Title
Dissection of Mitotic Ran Pathway Function Using the Small Molecule Importazole

Author
Bird, Stephen Lucien

Publication Date
2012

Peer reviewed|Thesis/dissertation

Dissection of Mitotic Ran Pathway Function Using the Small Molecule Importazole

by

Stephen Lucien Bird

A dissertation submitted in partial satisfaction of the

requirements for the degree of

Doctor of Philosophy

in

Molecular and Cell Biology

in the

Graduate Division

of the

University of California, Berkeley

Committee in charge:

Professor Rebecca Heald, Co-chair
Professor Karsten Weis, Co-chair
Professor David G. Drubin
Professor Gerard Marriott

Spring 2012

Dissection of Mitotic Ran Pathway Function Using the Small Molecule Importazole

by

Stephen Lucien Bird

Abstract

Dissection of Mitotic Ran Pathway Function Using the Small Molecule Importazole

by

Stephen Lucien Bird

Doctor of Philosophy in Molecular and Cell Biology

University of California, Berkeley

Professor Rebecca Heald and
Professor Karsten Weis, co-chairs

The faithful and proper segregation of the genome between dividing cells is of paramount importance to all organisms. In order to maintain the integrity of the genetic information during division, cells make use of an extremely complex and highly regulated set of processes known collectively as mitosis. A key aspect of mitosis is the generation and maintenance of the mitotic spindle, a large and complex microtubule based structure that is responsible for organizing and transporting the chromosomes to the daughter cells. The mitotic spindle is of vital importance to the life of the cell, and multiple partially redundant pathways have evolved to regulate its assembly and operation. The small GTPase Ran governs one such pathway functioning in the vicinity of the chromosomes to control the activation of a variety of proteins that contribute to mitotic spindle assembly. However, in addition to promoting spindle assembly, the Ran pathway also regulates a number of other essential processes during the cell cycle such as nucleocytoplasmic transport and nuclear envelope dynamics. Due to this fact, studying the mitotic roles of the Ran pathway *in vivo* is challenging, as mitosis comprises only a small portion of the cell cycle. In order to overcome this obstacle, we took a small molecule inhibitor based approach, and sought to identify a compound capable of disrupting Ran pathway function with great temporal precision in living cells. In the following dissertation, we first provide an introduction to the cellular processes regulated by mitotic Ran pathway function, and then follow with descriptions of our efforts to develop and improve an inhibitor of RanGTP/importin-β function. Finally, we describe how we made use of this inhibitor to gain insight into a newly discovered role for Ran in the regulation of mitotic spindle positioning.

First we set out to develop a small molecule inhibitor capable of disrupting Ran pathway function. During interphase, the transport receptor importin-β carries cargoes into the nucleus, where RanGTP releases them. A similar mechanism operates in mitosis to generate a gradient of active spindle assembly factors around mitotic chromosomes. We implemented a FRET-based, high-throughput small molecule screen for compounds that interfere with the

interaction between RanGTP and importin-β and identified importazole, a 2,4-diaminoquinazoline. We found that importazole specifically blocked importin-β-mediated nuclear import both in *Xenopus* egg extracts and cultured cells, without disrupting transportin-mediated nuclear import or CRM1-mediated nuclear export. When added during mitosis, importazole impaired the release of an importin-β cargo FRET probe and caused both predicted and novel defects in spindle assembly. Together, our results identified importazole as a compound suitable for study of the Ran pathway in mitosis that specifically inhibits importin-β function, and suggest a possible molecular mechanism for importazole in which it alters importin-β interaction with RanGTP.

With an inhibitor of the pathway in hand, we attempted to improve importazole as a tool for study of mitotic Ran pathway function by elucidating its mechanism of action and devloping more potent analogues to maximize compound specificity. In order to gain further insight into importazole's molecular mechanism, we made use of surface plasmon resonance to directly measure the *in vitro* association between RanGTP and importin-β in the presence of importazole. In concordance with our previous observations, these experiments suggested that importazole does not destabilize the RanGTP/importin-β complex. However, the data was ultimately not reproducible enough to provide additional information about importazole function. In an effort to produce more potent inhibitors of RanGTP/importin-β function, we developed small molecule analogues based on the structure of importazole. One of these second generation compounds was capable of disrupting nucleocytoplasmic transport and mitotic spindle assembly, though it was not shown to be a significantly more potent inhibitor than importazole. Thus, we determined that importazole remains the best currently available tool for study of the Ran pathway in mitosis.

Finally, we took advantage of importazole to explore RanGTP/importin-β involvement in regulating mitotic spindle positioning, a mitotic function of the Ran pathway that has only recently been discovered. Proper positioning of the spindle is required to ensure correct segregation of the chromosomes during mitosis, and is mediated through pulling forces exerted on the astral microtubules by dynein/dynactin complexes linked to the cell cortex with Gαi, LGN, and the importin-β cargo protein NuMA. We found that importazole treatment disrupted mitotic spindle positioning in living cells without preventing formation of astral microtubules, and that it affected the cortical localization of both LGN and NuMA. These results demonstrated a role for RanGTP/importin-β function in spindle positioning, and our data suggest a model in which Ran may control this process through regulation of the stability of cortical positioning factors. A great deal remains to be learned about the role of the Ran pathway in mitotic spindle positioning, but importazole provides a promising avenue of study for this and other Ran mediated cellular processes.

Table of Contents

List of Figures

List of Abbreviations

APC: Adenomatous polyposis coli

ATP: Adenosine triphosphate

CFP: Cyan fluorescent protein

CPC: Chromosomal passenger complex

CV: Coefficient of variation

DMSO: Dimethyl sulfoxide

DNA: Deoxyribonucleic acid

FLIM: Fluorescnenc-lifetime imaging microscopy

FRET: Fluorescence resonance energy transfer

GAP: GTPase activating protein

GFP: Green fluorescent protein

GTP: Guanosine triphosphate

GTPase: Guanosine triphosphatase

GDP: Guanosine diphosphate

GEF: Guanine nucleotide exchange factor

γ-TURC: γ-tubulin ring complex

HTS: High-throughput screen

IBB: Importin-β binding domain

IPZ: Importazole

LMB: Leptomycin B

MAPs: Microtubule associated proteins

MTs: Microtubules

MTOC: Microtubule organizing center

NCC: Nucleus centrosome complex

NES: Nuclear export signal

NLS: Nuclear localization sequence

NMR: Nuclear magnetic resonance

NPC: Nuclear pore complex

PCM: Peri-centriolar material

RNA: Ribonucleic acid

RNAi: RNA interference

RT-PCR: Real-time polymerase chain reaction

SAFs: Spindle assembly factors

SPR: Surface plasmon resonance

YFP: Yellow fluorescent protein

Acknowledgements

I have received a great deal of help and advice throughout my graduate career for which I am eternally grateful. First of all, I would like to thank both of my graduate advisors: Rebecca Heald and Karsten Weis. Rebecca and Karsten have always been there to support me through both thick and thin with great patience and understanding. Thank you both! I would also like to thank all the members of the Weis and Heald labs that have made graduate school such a memorable and rewarding experience, especially Jon Soderholm, Yasaswini Sampathkumar, and Petr Kalab, the members of the "Ran fan club" without whom completion of this dissertation would not have been possible. Furthermore, I would like to thank all the other members of the trilab for making the third floor of LSA such an interesting and enjoyable place to work.

I am also thankful to the members of my thesis committee David Drubin and Gerard Marriott, as well as the other faculty members both at UC Berkeley and other institutions that have aided my graduate career, including Robert Fletterick, Susan Marqusee, Michael Rape, Kevin Vaughan, and David Wemmer. Additionally, I would like to thank Brian Wolff, Janice Williams, Brian Feng, James Wells, and Michael Uehara-Bingen for their involvement in the importazole screen, Keisuke Hasegawa for the FLIM imaging, Elisa Dultz and Steve Duleh for their help with live cell imaging, Karin Reif for NFAT cDNA, David Halpin for biotin-labeled RCC1, Jeremy Wilbur and Peter Hwang for their help with SPR, Tim Lewis and Lili Wang for their development of the importazole analogues, Quansheng Du for the LGN antibody, and Duane Compton for the NuMA antibody.

Finally, I would like to all of my friends and family that have made this entire journey worthwhile, including Roman Barbalat, Steve Duleh, Jose Estrada, Daniel Richter, Alberto Stolfi, and Maylee Wu, my parents Stephen and Rosemary Bird, and my siblings Daniel, Holly, and Angela.

Dedicated to:

My parents, brother, and sisters for their constant support these past six years.

Chapter 1:

Introduction

Introduction to Mitosis

One of the most challenging problems faced by any organism is how to efficiently and accurately segregate its genome between dividing cells. This problem is especially apparent in complex multicellular organisms, in which failure to properly segregate the genome of individual cells can result in a variety of serious consequences for the organism as a whole including cell death, developmental defects, aneuploidy, and cancer (O'Connell and Khodjakov, 2007). In order to overcome this problem, eukaryotic cells make use of a highly complex and coordinated process known as mitosis in order to accurately segregate their genome between daughter cells.

Considering the importance of mitosis to the life of the cell, it should come as no surprise that this is an area of study that has been a source of great fascination to biologists ever since Walter Flemming first described the mitosis of salamander cells in 1882 (Wolpert, 1995) (Figure 1.1, panel a). Despite this natural interest, however, knowledge of this process had long been limited to what could be observed by eye or with light microscopy. The turning point in the study of mitosis came with the discovery of GFP in the early 1990s, which allowed scientists to observe the localization and dynamics of proteins involved in mitosis in living cells (Chalfie et al., 1994) (Figure 1.1, panel b). In the twenty years following this breakthrough, the scientific community's understanding of mitosis has expanded greatly, leading to a much greater understanding of both the components involved in mitosis, as well as how those components are organized and controlled. In the following sections, I will discuss the major protein components now known to be involved in mitotic spindle assembly, and how these components are organized to lead to the creation of the mitotic spindle.

Microtubules

Microtubules are protein polymers that comprise the major structural component of the mitotic spindle. The basic unit from which microtubules are constructed is the tubulin heterodimer, composed of an individual α-tubulin subunit and an individual β-tubulin subunit arranged head to tail (Nogales, 1999). Both α and β-tubulin subunits bind GTP, but only β-tubulin hydrolizes GTP in to GDP, which results in a conformational change in the tubulin heterodimer known to contribute to microtubule destabilization. Individual tubulin heterodimers are also arranged uniformly with α subunits always bordering β subunits to create a tubulin protofilament. Typically, thirteen tubulin protofilaments are arranged parallel and in the same orientation with respect to one another, and fold together to create a 25nm diameter tube, known as a microtubule (Desai and Mitchison, 1997). Because the inherent polarity of the tubulin heterodimer is maintained throughout the structure of the microtubule, β-tubulin subunits will always be exposed at one end of the microtubule, known as the plus end, while α-tubulin subunits are exposed at the other end of the microtubule, known as the minus end (Figure 1.2, panel a).

Figure 1.1

a

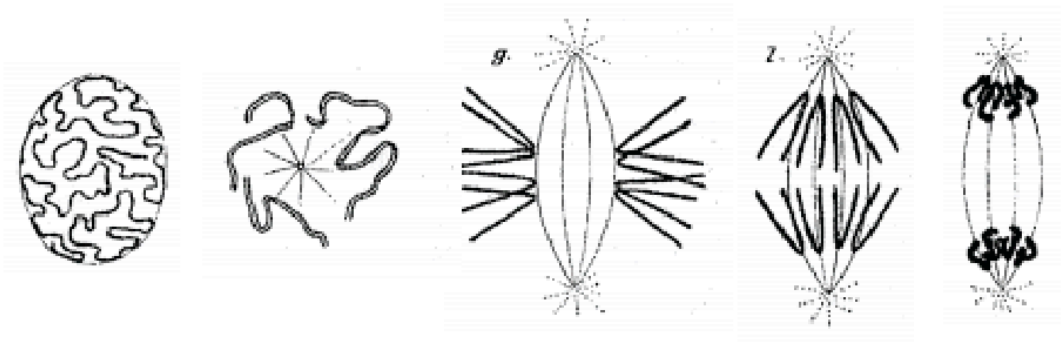

b

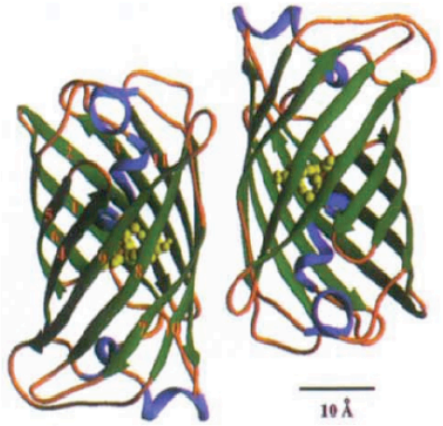

Figure 1.1: Observing mitosis
(a) Walter Fleming's original drawings of mitosis in salamander cells from 1882. (Adapted from (Wolpert, 1995))
(b) The crystal structure of green fluorescent protein (GFP) from the Pacific jellyfish *Aequorea victoria*, used by modern day biologists to visualize the process of mitosis in living cells. (Adaped from (Yang et al., 1996))

Figure 1.2

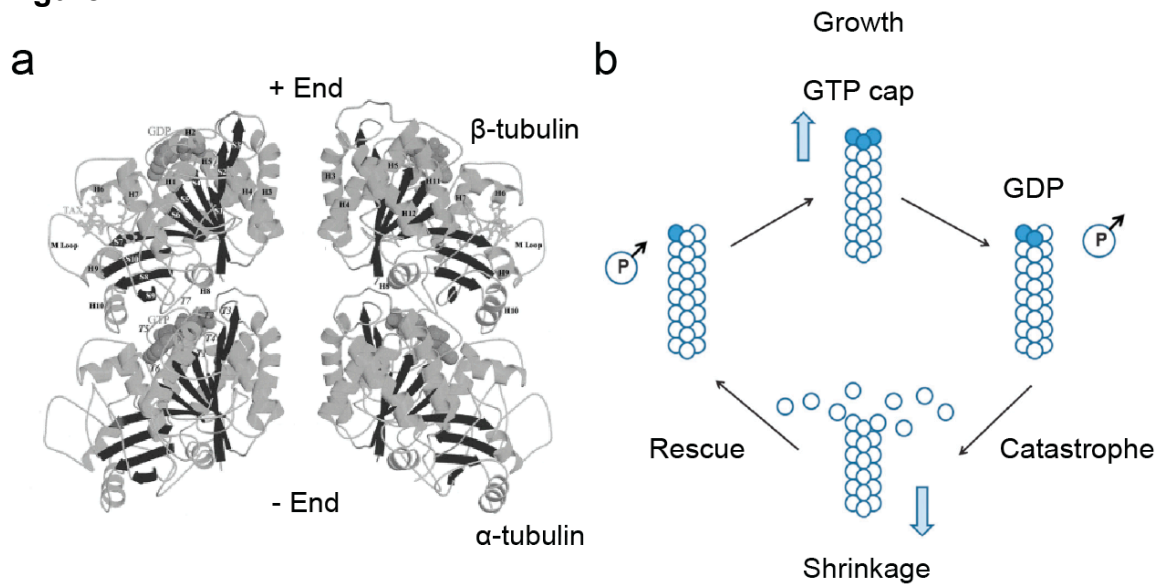

Figure 1.2: Microtubule structure and dynamics
(a) Microtubules are made up of individual tubulin heterodimers each composed of an individual α-tubulin subunit and an individual β-tubulin subunit arranged end to end. (Adapted from (Nogales, 1999))
(b) Dynamic instability of microtubules. At a given concentration of free tubulin, individual microtubules may cycle between periods of growth or shrinkage dependent upon the loss or gain of a cap of GTP tubulin at the microtubule plus end. (Adapted from (Kilner et al., 2011))

The inherent polarity of microtubules also leads to distinct growth and shrinkage rates at the plus and minus ends, with the plus end growing or shrinking faster than the microtubule minus end at a given concentration of free tubulin (Summers and Kirschner, 1979). In addition, microtubules possess a unique property known as dynamic instability, which describes the striking coexistence of both growing and shrinking microtubules at steady state (Mitchison and Kirschner, 1984). Key to this phenomenon is that tubulin dimers added to the microtubule have their β subunit bound to GTP, creating a cap of GTP tubulin at the growing plus end (Walker et al., 1989). However, over time, the GTP of β subunits in the microtubule lattice is hydrolyzed to GDP, and if the cap of GTP tubulin is lost it leads to destabilization and subsequent shrinking of the microtubule, known as catastrophe. Conversely, shrinking microtubules can also regain their GTP caps, possibly by encountering dimers in the microtubule lattice which have yet to hydrolize GTP, and can start growing again in a process known as rescue (Dimitrov et al., 2008) (Figure 1.2, panel b). In addition to these complicated inherent features of the microtubule polymer, the cellular tubulin concentration is much lower than the concentration required for microtubule nucleation *in vitro*, demonstrating that microtubule dynamics in the cell must be highly regulated (Amos and Amos, 1991; Mitchison and Kirschner, 1984; Mitchison and Salmon, 2001).

Microtubule associated proteins

Cells modify microtubule dynamics through microtubule associated proteins, or MAPs. The number of known MAPs is legion, so for simplicity's sake, we will focus on only a few important examples from each class of MAP. There are four major classes of MAPs involved in mitotic spindle assembly: microtubule stabilizers, microtubule destabilizers, microtubule nucleators, and microtubule motor proteins.

The first major class of MAPs is the microtubule stabilizers. As the name implies, this class of MAPs functions by binding to and stabilizing microtubules through a variety of mechanisms. For example, XMAP215 is a major microtubule stabilizer that functions by reducing the frequency of microtubule catastrophe (Andersen et al., 1994), while XMAP130 stabilizes microtubules by increasing the rescue frequency (Andersen and Karsenti, 1997). Additional examples of microtubule stabilizers include microtubule bundlers such as TPX2, and tip-tracking proteins such as EB1 and Orbit (Maiato et al., 2005; Schatz et al., 2003; Schuyler and Pellman, 2001; Wittmann et al., 2000). Tip-tracking proteins localize to the plus-ends of growing microtubules, where they help to mediate microtubule/cortex and microtubule/kinetochore interactions in addition to stabilizing microtubules by regulating plus-end dynamics.

The second major class of MAPs is microtubule destabilizers, which can be further classified based on the manner in which they function. Members of the kinesin-13 family such as MCAK are non-motor kinesins that depolymerize microtubules by using ATP hydrolysis to physically peel back the protofilaments at either end of the microtubule (Desai et al., 1999; Niederstrasser et al., 2002). Microtubule severing proteins such as katanin cut microtubules internally,

exposing additional microtubule ends for depolymerization (McNally and Vale, 1993). Finally, tubulin sequestering proteins such as Stathmin/Op18 bind and sequester free tubulin subunits, making them unavailable for polymerization, but can also bind subunits at the microtubule plus-end, leading to catastrophe (Cassimeris, 2002).

The third major class of MAPs is microtubule nucleators. The major site of microtubule nucleation in the cell is the centrosome, which also acts as the cell's microtubule organizing center (MTOC). Each centrosome is composed of a pair of microtubule like structures know as centrioles, which are surrounded by a poorly-understood mixture of proteins known as the peri-centriolar material, or PCM. One known component of the PCM is the γ-tubulin ring complex, or γ-TURC, which nucleates microtubules by providing a template for tubulin dimers to assemble in to ring structures containing thirteen protofilaments (Moritz et al., 1995; Zheng et al., 1995). While the centrosome is the major site of microtubule nucleation, γ-TURC can also exist free of the PCM and nucleate microtubules throughout the spindle. Additionally, the multi-functional protein TPX2 can nucleate microtubules in a chromatin-mediated manner (Schatz et al., 2003).

The final major class of MAPs is the microtubule-based motor proteins. All microtubule motor proteins make use of ATP hydrolysis to power their movement along the outer surface of the microtubule lattice. There are two major types of microtubule motors: cytoplasmic dynein and the kinesins. Cytoplasmic dynein is a multi-subunit minus-end directed motor protein complex that functions in association with the dynein activating dynactin complex (Heald and Walczak, 1999). Dynein is involved in a variety of aspects of mitotic spindle assembly and function including spindle length determination, spindle pole focusing, spindle/cortex interactions, spindle positioning, and chromosome movement during anaphase (Figure 1.3). Many of these functions are mediated by dynein's ability to transport other proteins to specific locations, such as spindle pole focusing, which is mediated by dynein's ability to transport TPX2 and NuMA to the poles (Merdes et al., 1996). Other dynien functions, such as spindle positioning and spindle length determination, rely directly on dynein's motor activity to generate force on microtubules.

The other group of microtubule motor proteins are the kinesins, of which there are three subgroups, which are defined both by the location of the motor domain within the protein and the consequent protein function (Lawrence et al., 2004). KinI kinesins possess an internal motor domain and are non-motile, but function as microtubule destabilizers, such as the previously discussed MCAK. KinN kinesins have a N-terminal motor domain and are plus end directed motor proteins (Antonio et al., 2000; Funabiki and Murray, 2000; Vernos et al., 1995). Notable examples of KinN kinesins include the chromokinesin Xkid, which is responsible for moving the chromosome arms towards the metaphase plate, and the homotetrameric Eg5, which organizes microtubules in to anti-parallel arrays with the minus ends extending outward (Funabiki and Murray, 2000; Kashina et al., 1996) (Figure 1.3). Eg5 is involved in spindle length determination and required for spindle bipolarity (Mayer et al., 1999). Finally, KinC kinesins are minus end directed kinesins with a C-terminal motor domain, and function in

Figure 1.3

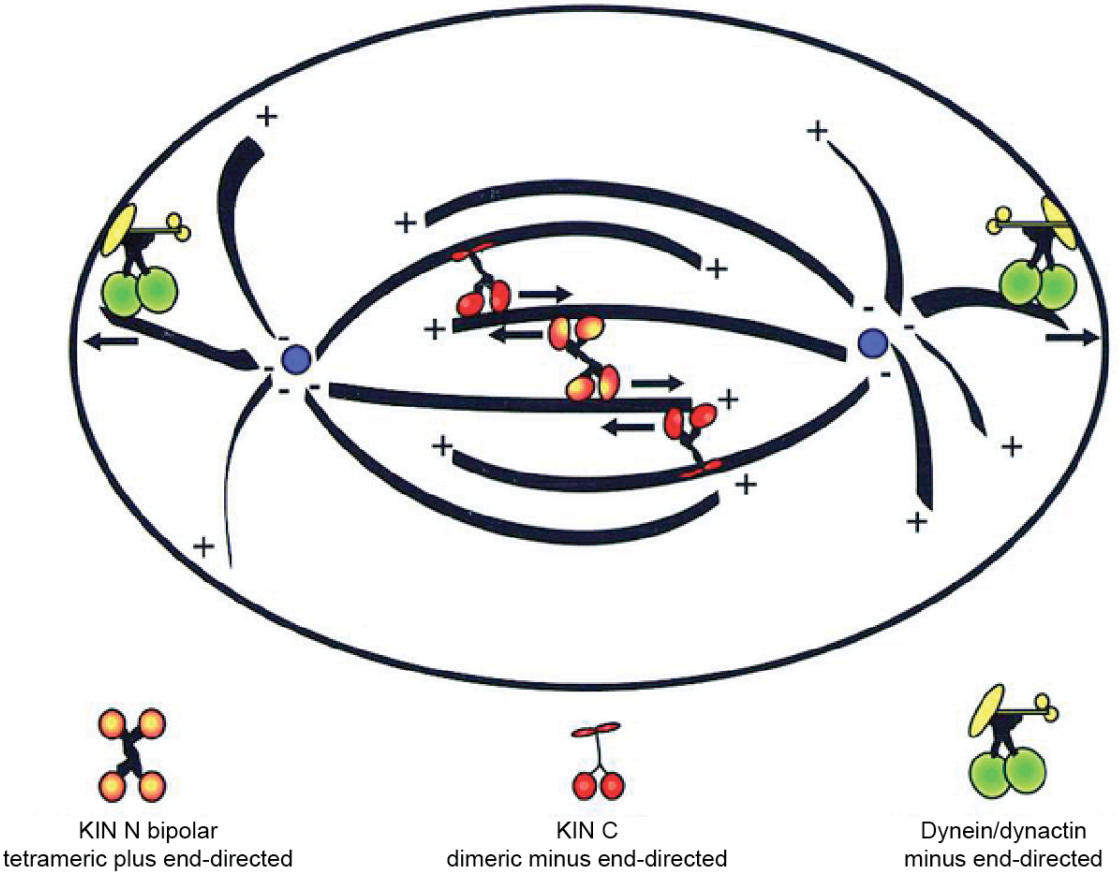

Figure 1.3: Microtubule motors help organize the spindle
A balance of forces from various microtubule motors maintains mitotic spindle structure. The tetrameric plus end-directed kinesin Eg5 pushes spindle poles apart while minus end-directed KinC kinesins pull the spindle poles together. The dynein/dynactin complex pulls spindle poles towards the cell cortex, where it is anchored. (Adapted from (Heald, 2000))

spindle pole organization and spindle length regulation in a manner similar to cytoplasmic dynein (Sharp et al., 1999; Walczak et al., 1997).

Mechanisms of mitotic spindle assembly

Because segregation of the genome is such an essential process for life, the cell has evolved two major partially redundant mechanisms that govern generation of the mitotic spindle. The "search and capture" model of mitotic spindle assembly describes the first of these mechanisms (Mitchison and Kirschner, 1985) (Figure 1.4, panel a). In this model, microtubules are nucleated at the centrosomes, located at the poles, and grow towards the center of the cell. As microtubules grow during this process, they "search" the cytoplasmic space for the kinetochores of chromosomes. Once a microtubule encounters a kinetochore, it "captures" the chromosome by attaching to the kinetochore and bringing it in to the structure of the spindle. However, it has been estimated that in a cell of normal size, if the cell relied only on the search and capture mechanism, the process of finding and attaching to the chromosomes would take longer than the entire length of mitosis (Wollman et al., 2005). Therefore, there must be a second mechanism of spindle organization.

Another mechanism to organize the mitotic spindle does indeed exist, and is described by the "chromatin mediated" model of mitotic spindle assembly (Figure 1.4, panel b). In this model, microtubules are nucleated around the chromosomes themselves, and their minus ends are organized and bundled to form the poles (Heald et al., 1996). Key to this model of spindle assembly is the presence of a diffusible factor located around the chromosomes capable of directing and organizing the various MAPs responsible for the nucleation and assembly of microtubules. This factor has been revealed to be the small GTPase Ran, which will be discussed further in the next section.

Both the "search and capture" and the "chromatin mediated" models of mitotic spindle assembly rely on nucleators, motor proteins, and other MAPs to generate, organize, and dynamically regulate the formation and maintenance of the mitotic spindle. While there are examples of cells, like meiotic *Xenopus* oocytes (Kalab et al., 2011) that use only one of these models to organize their spindles, the reality is that most cell types rely on both mechanisms to organize their spindles to some degree, and therefore both models are essential to understanding the process of mitotic spindle assembly (Gadde and Heald, 2004; Khodjakov et al., 2000) (Figure 1.4, panel c).

Ran

The small GTPase Ran is the diffusible factor that has been shown to direct chromosome mediated spindle assembly. Ran is a Ras-related GTPase and plays essential roles throughout the cell cycle in the regulation of nucleocytoplasmic transport and nuclear envelope dynamics, as well as in proper segregation of the genome (Clarke and Zhang, 2004; Goodman and Zheng, 2006; Pemberton and Paschal, 2005; Terry et al., 2007). The key to Ran's

Figure 1.4

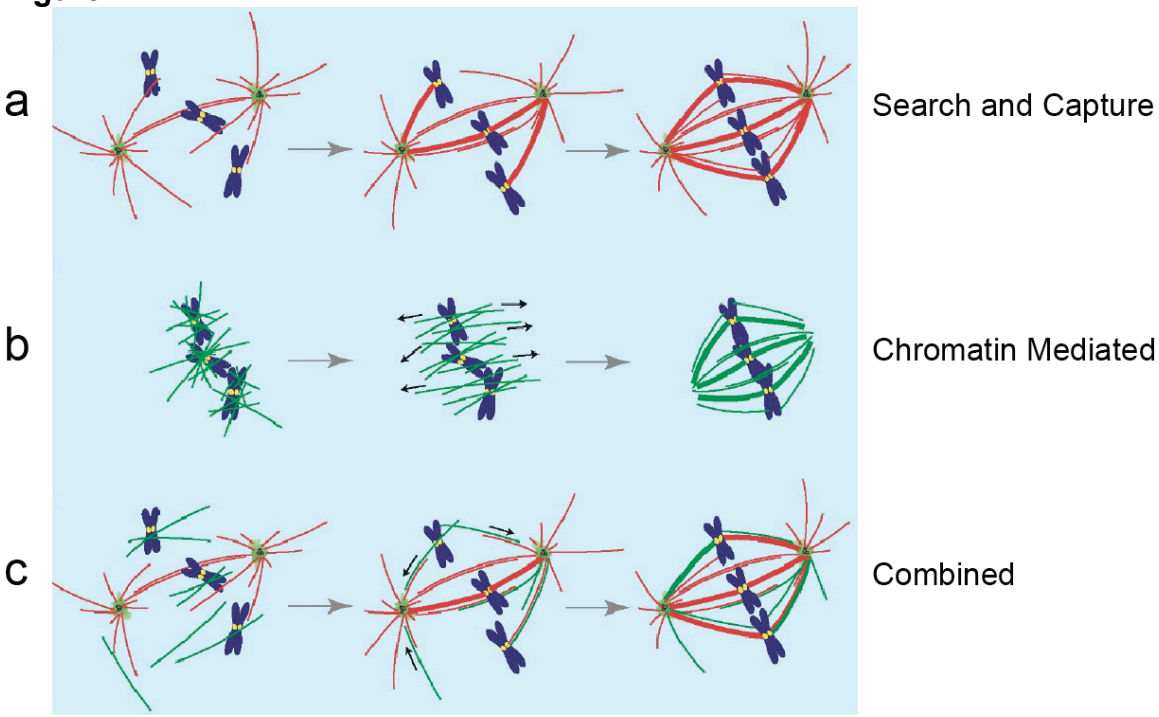

Figure 1.4: Models of mitotic spindle assembly
(a) In the search and capture model of spindle assembly, microtubules are nucleated by the centrosomes and probe the cytoplasmic space to find the kinetochores.
(b) In the chromatin mediated model of spindle assembly, microtubules are nucleated around the chromosomes and then organized and bundled by microtubule motor proteins to form the spindle poles.
(c) Both models of spindle assembly play a part in most cell types. (Adapted from (Gadde and Heald, 2004))

functions throughout the cell cycle is its ability as a small GTPase to exist in either a GTP or GDP bound form. The regulators of Ran's nucleotide state function due to their high specificity for Ran and distinct localizations within the cell (Figure 1.5). The first of these regulators is RCC1, which serves as Ran's guanine nucleotide exchange factor, or GEF, and is imported to the nucleus where it binds chromatin (Nemergut et al., 2001; Ohtsubo et al., 1989). RCC1 promotes GDP to GTP exchange about 10^5-fold by promoting release of GDP from Ran (Klebe et al., 1995). Because free GTP is far more abundant in the cell than free GDP, RCC1 promoted nucleotide release by Ran preferentially results in Ran binding to GTP. The other regulator of Ran's nucleotide state is its GTPase activating protein (GAP) RanGAP (Figure 1.5). While Ran itself is a GTPase, and therefore capable of hydrolyzing GTP to GDP, the GTPase activity of Ran alone is very low, resulting in a slow rate of GTP hydrolysis. However, when in the presence of RanGAP and its binding partner RanBP2, the GTP hydrolysis activity of Ran increases approximately 10^5-fold (Klebe et al., 1995). RanGAP localizes to the cytoplasm and to the outside of the nuclear envelope at nuclear pores, ensuring that RanGTP is quickly hydrolyzed to RanGDP once outside of the nucleus during interphase (Mahajan et al., 1997; Matunis et al., 1996).

The Ran pathway

Ran's various functions throughout the cell cycle are mediated by its binding or release from nuclear transport receptors of the importin-β superfamily, which are capable of transporting cargo molecules through the nuclear pore complex (NPC) (Mans et al., 2004; Pemberton and Paschal, 2005). Ran's binding to GTP or GDP changes its conformational state; when Ran binds GTP the conformation of its switch I and switch II loops changes, thus allowing Ran to bind to nuclear transport factors such as importin-β (Stewart et al., 1998). Importin-β is capable of binding RanGTP through three regions located in its N-terminal half, during which it is unable to bind to cargo proteins (Lee et al., 2005) (Figure 1.6). When GTP is hydrolyzed to GDP, however, Ran and importin-β no longer bind, allowing importin-β to bind to cargo proteins either directly or through the adaptor protein importin-α (Nilsson et al., 2001). Importin-α is able to bind to proteins that contain an NLS, or nuclear localization sequence, a short sequence of basic amino acids that directs a protein for nuclear import (Kalderon et al., 1984; Lanford and Butel, 1984; Weis, 2003). While importin-β is the most well-know mediator of nuclear import, other karyopherins such as transportin are also involved. Transport receptors involved in nuclear import are known collectively as importins. Additionally, some transport receptors, known as exportins, mediate nuclear export. One example is the transport receptor protein CRM1, which binds to RanGTP and cargo proteins containing an NES, or nuclear export signal, in a trimeric complex and transports them out of the nucleus through the NPC and into the cytoplasm (Moroianu, 1998).

Figure 1.5

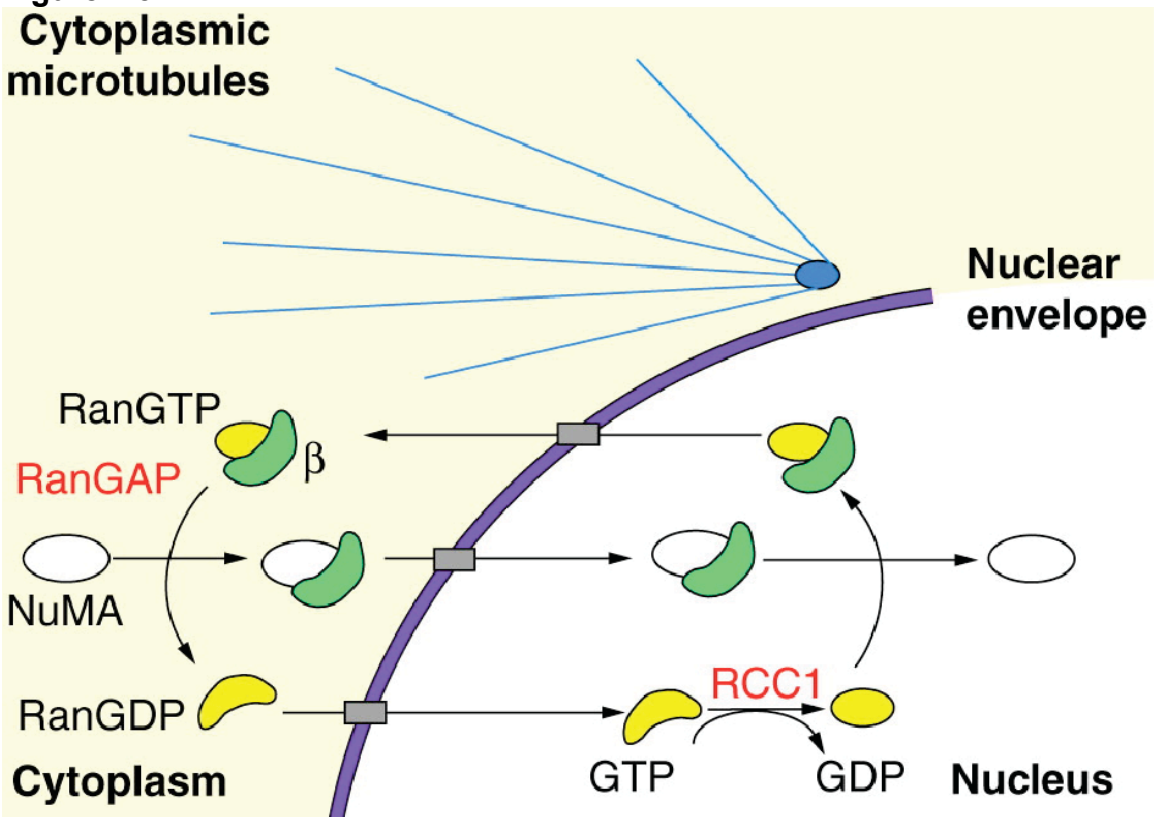

Figure 1.5: The Ran transport pathway
Ran's GEF RCC1 is bound to chromatin in the nucleus, creating high nuclear levels of RanGTP. Ran's GAP RanGAP is located in the cytoplasm, leading to rapid hydrolysis of RanGTP outside of the nucleus. In the cytoplasm, low levels of RanGTP allow transport receptors including importin-α/β to bind to NLS-containing cargo proteins such as NuMA and transport them into the nucleus. Once inside the nucleus, RanGTP binding to importin-β forces cargo release (Melchior, 2001).

Figure 1.6

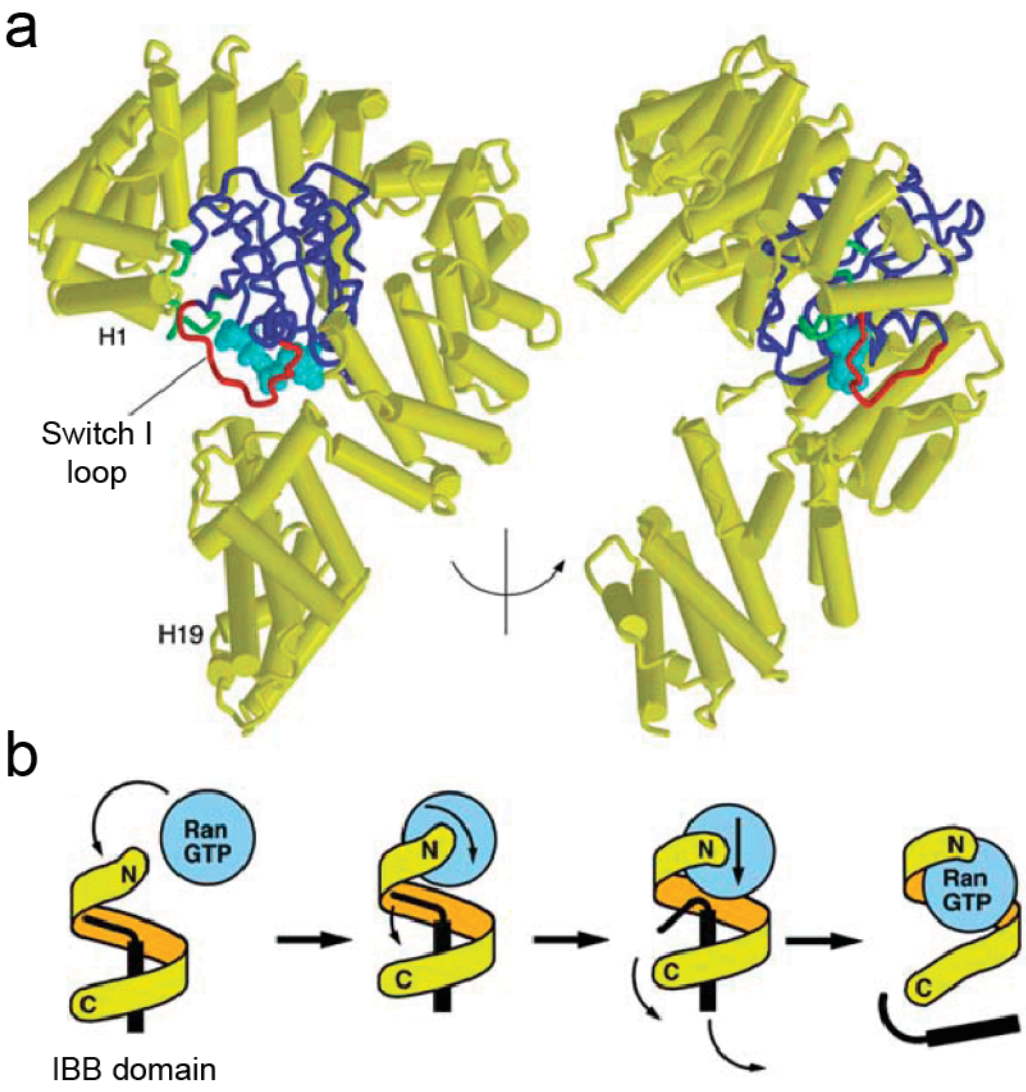

Figure 1.6: The RanGTP/importin-β structure
(a) Crystal structure of Kap95 (yeast importin-β, yellow) bound to RanGTP (blue). The switch 1 loop of Ran enveloping GTP is shown in red.
(b) Diagram of potential mechanism for RanGTP (blue) displacement of importin-β binding domain (IBB) containing cargo (black) from importin-β (yellow).
(Adapted from (Lee et al., 2005))

Nucleocytoplasmic transport

The distinct spatial localizations of Ran's GEF and GAP, along with Ran's ability to bind or release nuclear transport receptors depending on its nucleotide state are key to understanding Ran's regulation of various processes throughout the cell cycle. In interphase, Ran's GEF RCC1 is bound to chromatin through its interaction with double stranded DNA as well as histones H3 and H4 (Bilbao-Cortes et al., 2002), creating high levels of RanGTP within the nucleus. On the other hand, RanGAP is located in the cytoplasm, causing any RanGTP that makes its way in to the cytoplasm to be either quickly hydrolyzed to RanGDP or bound to the abundant free transport factors found there. The physical barrier of the nuclear envelope creates a sharp contrast between the RanGTP rich nucleus and the RanGDP containing cytoplasm (Hetzer et al., 2002). Consequently, This environment causes NLS containing cargos located in the cytoplasm to bind importin-β and other transport factors in the absence of RanGTP. The importin-β bound cargoes are then transported through the NPC in to the nucleus, where the high levels of RanGTP quickly force their release (Figure 1.5). This distinct contrast in nucleotide state also allows for efficient export of NES containing cargos, though in this case the localization of RanGAP to the cytoplasmic face of the NPC is key in promoting quick GTP hydrolysis and subsequent cargo release upon exit from the nucleus.

The RanGTP gradient

As with nucleocytoplasmic transport, Ran's ability to direct mitotic spindle assembly is tied to its ability to bind either GTP or GDP. The major difference between the two situations, however, is the lack of a physical barrier between the regulators of Ran's nucleotide state that is normally provided by the nuclear envelope in interphase. Following nuclear envelope breakdown, RCC1 is still bound to chromatin, but RanGAP is distributed throughout the cytoplasm. The distribution of these two proteins causes a gradient of RanGTP to concentrate around the chromosomes (Caudron et al., 2005; Kalab et al., 2002; Kalab et al., 2006; Li and Zheng, 2004) (Figure 1.7). The presence of this Ran gradient causes importin-β and other transport factors to release their cargo proteins when they encounter RanGTP in the proximity of the chromosomes. Many of these cargo proteins function as spindle assembly factors (SAFs) in mitosis, and serve to generate and organize the spindle in conjunction with microtubule motor proteins. For example, TPX2 (involved in the nucleation of spindle microtubules) and NuMA (involved in the organization of the spindle poles in combination with cytoplasmic dynien) are both examples of the many Ran/importin-β regulated cargoes that function as SAFs (reviewed in (Kalab and Heald, 2008)). The size of the Ran gradient is fairly small, both in the distance it extends away from the chromosomes (approximately 5 μm in HeLa cells) as well as the additional percentage importin-β cargo proteins it releases (approximately 15% in HeLa cells) (Kalab et al., 2006). However, this difference has been shown to be large enough to induce microtubule polymerization in *Xenopus* egg extract.

Figure 1.7

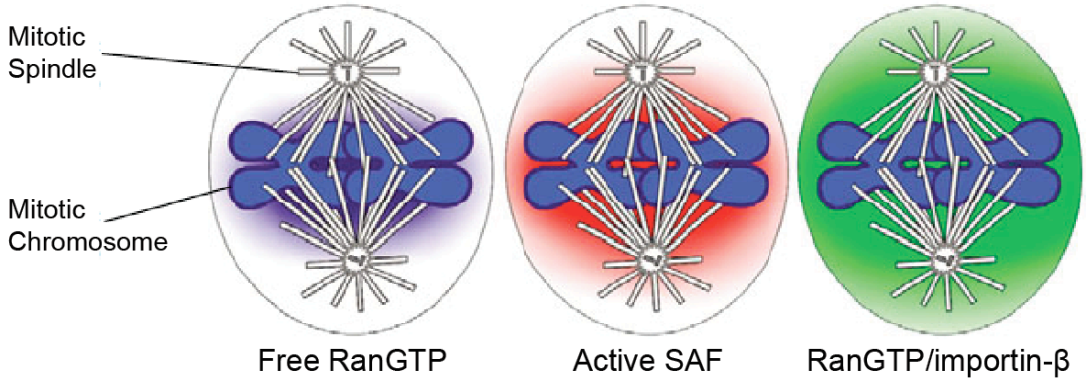

Figure 1.7: Mitotic gradients created by the Ran pathway
RCC1 bound to chromatin in mitosis causes a shallow gradient of free RanGTP to form that extends approximately 5 μm away from the chromosomes. This in turn frees importin-β bound cargoes in the proximity of the chromosomes, some of which act as spindle assembly factors (SAFs). The gradient of RanGTP bound to importin-β extends further towards the cell periphery. (Adapted from (Kalab and Heald, 2008))

Additional regulation of chromatin mediated spindle assembly

In addition to RanGTP gradient, multiple chromatin bound kinases contribute to chromatin mediated spindle assembly by regulating the phosphorylation of various MAPs. For example, polo kinase locally phosphorylates and inhibits the microtubule catastrophe factor Op18 in the vicinity of chromosomes (Andersen et al., 1997; Budde et al., 2001; Niethammer et al., 2004). Another important regulator of mitotic spindle assembly is the chromosomal passenger complex (CPC), a protein complex that localizes to the chromatin during mitosis, and later the spindle midzone during anaphase. The CPC includes INCENP, survivin, Dasara A/B, and the kinesin Aurora B, which phosphorylates and inhibits microtubule destabilizers such as MCAK near the chromosomes, thereby promoting microtubule stability (Gassmann et al., 2004; Ohi et al., 2004; Sampath et al., 2004; Zhang et al., 2007). Aurora B substrates are dephosphorylated farther away from the chromosomes by cytoplasmic phosphatases, creating a gradient of Aurora B phosphorylation that contributes to mitotic spindle stability (Fuller et al., 2008; Kelly et al., 2007). It is likely that additionally pathways that contribute to chromatin mediated spindle assembly have yet to be discovered.

Studying the role of Ran in mitosis

Due to the role Ran plays in spindle assembly and cell division, mis-regulation of the Ran pathway can have disastrous consequences for cell proliferation. In fact, Ran pathway members have been shown to be upregulated in several cancer cell lines, most notably those with mutated Ras (Morgan-Lappe et al., 2007; Yuen et al., 2012). Because of this association, understanding the Ran pathway's role in mitosis is essential to better understanding multiple cancer systems. While the need to understand the Ran pathway is clear, studying Ran in mitosis is complicated by its essential roles throughout the cell cycle, making the used of traditional means such as genetics and RNAi difficult. Due to these unusual circumstances, the ideal tool with which to study the Ran pathway in mitosis would be a small molecule inhibitor capable of specifically disrupting Ran/importin-β function. Such an inhibitor should allow for disruption of the Ran pathway with great spatial and temporal precision, and should reveal new insights on the role of the Ran pathway in living mitotic cells.

Spindle Positioning

While the Ran pathway has previously shown to play a role in processes related to the containment and segregation of the genome throughout the cell cycle including assembly of the mitotic spindle, recent work suggests that the Ran pathway may also play an important role in regulating the position of the mitotic spindle (Kiyomitsu and Cheeseman, 2012). Regulation of spindle positioning has primarily been studied in systems that undergo asymmetric cell division, like yeast. However, even in cells types that undergo symmetric cell division, regulation of spindle positioning is essential (Gonczy, 2008). Improper positioning of the spindle may result in mis-segregation of the genome during

cytokinesis, which can lead to aneuploidy and create further complications such as cancer or cell death. Spindle positioning is mediated by contact of the spindle's astral microtubules with the cell cortex, and interactions between the astral microtubules binding partners at the cortex are thought to be the primary source of information for spindle alignment (Pearson and Bloom, 2004). As these astral microtubules exhibit dynamic instability, the cell must be able to regulate their length with respect to the cortex, usually through pulling forces exerted on the microtubule plus-ends. These pulling forces can consist of plus-end depolymerization of microtubules still attached to the cortex, cortically attached minus end directed microtubule motors, or attachment of microtubules to actin-based motors associated with the cortical actin network (Siller and Doe, 2009).

Positioning in yeast

The system in which spindle orientation is best understood is the budding yeast *Saccharomyces cerevisiae*, and many of the relevant yeast proteins are evolutionarily conserved. As an asymmetrically dividing unicellular eukaryote, proper spindle orientation is essential for yeast to properly segregate their DNA to mother and daughter cells. As such, two partially redundant pathways that control different aspects of spindle positioning control the process in yeast. The first or "early" pathway is responsible for the alignment of the spindle along the bud axis of the mother cell before anaphase, while the "late" pathway is responsible for the proper translocation of the spindle through the bud neck during anaphase (Siller and Doe, 2009) (Figure 1.8).

In the early pathway of yeast spindle orientation, the APC (Adenomatous polyposis coli) related protein Kar9 is recruited to the daughter spindle pole body by the EB1 related Bim1 (Miller et al., 2006). This complex is then transported to the astral microtubule plus ends, allowing Kar9 to bind the myosin protein Myo2, which in turn transports the complex along actin cables in to the bud, where it associates with the cortically-associated Bud6 protein (Adames and Cooper, 2000; Hwang et al., 2003).

In the late pathway of yeast spindle orientation, the dynein/dynactin complex is transported to the cortex of the bud cell by association with the proteins Bik1 (related to CLIP-170), Pac1 (Lis1), and Ndl1 (Ndl) (Carminati and Stearns, 1997; Eshel et al., 1993; Li et al., 1993; Miller et al., 2006). These proteins first recruit dynein to the spindle pole body and then transport it to the cortex along the microtubule through association with the plus-end directed kinesin Kip2. Once at the cortex, dynein is activated by the membrane-bound Num1, and then regulates positioning of the spindle through its minus-end directed motor activity, pulling the spindle pole body through the bud neck (Farkasovsky and Kuntzel, 2001; Heil-Chapdelaine et al., 2000; Lee et al., 2003; Sheeman et al., 2003).

Figure 1.8

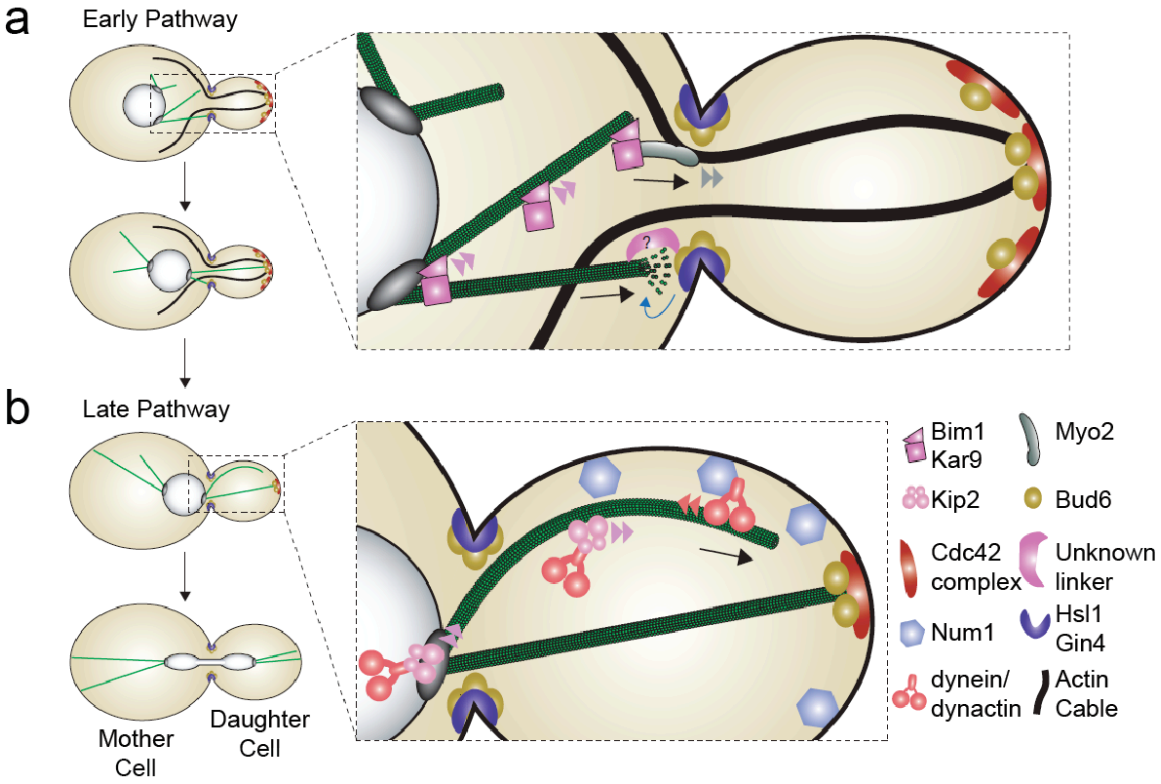

Figure 1.8: Spindle positioning in *S. cerevisiae*
(a) The early pathway of yeast spindle positioning. Kar9 bound to microtubules through Bim1 is transported in to the bud along actin cables by Myo2 to associate with Bud6 at the cortex.
(b) The late pathway of yeast spindle positioning. Dynein/dynactin is transported to the microtubule plus end by the kinesin Kip2 where it associates with membrane bound Num1 and exerts pulling forces on the mitotic spindle.
(Adapted from (Siller and Doe, 2009))

Positioning in worms

Another well-studied model of mitotic spindle positioning is the asymmetrically dividing *C. elegans* zygote (Schneider and Bowerman, 2003). Positioning in this system consists of three distinct steps defined as centration, spindle orientation, and spindle positioning (Figure 1.9). In the first step of centration, the posteriorly located nucleus centrosome complex (NCC) generates longer microtubules in the anterior direction, which are in turn preferentially pulled towards the cell center by the dynein/dynactin complexes linked to unknown cytoplasmic anchors (Kimura and Onami, 2005; Reinsch and Gonczy, 1998). Additionally, the cortical factors GPR-1/2 and LIN-5 are transiently enriched at the anterior cortex during centrarion, and may help direct the anterior movement of the NCC, though they are not required for this process (Park and Rose, 2008).

Both of the steps of spindle orientation and spindle positioning rely upon interaction between astral microtubule plus-ends and the dynein/dynactin complex at the cortex in order to move the spindle. Polarity is estabilished by the localization of the evolutionarily conserved Par complex (Par-3, Par-6, and aPKC) to the anterior cortex of the zygote, as well as PAR-1 and PAR-2 at the posterior cortex (Colombo et al., 2003; Gotta et al., 2003; Park and Rose, 2008; Tsou et al., 2003). Polarity cues from the Par proteins result in the enrichment of GPR-1/2 (Pins in flies and LGN in mammals) to the anterior cortex through activation of the receptor-independent heterotrimeric G-protien pathway and subsequent activation of cortical dynein/dynactin, resulting in rotation of the spindle to align the centrosomes along the anterior-posterior axis of the cell (Couwenbergs et al., 2007; Du and Macara, 2004; Nguyen-Ngoc et al., 2007; Nipper et al., 2007). Finally, in the spindle positioning step during anaphase, Par polarity cues lead to the enrichment of GPR-1/2 at the posterior cortex through the same mechanisms described above, leading to posterior displacement of the spindle and the generation of asymmetrically sized blastomeres.

Positioning in other organisms

Asymmetric cell division in other higher eukaryotes is controlled by mechanisms similar to those used by *C. elegans* embryos. *Drosophila* neuroblasts direct their asymmetric division by making use of the Par complex proteins Bazooka, Par-6, and aPKC to establish cortical polarity in late interphase/early prophase, along with the associated proteins Inscuteable, Pins and Gαi (Knoblich, 2008). Spindle polarity is established in prometaphase/metaphase through use of the conserved Gα-Pins-Mud pathway to recruit dynein/dynactin to the apical cortex, pulling the spindle to align along the apical/basil polarity axis (Bowman et al., 2006; Izumi et al., 2006; Parmentier et al., 2000; Schaefer et al., 2000; Schaefer et al., 2001; Siller et al., 2006; Yu et al., 2000). A second pathway exists in flies to organize the polar orientation of the spindle that involves Pins, Dlg, and the plus-end directed kif13A-related kinesin Khc73 (Siegrist and Doe, 2005). Like the Gα-Pins-Mud pathway, the Pins-Dlg-Khc73 pathway serves to orient the spindle by attaching astral

Figure 1.9

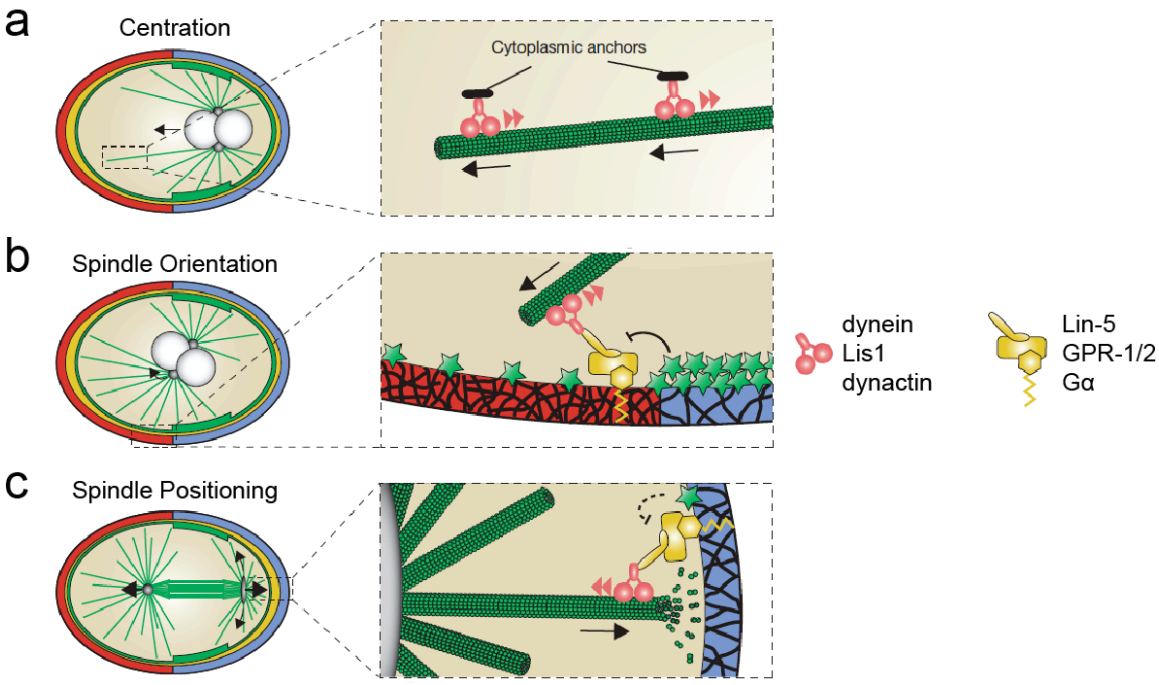

Figure 1.9: Spindle positioning in *C. elegans*
(a) During centration, the nucleus centrosome complex (NCC) is pulled anteriorly towards the cell center by dynein/dynactin complexes linked to unknown cytoplasmic anchors.
(b) During spindle orientation the Par complex (red) is localized to the anterior cortex of the cell, resulting in anterior enrichment of Gα/GPR-1/2/Lin-5 and subsequent activation of the dynein/dynactin complex, and rotation of the NCC to align with the anterior/posterior axis of the cell.
(c) In spindle positioning, polarity cues from PAR-1 and PAR-2 (blue) at the posterior cortex lead to posterior cortex enrichment of GPR-1/2 and posterior displacement of the spindle (Adapted from (Siller and Doe, 2009))

microtubules to microtubule motor proteins attached to linkers at the apical cortex. As with *C. elegans* zygotes, asymmetric cell division in *Drosophila* is accomplished through asymmetry of the mitotic spindle during anaphase.

Mammalian neuroepithelia also make use of polarized cell division, where spindle orientation may play a role in determining cell fate in the polarized tissues of the cerebral cortex and the retina (Cayouette and Raff, 2003; Cayouette et al., 2003; Konno et al., 2008). While the importance of controlling the polarity of these divisions in not completely clear, polarity in this system is also established by the Par complex proteins Cdc42, Par3, aPKC, and Par-6, and the Gα-LGN-NuMA complex accomplishes orientation of the spindle by linking astral microtubules to the cortex through use of the dynein/dynactin complex.

Positioning in symmetrically dividing cells

While the major focus of those involved in the positioning field has revolved around systems that divide asymmetrically, proper regulation of spindle position is also essential in symmetrically dividing cells (Figure 1.10). Examples of asymmetric cell division are rare in mammals, but members of the Gα-LGN-NuMA pathway still control spindle positioning by linking astral microtubules to the cortex through the dynein/dynactin complex. In *Drosophila*, the Gα-Pins-Mud (Gα-LGN-NuMA) pathway has been shown to be regulated by Ran without the use of importin-β through canoe (Wee et al., 2011). However, further Ran regulation of this pathway is likely in mammalian cells, especially due to the involvement of NuMA, a protein involved in spindle assembly known to be regulated by Ran and importin-β. Additionally, in HeLa cells, NuMA association with LGN is required for association of LGN with the cell cortex (Du and Macara, 2004). In fact, a likely role for the Ran/importin-β pathway in mitotic spindle positioning has recently been identified, though the details of its mechanism are still unclear (Kiyomitsu and Cheeseman, 2012).

Studying Ran pathway regulation of spindle positioning

Studying mitotic functions of the Ran pathway is challenging due to the involvement of Ran in multiple essential cellular processes throughout the cell cycle. Historically, researchers have been able to circumvent this problem by using the biochemically tractable *Xenopus* egg extract system to precisely manipulate the Ran pathway under conditions that mimic the mitotic cytoplasm (Heald, 1996). However, study of RanGTP/importin-β regulation of mitotic spindle positioning excludes use of this system, as spindles generated in extract have no cell cortex with which to interact. Therefore, use of a cell-permeable small molecule inhibitor to precisely disrupt Ran pathway function in mitotic cells provides the most straightforward approach toward study of Ran regulation of spindle positioning. In the following chapters, we describe our discovery of just such a small molecule, and use this inhibitor to examine various mitotic Ran pathway functions including spindle positioning.

Figure 1.10

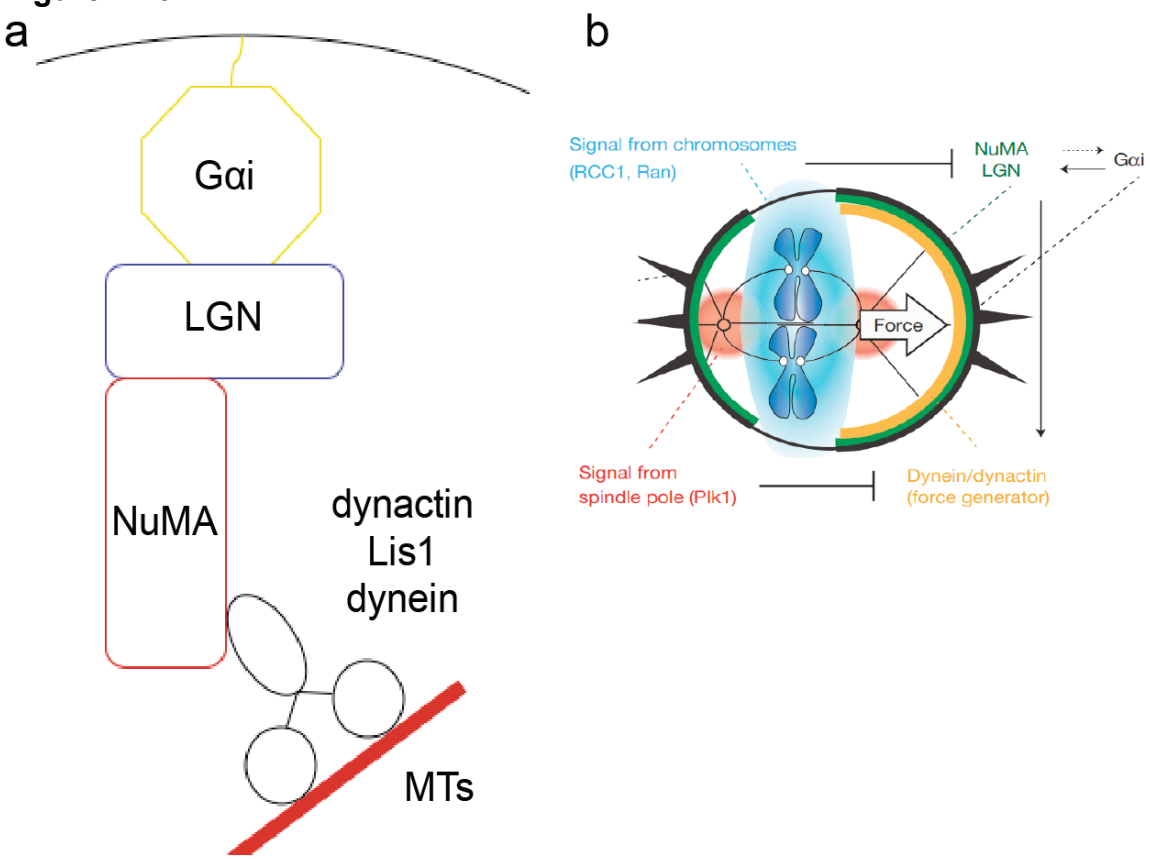

Figure 1.10: Spindle positioning in symmetrically dividing mammalian cells
(a) Spindle positioning in symmetrically dividing mammalian cells is regulated by interaction of dynein/dynactin with the evolutionarily conserved (Gα-LGN-NuMA) pathway.
(b) Proposed role for the Ran pathway in mitotic spindle positioning of mammalian cells. (Adaped from (Kiyomitsu and Cheeseman, 2012))

Chapter 2:

Importazole, a Small Molecule Inhibitor of the Transport Receptor Importin-β

Background

Importin-β transport receptors, which comprise at least 22 members in vertebrates (Strom and Weis, 2001), bind to cargo molecules and mediate their import or export through nuclear pores (Harel et al., 2003). Directionality of transport depends on the nature of the receptor as well as the asymmetric distribution of nucleotide states of the small GTPase Ran, which is GTP-bound in the nucleus due to the chromatin interaction of its guanine exchange factor (GEF) RCC1, and GDP-bound in the cytoplasm where its GTPase activating protein, RanGAP, is localized. The founding member of this family, importin-β, together with its partner importin-α, recognize nuclear localization signal (NLS)-containing cargo molecules and transport them into the nucleus where RanGTP binds directly to importin-β, causing a conformational change that releases importin-α and NLS-containing cargoes. In addition to its vital interphase functions, importin-β and Ran are also important regulators during mitosis, contributing to chromatin-mediated spindle assembly (Gruss et al., 2001; Nachury et al., 2001; Wiese et al., 2001). During mitosis, importin-β has an inhibitory function towards NLS-containing spindle assembly factors, binding them in the cytoplasm and impairing their microtubule-stabilizing or organizing activities. However, RanGTP remains enriched around condensed mitotic chromosomes in mitosis and generates a gradient of released cargoes that triggers spindle assembly (Kalab et al., 2002; Kalab et al., 2006). The importin-β/RanGTP pathway has also been implicated in a variety of other cellular processes including postmitotic nuclear envelope assembly, nuclear pore complex assembly, protein ubiquitylation, and primary cilium formation (Dishinger et al., 2010; Harel et al., 2003; Ryan et al., 2007; Song and Rape, 2010; Walther et al., 2003).

Small-molecule inhibitors provide a promising approach to study the multifunctional importin-β/Ran pathway in living cells by acting like conditional mutations that allow disruption of a protein with temporal precision, at any phase of the cell cycle. Compounds targeting microtubules or microtubule-based motors have been successfully used to dissect their mitotic functions and also gain mechanistic insight into the complex events of mitosis. For example, the drug monastrol inhibits kinesin-5 (Eg5) (Mayer et al., 1999) and causes a loss of spindle bipolarity, consistent with this motor's microtubule cross-linking and sliding function, as well as the results of immunodepletion and antibody microinjection experiments (Blangy et al., 1995; Sawin et al., 1992). However, monastrol has also provided novel insights through drug-washout experiments and in combination with other inhibitors, to assess how spindle bipolarity and microtubule attachment to chromosomes are established (Kapoor et al., 2000; Khodjakov et al., 2003) and how the cell division cleavage plane is positioned (Canman et al., 2003). Because of its fundamental role in many cellular functions including mitosis, nuclear transport is also an attractive target for small molecule inhibition. However, despite the importance of this process, surprisingly few inhibitors have been identified. With respect to nuclear export, leptomycin is a potent inhibitor, but binds covalently to its target, preventing

washout experiments (Ossareh-Nazari et al., 1997). Peptide inhibitors (Kosugi et al., 2008) and small molecule peptidomimetic inhibitors (Ambrus et al., 2010) of importin-α/β have been designed and used to study nuclear import *in vivo*. However, these inhibitors are not cell permeable. Recently, a new cell permeable small molecule inhibitor of the RanGTP/importin-β interaction named karyostatin 1A that binds specifically to importin-β and blocks importin-β-mediated nuclear import has been identified (Hintersteiner et al., 2010). However, the effects of karyostatin 1A on mitotic events have not yet been demonstrated.

To gain a better understanding of the functions of the importin-β/Ran pathway in mammalian cells without the limitations associated with microinjection of proteins or antibodies, or the time required for efficacy of RNA interference or peptide inhibitors (Kalab et al., 2006), we aimed to identify a cell permeable, specific and reversible small molecule inhibitor that would provide high temporal precision, allowing dissection of the role of importin-β/RanGTP throughout the cell cycle. Here we report the discovery of importazole, which meets these criteria and suggests at least one previously uncharacterized role for this pathway in mitosis.

Results and Discussion

Identification of importazole in a high throughput screen

We applied a reverse chemical genetic high-throughput screen (HTS) to identify compounds that affect the interaction between RanGTP and importin-β using a fluorescence resonance energy transfer (FRET)-based assay with CFP-tagged Ran and YFP-tagged importin-β. These proteins bind one another only when CFP-Ran is GTP-bound, which can be detected by changes in FRET (Figure 2.1, panels a and b). When CFP-Ran is incubated with RCC1, GTP, and YFP-importin-β, and the mixture is excited with 435 nm fluorescence in a fluorometer, a strong FRET signal is generated, as indicated by a decrease in the fluorescence intensity at 475 nm (the emission wavelength of CFP) and an increase in the fluorescence intensity at 525 nm (the emission wavelength of YFP). No FRET signal is generated if GDP is substituted for GTP, and nucleotide-specific interaction could also be observed biochemically, as S-tagged YFP-importin-β pulls CFP-Ran out of solution only in the presence of GTP (Figure 2.2). These results demonstrate that the FRET signal generated by CFP-RanGTP and YFP-importin-β is due to a physical interaction dependent upon the nucleotide state of Ran, and that our approach could be used to identify compounds that interfere with the interaction between CFP-RanGTP and YFP-importin-β, resulting in a reduced FRET signal.

The assay was tested for suitability for HTS using a 384-well format and a fluorescence plate reader. We calculated FRET ratios (I_{FRET}/I_{CFP}) for each well and determined two commonly used statistical parameters, the coefficient of variation (CV), which was 0.95% and 1.24% for reactions containing the GDP and GTP, respectively, and the Z' value, which was 0.81, indicating that our assay was robust and appropriate for HTS (Zhang et al., 1999). To

Figure 2.1

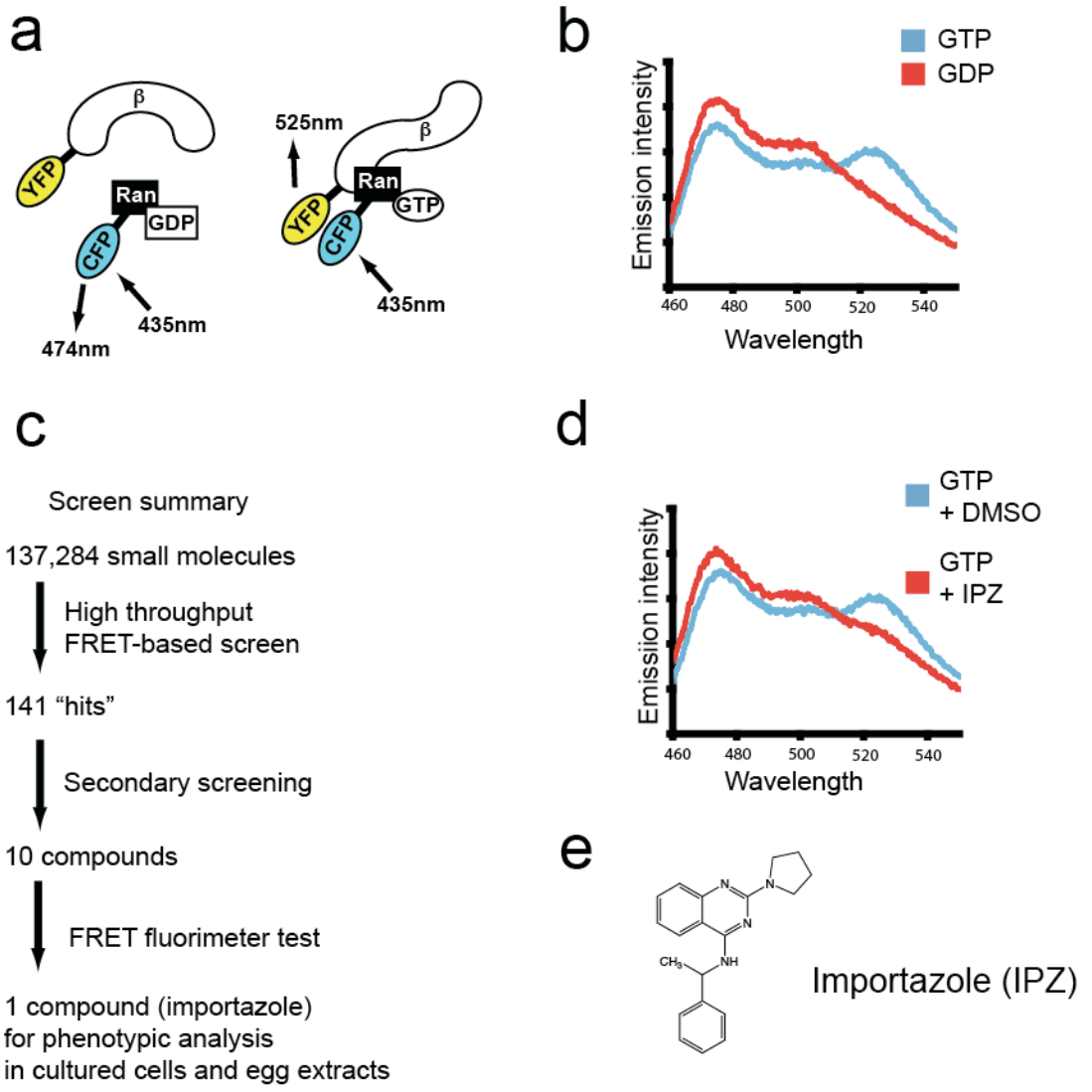

Figure 2.1: A high-throughput screen identifies importazole as an inhibitor of FRET between CFP-Ran and YFP-importin-β

(a) Schematic of the fusion proteins that bind and undergo FRET in the presence of Ran-GTP but not Ran-GDP.

(b) Fluorescence emission of the FRET pair detected between 460 nm and 550 nm following excitation at 435 nm, showing strong emission of CFP (475 nm) in the presence of GDP (red curve) that decreases in the presence of GTP (blue curve) concomitant with an increase at the emission wavelength of YFP (525 nm), indicative of FRET.

(c) Summary of the screen. Of 137,284 small molecules screened in duplicate using the FRET-based assay, 141 putative hits were subjected to three secondary screens designed to eliminate false positives. Of the 10 compounds remaining after the secondary screens, only a single compound reproducibly

diminished the FRET signal generated by CFP-Ran and YFP-importin-β in the original assay (d).
(e) The structure of importazole, a 2,4-diaminoquinazoline.

Figure 2.2

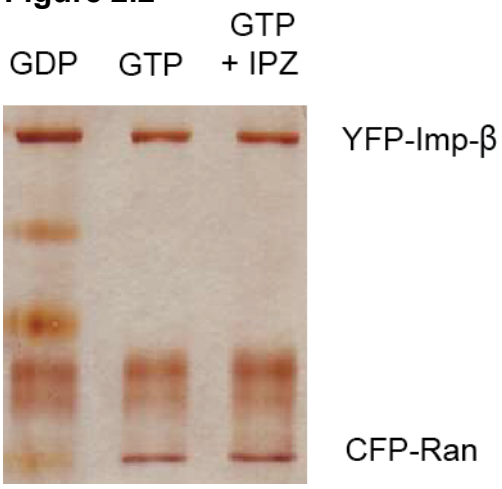

Figure 2.2: Importazole does not affect the ability of YFP-importin-β to pull down CFP-Ran in the presence of GTP
Pull down of CFP-Ran using YFP-importin-β in the presence of GDP, GTP, or GTP plus 200 μM importazole.

facilitate rapid data analysis, we developed software to generate color-coded plate maps to identify compounds that reduced the FRET ratio by both an increase in CFP emission *and* a decrease in YFP emission, thereby eliminating compounds that altered the FRET ratio by contributing their own fluorescence at wavelengths in the range of our probes (Figure 2.3).

In total, we screened 137,284 compounds in duplicate (Figure 2.1, panel c), and selected 141 "hits" for further analysis. Compounds that showed activity upon retesting in the original assay were analyzed in a unimolecular CFP and YFP FRET-based assay using a YIC sensor (Kalab et al., 2002) to confirm that the observed changes were not due to non-specific quenching or augmentation of either CFP or YFP emission. In a third assay, each compound was tested for its tendency to form aggregates that non-specifically inhibit β-lactamase (Feng and Shoichet, 2006). The 10 compounds that survived the secondary assays were obtained in larger quantities and tested again in the original CFP-Ran/YFP-importin-β FRET assay using a spectrofluorimeter. Only one of these compounds, a 2,4-diaminoquinazoline which we named "importazole", reproducibly disrupted the FRET signal generated by CFP-Ran and YFP-importin-β and was analyzed further (Figure 2.1, panels d and e).

Importazole binds importin-β *in vitro*

Although importazole blocked the FRET interaction between CFP-RanGTP and YFP-importin-β *in vitro*, it did not obviously affect the binding of the two proteins in pull-down assays (Figure 2.2). To begin elucidating the mechanism of importazole action, we tested whether importazole could alter the ability of importin-β to protect RanGTP from RanGAP-stimulated hydrolysis *in vitro* (Bischoff and Gorlich, 1997; Floer and Blobel, 1996). Binding curves calculated from these data do not indicate that importazole disrupts the RanGTP/importin-β interaction, and if anything, suggest that importazole may slightly stabilize the complex (Figure 2.4). The inability of importazole to disrupt the RanGTP/importin-β interaction is not entirely surprising considering the multiple large interaction surfaces between the two proteins (Lee et al., 2005). One possible explanation for the importazole-induced FRET change is that importazole binding causes a conformational change that disrupts the CFP-RanGTP/YFP-importin-β FRET interaction without preventing binding.

To test whether importazole binds to importin-β *in vitro*, we used a fluorescent thermal shift assay with the dye Sypro® Orange, since small molecule binding is expected to affect the thermal stability of a protein (Niesen et al., 2007). Importazole reduced the melting temperature of importin-β by 1.72+/-0.27 ^{o}C (Figure 2.5, panels a and b), but was unaffected by a related compound of comparable hydrophobicity that did not interfere with CFP-RanGTP/YFP-importin-β FRET (compound 3016, Figure 2.6, panels c and d, and data not shown). In contrast, importazole did not significantly affect the melting curves of related importin-β family members transportin and CRM1, or that of RanGTP, suggesting that importazole binds preferentially to importin-β (Figure 2.5, panel c, Figure 2.7). Going forward, a crystal structure of the RanGTP/importin-β

Figure 2.3

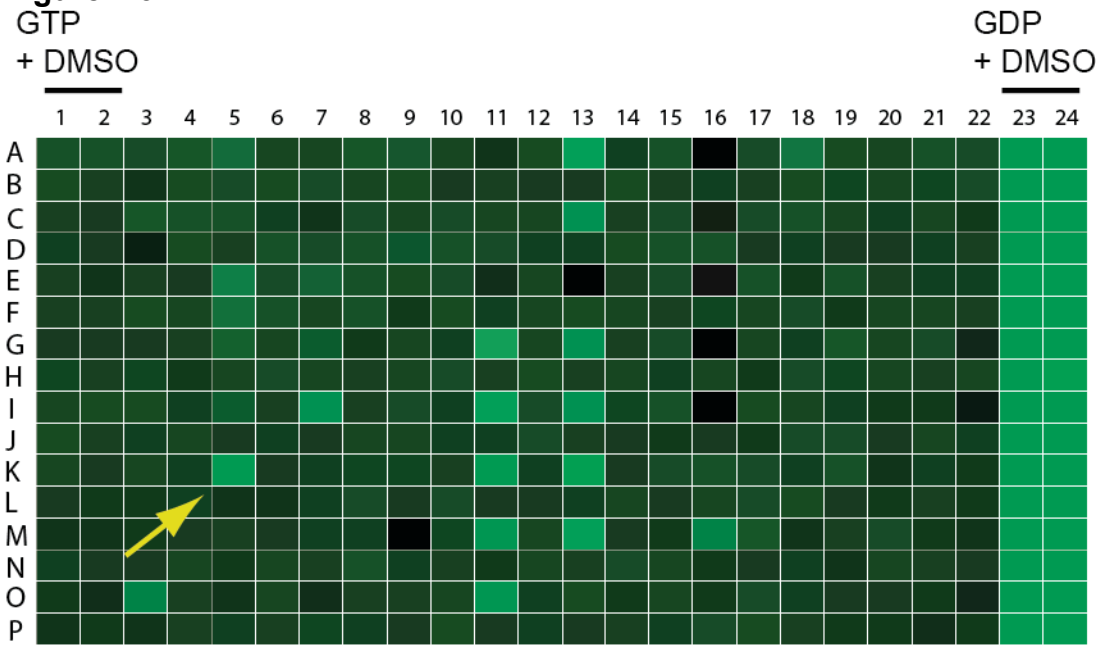

Figure 2.3: Heat map of a 384-well plate showing changes in FRET that monitor the interaction between CFP-Ran and YFP-importin-β

The green color represents I_{FRET}/I_{CFP}. Darker wells correspond to samples with a high I_{FRET}/I_{CFP} and lighter wells correspond to samples with a low I_{FRET}/I_{CFP}. Negative control wells occupy columns 1 and 2 (dark green). These wells include CFP-Ran, YFP- importin-β, GTP, and DMSO but no compound. Positive control wells occupy columns 23 and 24 (light green). These wells include CFP-Ran, YFP-importin-β, GDP, and DMSO but no compound. Wells in columns 3 through 22 include GTP plus compounds. The well marked with a yellow arrow showed a diminished FRET signal that was specifically due to a decrease in I_{FRET} and an increase in I_{CFP} as determined using our software, and thus was scored as a hit. Other light green wells in this plate were not scored as hits because they did not meet the criteria for a hit, which are listed in the materials and methods section.

Figure 2.4

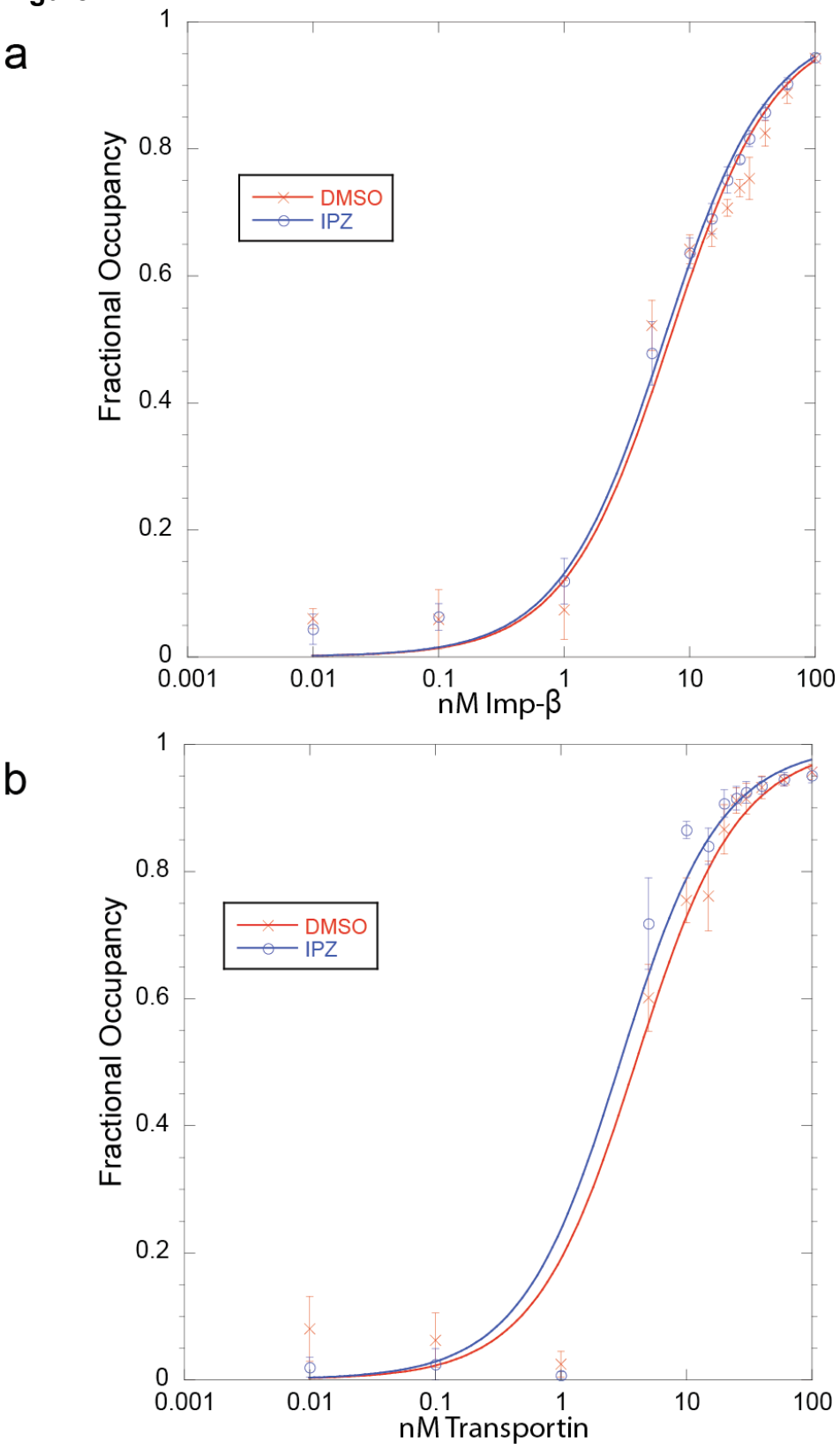
a
Fractional Occupancy
DMSO
IPZ
nM Imp-β
b
Fractional Occupancy
DMSO
IPZ
nM Transportin

Figure 2.4: Importazole does not destabilize the Ran/importin-β complex *in vitro*

(a) Fractional occupancy of the Ran/importin-β complex was determined via a RanGAP protection assay with increasing concentrations of importin-β in the presence of DMSO or importazole. For DMSO the K_d was estimated as 6.53 nM and for importazole the K_d was estimated as 5.86 nM.

(b) Fractional occupancy of the Ran/transportin complex with increasing concentrations of transportin in the presence of DMSO or importazole. For DMSO the K_d was estimated as 3.52 nM and for importazole the K_d was estimated as 2.51 nM.

Figure 2.5

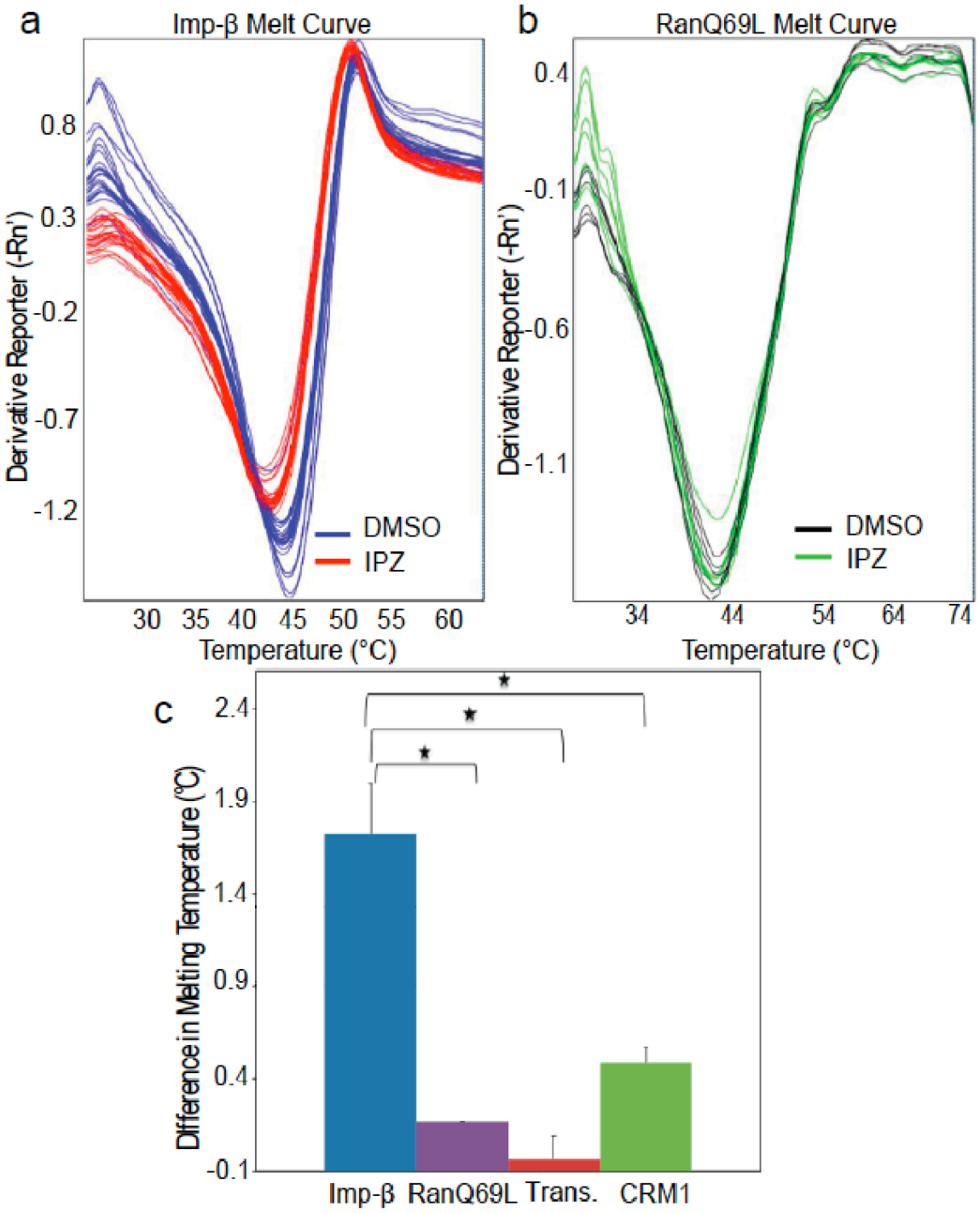

Figure 2.5: Importazole binds specifically to importin-β
(a) Negative first derivatives of melting curves of 2 μM importin-β in the presence of 50 μM importazole or DMSO where the minima indicate the melting temperature. Melting curves show the results from six experiments conducted in quadruplicate using the Applied Biosystems 7500 qPCR machine.

(b) Negative first derivatives of melting curves of 2 μM RanQ69L in the presence of 50 μM importazole or DMSO as control where the minima indicate the melting temperature.
(c) Mean changes in melting temperature of 2 μM importin-β, RanQ69L, transportin and CRM1 in the presence of 50 μM importazole. Error bars indicate standard error; asterisks denote statistical significance ($p < 0.01$).

Figure 2.6

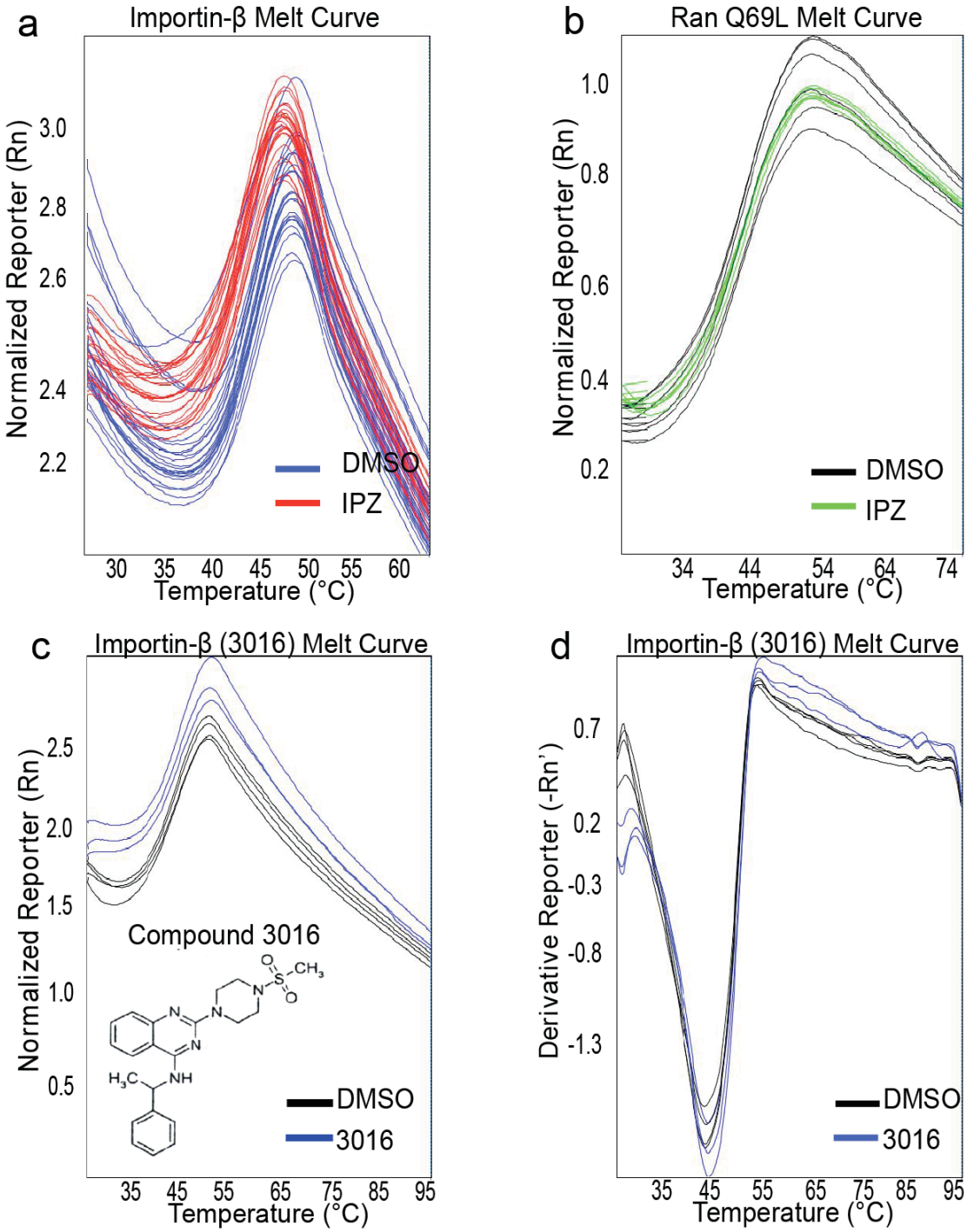

Figure 2.6: Importin-β melting temperature is unaffected by the importazole related compound 3016

(a) Melting curves of 2 μM importin-β in the presence of 50 μM importazole or DMSO.

(b) Melting curves of 2 μM RanQ69L in the presence of 50 μM importazole or DMSO.

(c) Melting curves of 2 μM importin-β in the presence of 50 μM compound 3016 or DMSO. The structure of compound 3016 is inset in (c). (d) Negative first derivatives of importin-β melting curves in the presence of compound 3016 or DMSO where the minima represent the melting temperature (Tm).

Figure 2.7

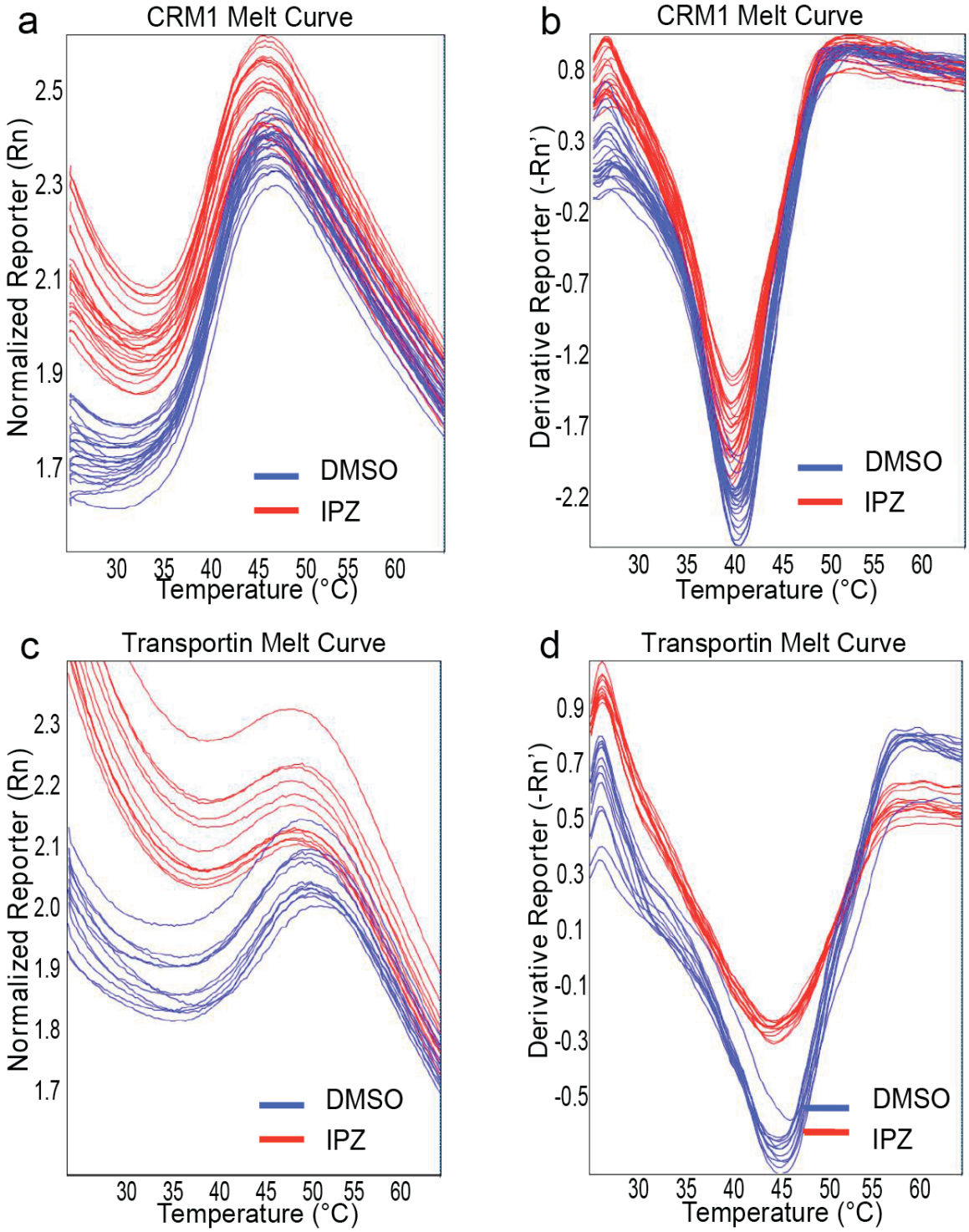

Figure 2.7: Analysis of importazole binding to transportin and CRM1
(a) Melting curves of 2 μM CRM1 (a) or 2 μM transportin (c) in the presence and absence of 50 μM importazole. Curves are the results from six experiments conducted in quadruplicate.

(b, d) Negative first derivatives of CRM1 or transportin melting curves, respectively, where the minima represent the melting temperature (Tm).

complex in the presence of importazole will likely be necessary to fully elucidate its biochemical mechanism of action.

Importazole disrupts importin-β/RanGTP-mediated nuclear import

If importazole binds importin-β and affects the RanGTP/importin-β interaction, it should inhibit the nuclear import of any protein bearing a classical NLS. We first tested this prediction using permeabilized HeLa cells, in which nuclear import of a GFP-NLS reporter can be reconstituted *in vitro* (Adam et al., 1990). Digitonin-permeabilized cells were incubated with a GFP-NLS reporter plus *Xenopus laevis* egg extracts as a source of soluble transport factors including Ran, importin-α, and importin-β. Whereas rapid nuclear accumulation of GFP-NLS occurred in the presence of the solvent DMSO, importazole blocked import and the reporter became enriched at the nuclear envelope, where RanGTP functions to induce cargo release from importin-β (Gorlich et al., 1996; Lowe et al., 2010) (Figure 2.8, panels a and b). In contrast, importazole did not block nuclear import mediated by transportin, an importin-β family member that utilizes the M9 import signal together with RanGTP to import hnRNP proteins (Figure 2.8, panel c) (Pollard et al., 1996).

To investigate whether importazole is cell permeable and active in living human cells, we generated a cell line that stably expresses a GFP-tagged version of the transcription factor NFAT, which shuttles between the nucleus and the cytoplasm in a calcium-regulated manner (Flanagan et al., 1991; Shibasaki et al., 1996) and is imported by importin-α/β and exported by CRM1 (Kehlenbach et al., 1998; Zhu and McKeon, 1999). At steady state NFAT is predominantly cytoplasmic. An increase in cytoplasmic calcium induced by the ionophore ionomycin leads to the accumulation of NFAT in the nucleus (Figure 2.9, panel a). NFAT import can be reverted upon ionophore withdrawal, (Figure 2.11, panel a) providing an inducible system ideal for testing the effects of importazole on importin-β-mediated nuclear import and CRM1-mediated nuclear export, both of which are dependent upon RanGTP.

Cells were pretreated with 40 μM importazole for 1 hour followed by 30 minutes of ionomycin treatment in the continued presence of importazole. Whereas control cells treated with DMSO or the control compound 3016 displayed a robust nuclear accumulation of the NFAT-GFP reporter after ionomycin addition, there was virtually no import of NFAT-GFP in importazole treated cells (Figure 2.9, panel b, quantified in panel c and Figure 2.10). Importazole displayed an IC_{50} of approximately 15 μM for inhibition of NFAT-GFP import (data not shown).

This effect was reversible upon importazole washout, which restored ionomycin-induced import of NFAT-GFP to near control levels (Figure 2.9, panels b and c). Thus, it should be possible to use importazole in drug-washout experiments to study the Ran/importin-β pathway in cells. The reversibility of importazole required 1 hour of recovery time between washing out the drug and adding ionomycin, and did not require new protein synthesis (data not shown).

To further assess the specificity of importazole, we tested its effects on CRM1-mediated export of NFAT-GFP. Export of NFAT-GFP occurred efficiently

Figure 2.8

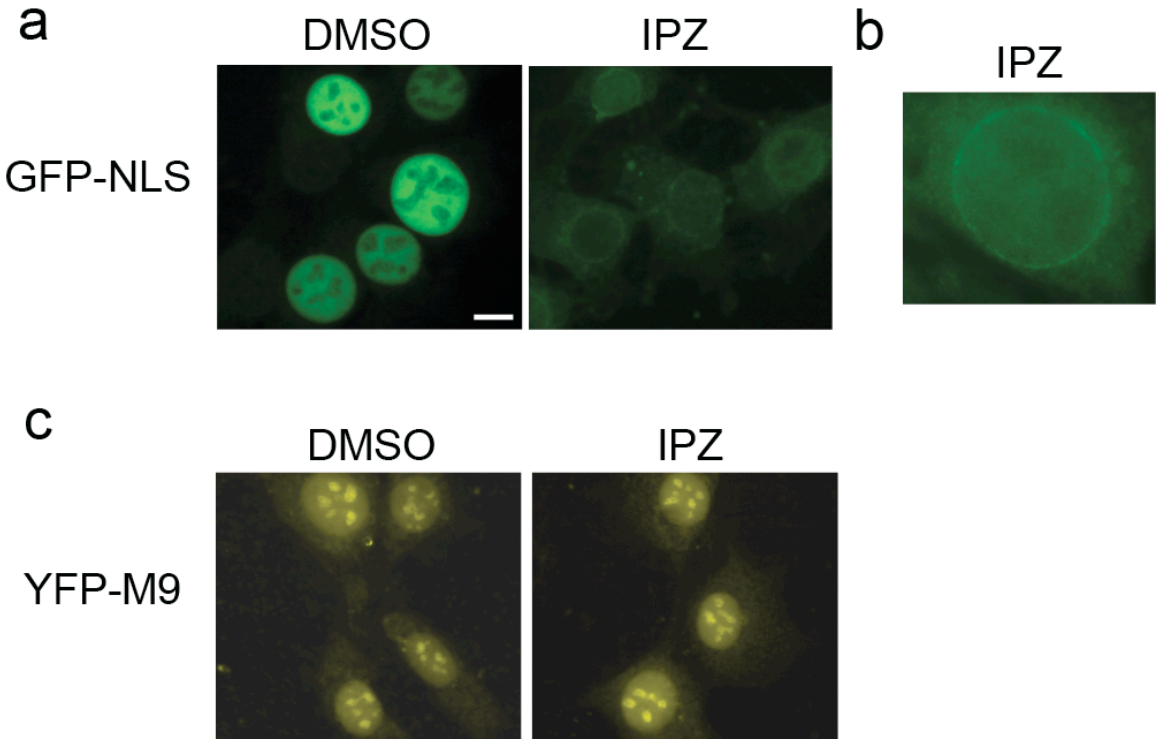

Figure 2.8: Importazole inhibits importin-β NLS-mediated nuclear import, but not transportin M9-mediated import

(a) NLS-GFP (importin-β import substrate) was added with *Xenopus* egg extract to permeabilized HeLa cells and assayed by fluorescence microscopy for nuclear import in the presence of DMSO or 100 μM importazole.
(b) NLS-GFP accumulation at the nuclear rim in the presence of importazole.
(c) M9-YFP (transportin import substrate) in the same assay. Scale bar = 10 μm.

Figure 2.9

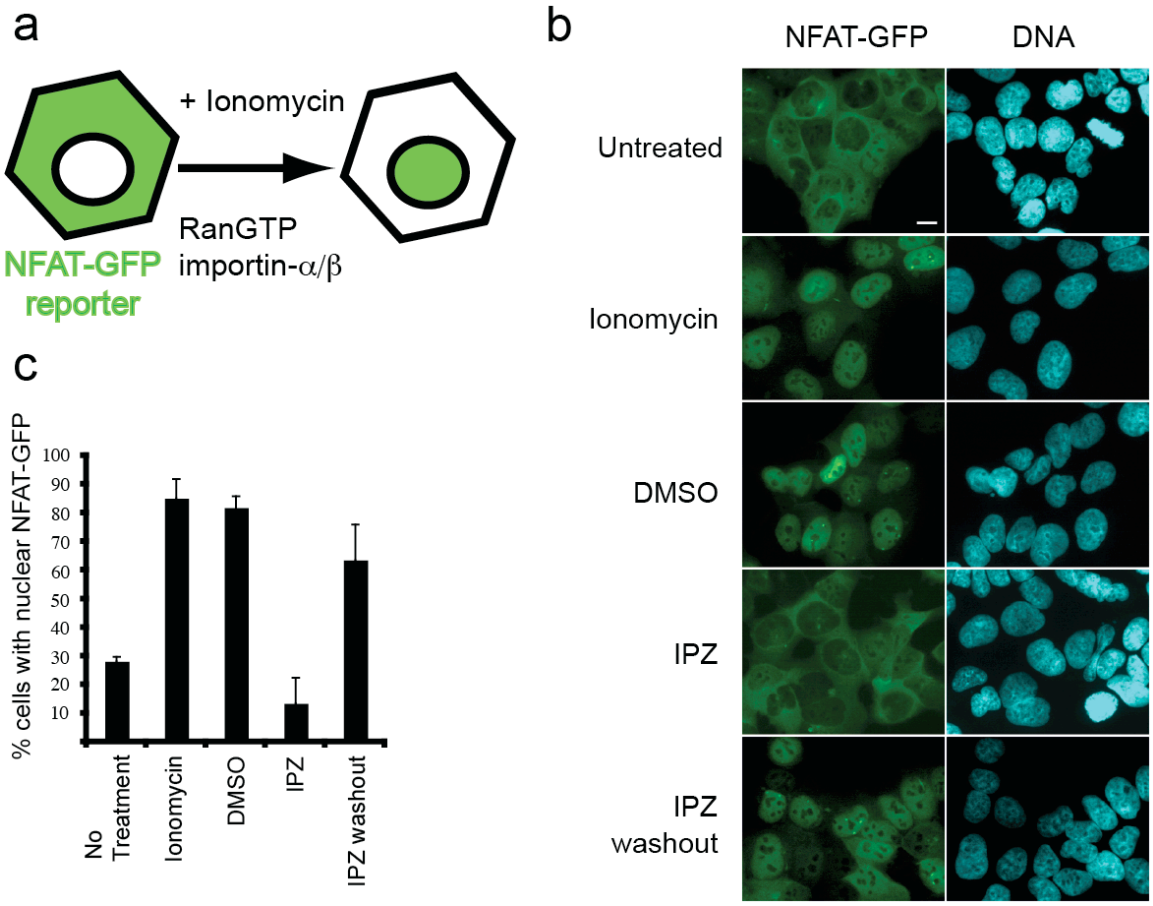

Figure 2.9: Importazole reversibly blocks importin-β-mediated nuclear import in living cells

(a) Schematic showing that the GFP-tagged, NLS-containing transcription factor NFAT enters the nucleus upon treatment with the ionophore ionomycin in a RanGTP and importin-β-dependent manner.

(b) HEK 293 cells stably expressing GFP-NFAT were treated with DMSO or 40 μM importazole for 1 hour prior to a 30 min treatment with ionomycin to induce nuclear import. Importazole was washed out and after 1 hour prior to ionomycin re-treatment. Scale bar = 10 μm.

(c) Results were quantified as the percentage of cells with nuclear NFAT-GFP. N=3, 100 or more cells counted under each condition. Bars represent standard error.

Figure 2.10

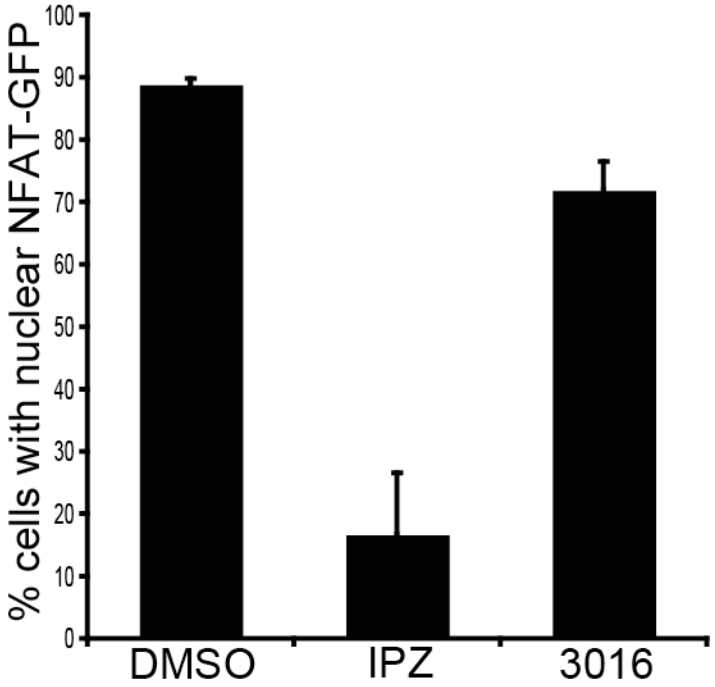

Figure 2.10: Compound 3016 does not block nuclear import in living cells
HEK 293 cells stably expressing GFP-NFAT were treated with DMSO, 20 μM importazole, or 20 μM compound 3016 for 1 hour prior to a 30 min treatment with ionomycin to induce nuclear import. Results were quantified as the percentage of cells with nuclear NFAT-GFP. N=3, 100 or more cells counted under each condition. Bars represent standard error.

Figure 2.11

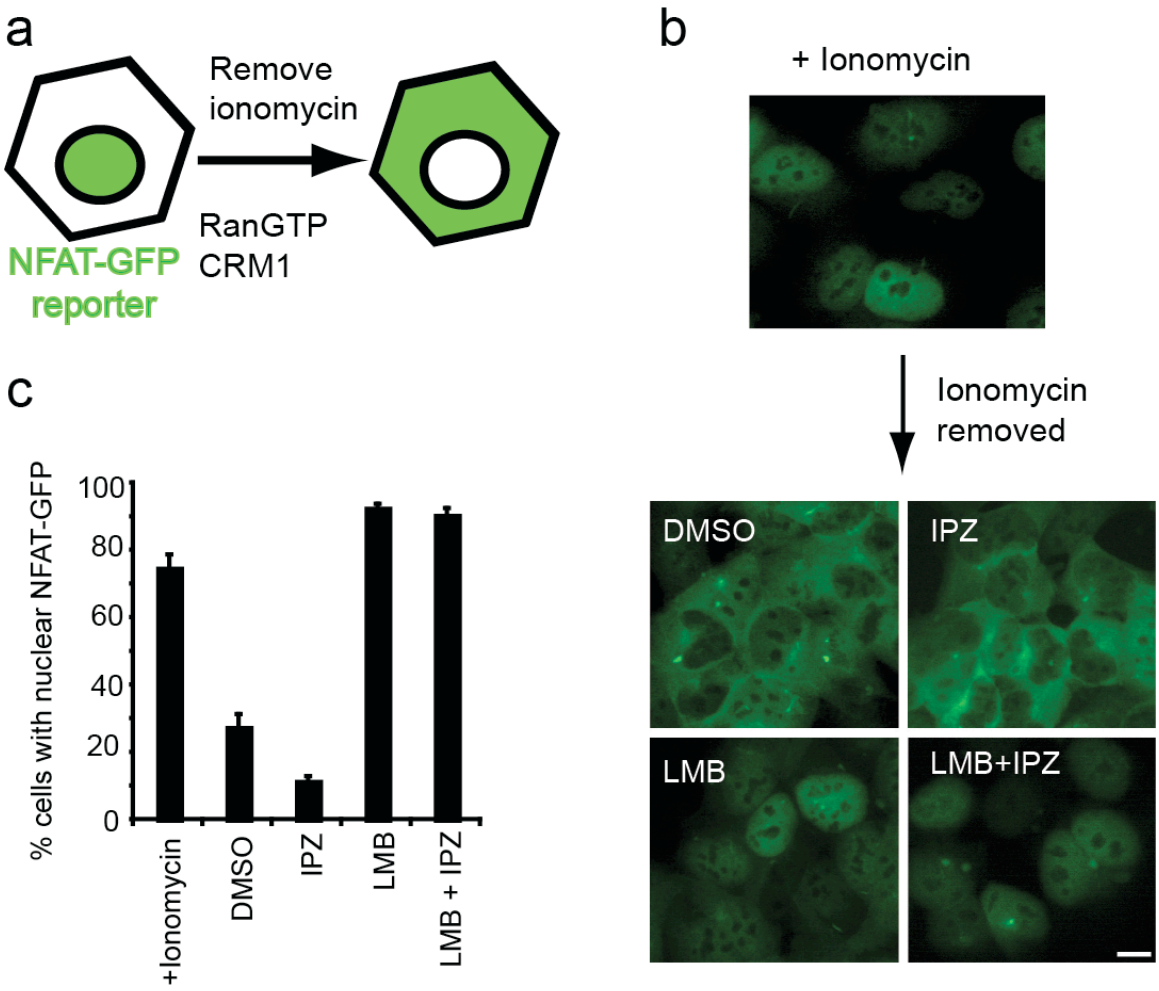

Figure 2.11: Importazole does not inhibit CRM1-mediated nuclear export
(a) Schematic illustrating that upon removal of the ionophore ionomycin, GFP-NFAT exits the nucleus in a RanGTP and CRM1-dependent manner.
(b) Cells were treated with ionomycin to induce nuclear import of NFAT-GFP, then washed and treated with DMSO, importazole, leptomycin B, or importazole + leptomycin B for 1 hour. Scale bar = 10 μm.
(c) Results were quantified as the percentage of cells with nuclear NFAT-GFP. N=3, 100 or more cells counted under each condition. Bars represent standard error.

in the presence or absence of importazole, but was blocked by leptomycin B, a specific CRM1 inhibitor (Nishi et al., 1994) (Figure 2.11 panel b, quantified in panel c). Importantly, when cells were treated with both leptomycin B and importazole upon ionomycin washout, NFAT-GFP was still restricted to the nucleus (Figure 2.11, panels b and c), confirming that importazole treatment does not non-specifically damage the nuclear envelope allowing proteins to leak out into the cytoplasm. Consistent with the concentration of importazole sufficient to impair nuclear import, we found that importazole has an IC_{50} of approximately 22.5 μM in HeLa cells following treatment over a 24-hour period (Figure 2.12). Taken together our nuclear import experiments indicate that importazole is likely specific for importin-β-mediated protein import. Although we have not tested importazole's effect on all importin-β family members, no effect on transportin-mediated import or CRM1-mediated export was detected. Furthermore, these results also suggest that importazole does not impair RCC1-dependent loading of Ran with GTP or the function of RanGTP itself since the export function of CRM1 critically depends on the formation and function of RanGTP.

Importazole blocks spindle assembly in *Xenopus* egg extracts, but does not affect pure microtubules

A specific inhibitor of importin-β/RanGTP should also disrupt mitosis. We first tested importazole in metaphase-arrested *Xenopus* egg extracts, which rely heavily on a RanGTP gradient for spindle assembly around sperm chromosomes. Addition of 100 μM importazole, but not the solvent DMSO, strongly inhibited spindle assembly, preventing normal bipolar microtubule structures from forming around 80% of sperm nuclei (Figure 2.13, panels a and b). The effect was similar to that of adding a truncated importin-β (amino acids 71-876), a version that no longer binds to RanGTP and therefore sequesters its cargoes (Chi et al., 1997). Although importazole significantly weakened spindle microtubule density, it was not a general microtubule inhibitor, since it did not impair the formation of microtubule asters in the extract induced by the microtubule stabilizing agent DMSO (Figure 2.13, panels c and d) or affect the polymerization of pure microtubules, in contrast to nocodazole (Figure 2.13, panel e). Thus, importazole caused dramatic effects on spindle assembly consistent with the known role of the importin-β /RanGTP pathway in the *Xenopus* egg extract system, and is not a general microtubule inhibitor.

Importazole impairs mitotic cargo release and reveals novel functions for the importin-β/RanGTP pathway in human cells

A major advantage of a cell-permeable importin-β/RanGTP inhibitor is its potential for dissecting novel roles of this pathway in dividing human cells, which also provide a system to analyze mitotic gradients of released cargos using FRET probes (Kalab et al., 2006). If importazole disrupts the interaction of importin-β with RanGTP, then the chromatin-localized FRET gradient of the cargo probe Rango should be reduced, since it undergoes FRET when released from importin-β in HeLa cells (Kalab et al., 2006). As predicted, the difference in

Figure 2.12

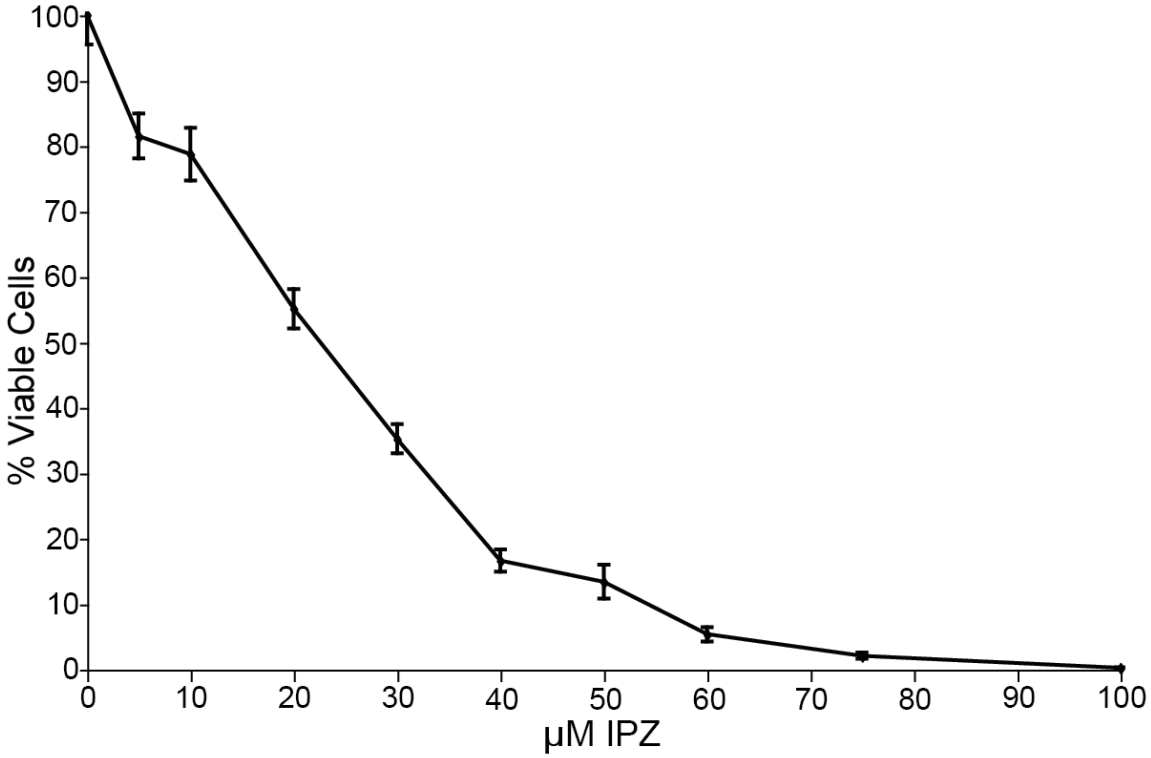

Figure 2.12: Importazole affects HeLa cell viability
HeLa cells were treated with the carrier DMSO or varying concentrations of importazole over a period of 24 hours, and the percentage of viable cells remaining was determined using the CellTiter-Glo assay from Promega. The percentage of viable cells was normalized to the number of cells remaining following DMSO treatment alone. The IC_{50} of importazole treatment for cell viability was determined to be 22.5 μM. The curve represents the results of three independent experiments performed in quadruplicate.

Figure 2.13

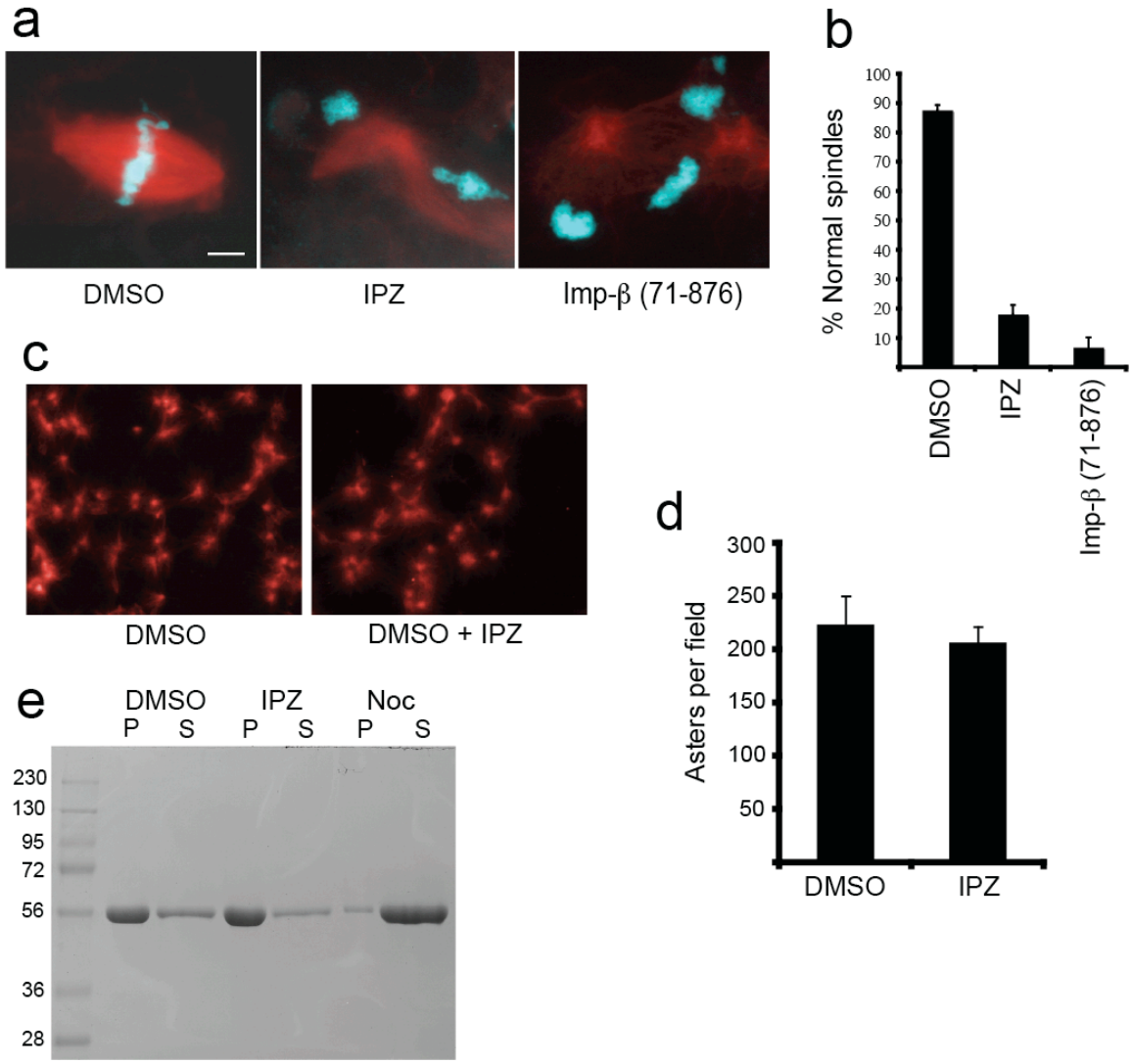

Figure 2.13: Importazole impairs spindle assembly in *Xenopus* egg extracts but does not affect pure microtubule polymerization

(a) Spindle assembly reactions containing X-rhodamine labeled tubulin in the presence of DMSO, 100 μM importazole, or a truncated form of importin-β that is unable to bind to RanGTP. Microtubules are red and DNA is blue. Scale bar = 10 μm.

(b) Quantification of the percentage of normal spindle structures. N=3, 100 structures counted under each condition. Bars represent standard error.

(c) Aster assembly induced by addition of 5% DMSO to extracts containing X-rhodamine labeled tubulin in the presence of DMSO or importazole.

(d) Quantification of the number of asters per field. 10 fields were counted under each condition.

(e) DMSO induced pure tubulin polymerization assay. Reactions were supplemented with additional DMSO, importazole, or nocodazole, and microtubules pelleted through a sucrose cushion and samples from the pellet (P) and supernatant (S) analyzed by SDS PAGE.

fluorescence lifetime of the donor GFP of the Rango-3 probe between the chromosomes and distal cytoplasm was significantly reduced in the presence of importazole compared to controls, from an average of 0.12 +/- 0.4 ns to 0.07+/- 0.03 ns due to reduced FRET (Figure 2.14, p-value: 1.3×10^{-7}). Thus, importazole impairs mitotic importin-β cargo release in HeLa cells.

To examine the consequences of importazole on mitosis, HeLa cells treated for one hour were fixed and stained for tubulin and chromosomes. Control metaphase figures displayed robust spindles with a mean area of 105 μm^2, and were centrally located within the cell with chromosomes aligned on the metaphase plate (Figure 2.15, panels a and d). Importazole treatment caused dose-dependent defects in spindle assembly, chromosome alignment, and spindle size (Figure 2.15). Interestingly, importazole also led to spindle positioning defects, with more than 40% of the cells displaying off-center spindles (Figure 2.15, panels a and b). Spindle positioning was not previously attributed to the Ran pathway and this phenotype may be a consequence of astral microtubule disruption by importazole (data not shown). Previous studies have most likely not revealed this role of the Ran pathway in mitosis because they were performed in cell free systems such as *Xenopus* extract where spindle positioning could not be assessed. The discovery of this spindle misalignment phenotype demonstrates the importance of importazole as a tool to study the Ran pathway in mitosis.

The Ran pathway members Ran and importin-β are highly conserved, and an inhibitor of the RanGTP/importin-β interaction may have considerable value as a research tool across multiple species. Additionally, as the Ran pathway has been shown to be upregulated in some forms of cancer (Xia et al., 2008), importazole may have some potential as a therapeutic compound. Development of more potent, related compounds should allow a more complete disruption of the Ran/importin-β interaction as well as limit any possible non-specific effects of compound treatment, further increasing the value of these inhibitors in both the academic and medical fields. Overall, we have shown importazole to be an effective inhibitor of the Ran/importin-β interaction *in vitro* and in cells with great potential for future use as a tool to study the Ran pathway in mitosis.

Figure 2.14

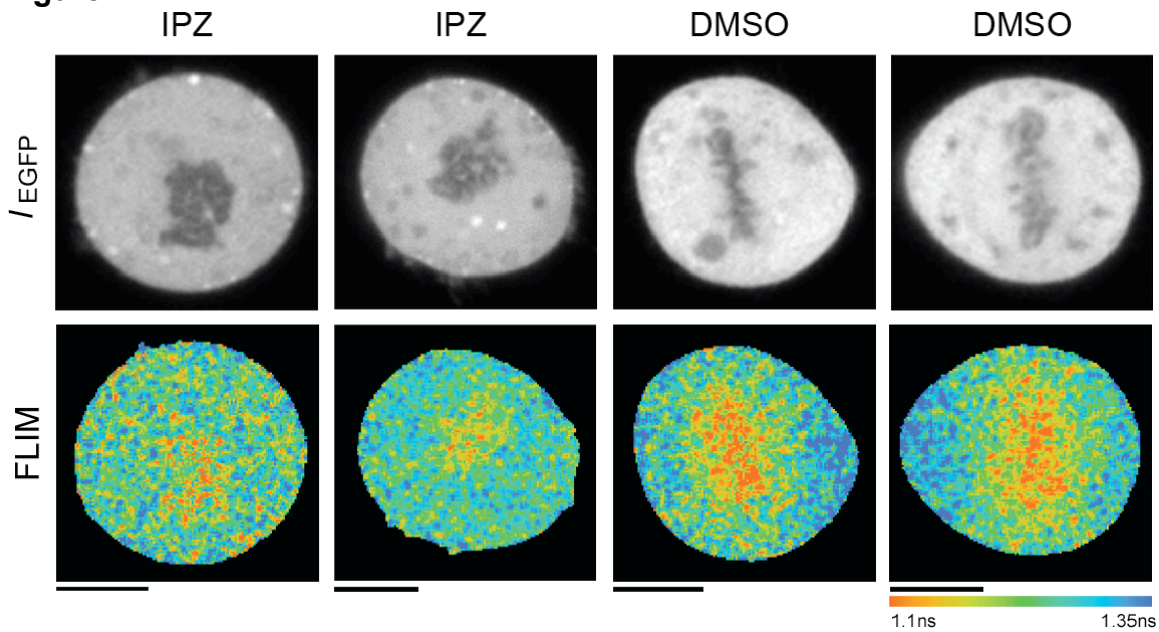

Figure 2.14: Importazole disrupts mitotic cargo release monitored by the FRET probe Rango

Donor fluorescence (top panels) and pseudo-colored FLIM images (bottom panels) of mitotic HeLa cells expressing the Rango-3 FRET sensor. Rango-3 displays a greater fluorescence lifetime around the chromosomes of cells treated with importazole compared to that of cells treated with DMSO, resulting from importazole's disruption of sensor release from importin-β. N=3, 30 cells counted for each condition. Scale bars = 10 μm.

Figure 2.15

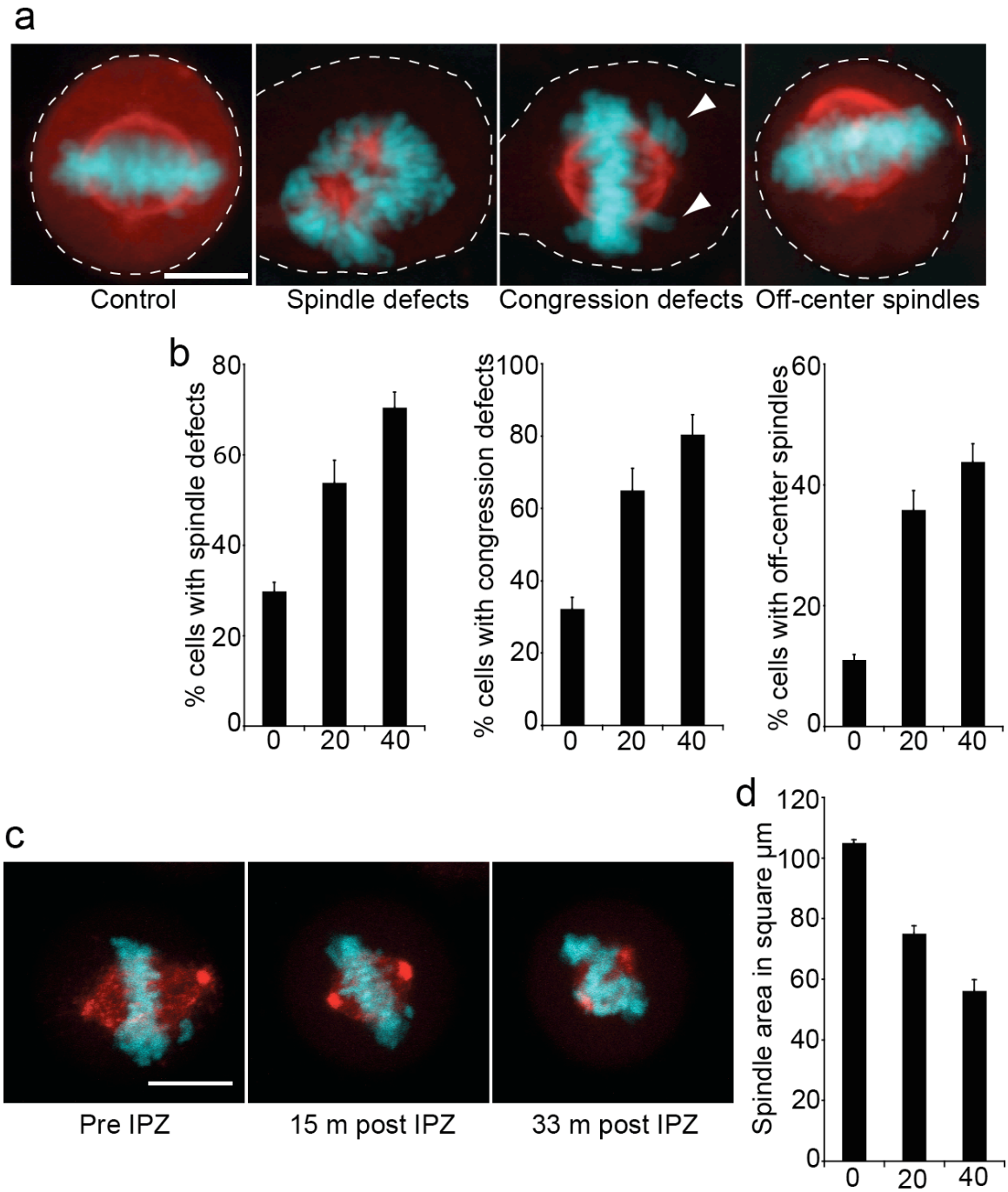

Figure 2.15: Importazole disrupts mitotic spindles in living HeLa cells
(a) Asynchronously growing cultures were treated with DMSO or importazole for 1 hour prior to fixation and staining for DNA (blue) and tubulin (red). Note defects including chromosome congression (white arrowheads point to misaligned chromosomes) and spindle positioning upon importazole treatment. Dashed white lines indicate cell boundaries. Scale bars = 10 μm.

(b) Quantification of spindle defects in cells treated with DMSO, 20 μM importazole, or 40 μM importazole. N=5. In each case, 100 metaphase cells were counted and the fraction of those displaying defects were scored.
(c) Time-lapse fluorescence microscopy of a metaphase HeLa cell treated with 50 μM importazole. Frames were captured every 3 minutes.
(d) Asynchronous HeLa cells were treated with 0 to 40 μM importazole for 1 hour prior to fixation, and the size of the spindle in mitotic cells was measured. N=4, 100 metaphase spindles were measured per condition. Bars represent standard error.

Materials and Methods

Protein expression and purification

pET30a-derived constructs encoding importin-β with an N-terminal YFP fusion (pKW1532), a CFP-Ran fusion (pKW1543), and importin-β (pKW485) were transformed into BL21 cells (Invitrogen). Additionally, pQE32-derived Ran constructs (pKW356 [WT Ran], pKW 590 [RanQ69L]), a pQE9-derived CRM1 construct (pKW812), and a pQE60-derived transportin construct (pKW738) were transformed in to SG13 cells. All constructs were induced with IPTG at room temperature. Harvested cells were lysed using a French press. Fusion proteins were purified with Ni NTA resin using a standard protocol followed by gel filtration. RCC1 was purified as described previously (Azuma et al., 1996).

FRET assay

The following reaction buffer was used for all FRET assays, including the high-throughput screen: 1X PBS, 5 % glycerol, 2 mM $MgCl_2$, 1 mM DTT, 0.01 % NP-40. For standard CFP-Ran/YFP-importin-β FRET assays, 50 – 100 nM CFP-Ran mixed with 20 nM RCC1 and 200 μM GDP or 200 μM GTP was immediately followed by addition of 50 – 100 nM YFP-importin-β. The reaction was excited using a Fluorolog 3 spectrofluorometer with 435 nm fluorescence and the emission was read between 460 nm and 550 nm. For the high-throughput screen, the concentrations of reaction components were as follows: CFP-Ran: 62.5 nM; YFP-importin-β: 62.5 nM; GTP or GDP: 200 μM; RCC1: 20 nM

The high-throughput screen

The screen was carried out in collaboration with the Small Molecule Discovery Center (SMDC) at the University of California, San Francisco. Compounds were from ChemBridge, ChemDiv, SPECS, ChemRX, and Microsource. The complete content of this library can be found through the Small Molecule Discover Center website (http://smdc.ucsf.edu/). The software used to analyze the screening data is available upon request.

In the first step of the screen, compound dilution plates were made using a Multimek liquid handler and a Wellmate bulk dispenser by transferring 5 μl of compounds from stock plates into 384-well dilution plates (Corning, polypropylene, square wells). A bulk dispenser (Wellmate) was then used to transfer 45 μl of 2.77% DMSO (diluted with reaction buffer). This yielded a compound concentration of 100 μM and a DMSO concentration of 12.5 %. In the second step, the Multimek liquid handler was used to transfer 5 μl of solution from the dilution plates into the 384-well assay plates (Greiner, black, flat bottom). Next, the Wellmate bulk dispenser was used to transfer 20 μl of a solution containing CFP-Ran, RCC1, and GTP (diluted in reaction buffer) on top of the diluted compounds in the 384-well assay plates. This step yielded the following concentrations for each reaction component: CFP-Ran: 125 μM, RCC1: 40 nM, GTP: 400 μM, DMSO: 2.5%, and compound: 20 μM. The Wellmate bulk dispenser was then used to add 25 μl of diluted YFP-importin-β to each well in

the assay plates. This step yielded the following final concentrations for each reaction component: CFP-Ran: 62.5 μM, YFP-importin-β: 62.5 μM, RCC1: 20 μM, GTP: 200 μM, DMSO: 1.25% and compound: 10 μM.

Each assay plate included 32 negative control wells (containing the GTP reaction + 1.25% DMSO) and 32 positive control wells (containing the GDP reaction). These control wells were used to set the maximum and minimum fluorescence values for each plate individually. Each compound was tested in duplicate.

In the next step the assay plates were loaded into the Analyst AD plate reader. Each well was excited with 435 nm fluorescence and emission was detected both at 475 nm (CFP) and 525 nm (YFP).

Because our high throughput screen generated a large amount of data, we designed our own software package using Perl to analyze it. Text files generated by the Analyst AD included raw fluorescence values at 475 nm and 525 nm for each well in a 384-well plate. As mentioned above, each plate included 32 negative control wells (containing the GTP mixture + 1.25% DMSO) and 32 positive control wells (containing the GDP mixture + 1.25% DMSO). Data were processed by our program in the following manner.

Positive control averages and standard deviations for the individual I_{CFP} and I_{FRET} emission values (475 nm and 525 nm respectively) were calculated using all 32 positive control wells. Similarly, the FRET ratio for each positive control well (I_{FRET}/I_{CFP}) was calculated and these values were used to generate an average I_{FRET}/I_{CFP} value and the standard deviation. The same calculations were performed using data from the negative control wells. Thus for each plate in the screen, our program calculated positive and negative control values that were used to set the maximum and minimum fluorescence intensities with which all other wells in the plate were compared. This allowed us to remove many fluorescent compounds that interfered with CFP or YFP fluorescence indirectly causing excessively high or low emission readings.

In the next step, fluorescence values from each well in the plate were compared to both the average positive control value and the average negative control value and their corresponding standard deviations, which were used to make error bars. Wells were removed from further consideration if:

1. I_{FRET} was greater than that of the negative control average plus three standard deviations.
2. I_{FRET} was less than that of the positive control average plus three standard deviations.
3. I_{CFP} was greater than that of the negative control average plus three standard deviations.
4. I_{CFP} was less than that of the positive control average plus three standard deviations.
5. I_{FRET}/I_{CFP} was either less than the average I_{FRET}/I_{CFP} value plus three standard deviations for the positive control wells, or greater than the average I_{FRET}/I_{CFP} value plus three standard deviations for the negative control wells.
6. I_{FRET}/I_{CFP} was not less than the average I_{FRET}/I_{CFP} value plus one standard deviation for the positive control wells. These compounds were considered to

have no measurable effect on the interaction between CFP-Ran and importin-β because they did not affect I_{FRET}/I_{CFP}. Some of these compounds were fluorescent (based on the emission intensities in the CFP and YFP channels) and were discarded as interfering compounds.

A compound was considered a "hit" and kept for further analysis if it satisfied all three of the following criteria:

1. It reproducibly (n = 2) reduced I_{FRET}/I_{CFP} to a level in between the positive control average value minus two standard deviations and the negative control average value minus two standard deviations.
2. It reproducibly (n = 2) reduced the I_{FRET} value to a level in between the negative control average value minus two standard deviations and the positive control average value minus two standard deviations.
3. It reproducibly increased the I_{CFP} value to a level in between the positive control average value plus one standard deviation and the negative control average value plus one standard deviation.

Secondary screening

141 hit compounds from the primary screen were tested for non-specific effects on fluorescence with FRET probe YIC that contains the importin-β-binding domain of importin-α flanked by CFP and YFP. When unbound in solution, this probe undergoes intramolecular FRET (Kalab et al., 2002). In the second assay, we tested our 141 hits for nonspecific inhibition due to aggregation using a β-lactamase-based assay as described (Feng and Shoichet, 2006). Importazole was found to be soluble up to approximately 100 μM in water. Additionally, importazole was characterized by mass spectrometry and NMR to confirm its identity and purity.

Fluoresecent thermal shift assay

Experiments were performed using Applied Biosystems StepOnePlus™ Real-Time PCR (RT-PCR) System as previously described (Niesen et al., 2007; Uniewicz et al., 2010). Protein stocks were diluted in PBS and added 70% v/v to a Microamp® Fast 96-well Reaction Plate and maintained on ice. Compounds (importazole and control compound 3016) were then added at 30% v/v in 3% DMSO. Freshly prepared 100X water based-dilution of Sypro® Orange Protein Gel Stain was then added at 1% v/v to reach a final reaction volume of 20 µl. Samples were mixed by gentle pipetting. After sealing the plates with Microamp™ Optical Adhesive Film, the plate was subjected to a heating cycle composed of a 10 sec prewarming step at 25°C and a gradient between 25°C and 95°C with a 0.3°C ramp. Data was analyzed using the StepOnePlus™Software v2.1.

Cell lines and tissue culture

A GFP-NFAT expression plasmid (pKW520) was generated by inserting a BamH I/Hind III-cleaved NFATC1 cDNA fragment into pEGFP-C1 (Clontech) digested with Bgl II and Hind III. The plasmid was a gift of K. Reif. The construct

was stably transfected into HEK 293 cells and a single clone expressing moderate levels of NFAT-GFP was selected and maintained in Opti-mem media (Gibco) plus 4 % fetal bovine serum, 1 % penicillin/streptomycin, and 200 μg/ml G418. HeLa cells were grown and maintained according to standard protocols.

Nuclear import with permeabilized HeLa cells

HeLa cells were permeabilized and treated with an import reporter and cytosol from *Xenopus laevis* oocytes as described previously (Adam et al., 1990).

NFAT-GFP nuclear import and export

For all import and export experiments, HEK 293 cells stably expressing NFAT-GFP were grown on glass coverslips to approximately 50% confluency prior to drug treatment. In all cases, importazole was used at 40 μM and leptomycin B was used at 10 ng/ml. For controls, DMSO was used at a concentration of 0.4%. Ionomycin was added at 1.25 μM. Importazole and leptomycin B treatments were all for 1 hour. In all experiments cells were fixed with 4% formaldehyde prior to fluorescence microscopy. DNA was visualized with 1 μg/ml Hoechst dye. For quantification, 100 cells from each condition were analyzed and the percentage that showed nuclear accumulation of NFAT-GFP calculated.

***In vitro* microtubule polymerization and spindle assembly**

Xenopus laevis egg extracts were prepared as described (Hannak and Heald, 2006). For *in vitro* spindle assembly, *Xenopus laevis* sperm DNA was added to egg extracts supplemented with rhodamine-labeled tubulin. Asters were formed by addition of 5% DMSO. DNA was stained with Hoechst dye. The formation of microtubule-based structures was assessed using epifluorescence microscopy after a 30 minute room temperature incubation. *In vitro* microtubule polymerization and pelleting assays were performed by incubating 25 μM bovine tubulin, 1 mM GTP, and 5% DMSO in BRB80 buffer (80 mM PIPES, 1 mM $MgCl_2$, 1 mM EGTA, pH 6.8) at 37ºC for 30 minutes. Polymerized microtubules were pelleted through a sucrose cushion, resuspended, and analyzed by SDS PAGE.

Fluorescence lifetime imaging microscopy (FLIM)

The Rango-3 FRET sensor is an improved version of Rango and was created by replacing Cerulean-EYFP donor-acceptor pair in Rango (Kalab et al., 2006) with EGFP as a donor and non-fluorescent acceptor sREACh (Murakoshi et al., 2008) which was modified by the introduction of mild dimerization mutations. Time-correlated single photon counting (TCSPC) datasets were acquired with a Plan-Apochromat 63x/1.40 NA oil immersion lens on an inverted Zeiss LSM710 NLO microscope equipped with a Becker & Hickl SPC-830 TCSPC controller. Samples were excited by one-photon 485nm pulses generated by a frequency doubling 970nm 80MHz Ti:Sapphire laser (Coherent MiraSHG). The emission was collected from a custom side port, filtered through a 525 nm bandpass filter (ET525/50 Chroma) and detected by a HPM-100-40

module (Becker & Hickl) containing a hybrid Hamamatsu R10467-40 GaAsP photomultiplier. Two to three days before the experiment, HeLa cells were transfected with a pSG8 plasmid containing the Rango-3 open reading frame (pK135) to induce sensor expression. Treatment with importazole or DMSO was started one hour before imaging and continued for up to one hour in an environmental chamber built on the microscope (37°C, 5% CO_2). Recording conditions were chosen to limit emission to approx 1-2x10^6 counts per second, and images of 128 x 128 pixels (1024 time bins/pixel) were averaged over 60 seconds. Fluorescence lifetime images were produced and analyzed using SPCI software (Becker & Hickl).

Immunofluorescence microscopy

Cells were fixed in 4% formaldehyde and 0.1% glutaraldehyde in PHEM (60 mM PIPES, 25 mM HEPES, 10 mM EGTA, 2 mM $MgSO_4$) at 37ºC for 15 minutes followed by permeabilization with 0.1% triton X-100 for 2 minutes at room temperature. Cells were then washed and blocked (PHEM + 5% FBS + 0.2% saponin) and stained by standard techniques using the E7-A anti β tubulin antibody (Developmental Studies Hybridoma Bank) diluted 1:1000 and Hoechst dye.

Pulldowns to detect interaction between CFP-Ran and YFP-importin-β

All reactions were performed in buffer consisting of PBS + 2 mM $MgCl_2$, 5% glycerol, 0.01% NP-40, and 1.0 mM DTT. Reaction buffer was combined with the following components in this order: CFP-Ran, RCC1, BSA, GDP or GTP, importazole or 100% DMSO, and YFP-importin-β, yielding the following final concentrations: CFP-Ran: 2.5 nM, RCC1: 20 nM, BSA: 0.1 mg/ml, GDP or GTP: 200 μM, importazole: 200 μM, YFP-importin-β: 5.0 nM. Reactions were incubated for 10 min at room temperature, 20.0 μl of S-protein agarose was added, and then incubated for an additional 30 min on a rotator before pelleting the agarose at 3,000 rpm for 1 min. The supernatant was removed followed by three washes with 500 μl reaction buffer. The S-protein pellet was resuspended in 15 μl of SDS PAGE sample buffer and boiled briefly. After spinning down the S-protein pellet, 10 μl of the sample was analyzed by SDS PAGE.

HeLa cell viability assay to obtain an IC_{50}

10,000 actively growing HeLa cells per well were transferred to opaque white 96 well tissue culture plates at a final volume of 100 µl per well in DMEM plus 4% fetal bovine serum and 1% penicillin/streptomycin. Cells were allowed to grow at 37ºC for 24 hours. Individual wells were then treated for 12 hours with one of the following conditions: 1% DMSO, 5, 10, 20, 30, 40, 50, 60, 75, 100 µM IPZ. Following this treatment, the media was replaced and cells were treated for another 12 hours under the same conditions. The plates were then allowed to equilibrate to room temperature for 30 min, after which 100 µl of room temperature CellTiter-Glo reagent from the Promega CellTiter-Glo Luminescent Cell Viability Assay kit was added to each well. Plates were shaken for 2 min, incubated at room temperature for 10 min, then read on a luminometer. The

average background signal for the plate was subtracted from the value of each individual well, and the resulting values were normalized to the signal level of the DMSO containing well.

RanGAP protection assay

All steps were performed in buffer containing 50 mM HEPES pH 7.6 with 2.5 mM $MgCl_2$. Loading the Ran with GTP: 40 nM Biotin labeled RCC1 was bound to streptavidin agarose resin for 30 min rotating at 4°C. The Biotin labeled RCC1 was a gift of D. Halpin. The beads were washed with fresh buffer to remove any free RCC1, and 16 µM nucleotide free Ran and 51 µM $GTP\gamma P^{32}$ were added and Ran was allowed to load for 30 min at room temperature. The beads were then removed using a spin column, and the remaining supernatant was filtered through a Sephadex G-50 column to remove free $GTP\gamma P^{32}$. The loaded Ran was then diluted to 1.6 µM for further use. Performing the assay: All reactions were performed in a final volume of 200 µL and in buffer containing 50 mM HEPES pH 7.6 with 2.5 mM $MgCl_2$. Importin-β was pre-incubated with either 0.5% DMSO or 50 µM importazole in 0.5% DMSO and 100 nM $RanGTP\gamma P^{32}$ at room temperature. 1 µM RanGAP was added to start each reaction, and the reaction was allowed to proceed for 5 min before the reaction was stopped using 1 ml of a solution containing 7% charcoal, 10% ethanol, 0.1 M HCl, and 10 mM KH_2PO_4. The resulting solution was spun at 10,000 RPM for 2 min in a tabletop centrifuge to pellet the charcoal, and the resulting supernatant was removed and counted for three min per sample in a liquid scintillation counter.

Chapter 3:

Efforts to Improve Importazole

Background

Studying the RanGTP/importin-β pathway in mitosis presents a variety of challenges. Ran's involvement in essential processes throughout the cell cycle such as nucleocytoplasmic transport and nuclear envelope dynamics makes studying the Ran pathway's involvement in mitosis difficult when employing traditional means such as genetics or RNAi (Clarke and Zhang, 2004; Goodman and Zheng, 2006; Pemberton and Paschal, 2005; Terry et al., 2007). To overcome this problem, we previously employed a small molecule inhibitor based approach and identified the compound importazole, which enabled us to rapidly interfere with the Ran/importin-β interaction, allowing specific inhibition of this pathway during mitosis (Soderholm et al., 2011). Similar small molecule based approaches have previously been used to inhibit the function of a variety of mitotic targets including the kinesin Eg5, whose inhibitor monastrol has been used to provide insight into several mitotic processes including establishment of spindle bipolarity and microtubule attachment to the chromosomes (Kapoor et al., 2000; Khodjakov et al., 2003; Mayer et al., 1999).

Using a small molecule inhibitor like importazole to study the Ran pathway offers several advantages. First, importazole can be applied with high temporal precision, shedding light on the importance of the Ran pathway at specific stages of mitosis. Second, importazole can be used in a wide variety of biological assays, both *in vitro* and *in vivo*, providing the versatility to observe protein interactions, localizations, and dynamics among many other qualities. Third, importazole has been shown to be effective in several commonly used model systems including *Xenopus* egg extract and mammalian cells (Soderholm et al., 2011), as well as budding yeast (data not shown). Fourth, importazole is a reversible inhibitor, allowing for temporary inhibition of the Ran/importin-β interaction during washout experiments. Fifth, use of importazole allows the Ran pathway to be studied under otherwise endogenous cellular conditions, minimizing the potential for artifacts produced as a result of experimental conditions. Finally, importazole can be used in combination with other inhibitors, or siRNA knockdowns, which has the potential to reveal new insights into redundant or synergistically acting pathways that operate during mitosis or interphase.

While small molecules provide a variety of advantages for studying mitosis, they can also present their own set of problems. The inhibitor leptomycin is a potent inhibitor of RanGTP/CRM1 mediated nuclear export, but it binds covalently to CRM1, preventing reversibility experiments and leading to high cytotoxicity (Ossareh-Nazari et al., 1997). Additional inhibitors of the Ran/importin-β interaction have been previously developed, but their lack of cell permeability has limited their usefulness as tools to study the Ran pathway *in vivo* (Ambrus et al., 2010; Kosugi et al., 2008). Fortunately, as a cell-permeable and reversible inhibitor, importazole avoids some of these potential issues. However, there still remain two potential drawbacks to using importazole for study of the Ran pathway in mitosis.

First, because importazole inhibits essential processes throughout the cell cycle such as nucleocytoplasmic transport, it displays dose dependent cytotoxicity, preventing its use in long term experiments (Figure 2.12). Another drawback is importazole's unknown mechanism of action. Importazole demonstrates an ability to disrupt a FRET interaction between CFP-RanGTP and YFP-importin-β (Figure 2.1) and specifically causes a shift in the melting temperature of importin-β (Figure 2.5), but the manner in which importazole affects the Ran/importin-β interaction remains unknown. Pull down assays (Figure 2.2) and RanGAP protection assays (Figure 2.4) have demonstrated that importazole does not robustly disassociate the RanGTP/importin-β complex *in vitro*. These results were not entirely surprising considering that the RanGTP/importin-β complex involves three separate interaction surfaces which are unlikely to all be disrupted by a single small molecule (Lee et al., 2005). How then, does importazole inhibit RanGTP/importin-β function? In an attempt to address this question, we turned to Surface Plasmon Resonance, a biochemical technique that can directly and kinetically measure the affinity between two ligands in order to determine a binding constant (van der Merwe and Barclay, 1996).

An additional potential drawback of importazole is its specificity to the RanGTP/importin-β interaction. In our previous work, we attempted to address the issue of importazole's specificity through a variety of means both *in vitro* and *in vivo*. We have addressed the functional specificity of importazole by testing its effects on several nucleocytoplasmic transport pathways, all of which demonstrated that importazole was specific to the RanGTP/importin-β and had no effect on other Ran regulated transport processes (Figures 2.8, 2.9, 2.11). We have also tested importazole's specificity in mitosis with *Xenopus* egg extracts, and shown that it is capable of disrupting spindle assembly without directly destabilizing microtubules (Figure 2.13). Additionally, we have demonstrated that importazole disrupts the gradient of importin-β cargo release in mitotic HeLa cells (Figure 2.14). However, despite these data, we cannot rule out the possibility that importazole may also affect other cellular targets. Inhibitors with lower a K_D for their target can be employed at lower concentrations and are thus less likely to exhibit off-target effects. While importazole's estimated IC_{50} of 22.5 μM (Figure 2.12) is on par with other mitotic inhibitors such as monastrol (14 μM (Mayer et al., 1999)), we sought to create a more potent analogue of importazole in order to minimize the potential for nonspecific drug effects.

Results and Discussion

Importazole may enhance the Ran/importin-β interaction *in vitro*

In an effort to understand the mechanism by which importazole affects the interaction between RanGTP and importin-β we made use of surface plasmon resonance (SPR), a technique that allows direct observation of the interactions between ligands in real time (van der Merwe and Barclay, 1996). We first

immobilized importin-β on to the surface of a CM5 sensor chip and used a Biacore T100 to measure the response generated when RanGTP was introduced in the presence of increasing concentrations of importazole (Figure 3.1, panel a). Surprisingly, increasing concentrations of importazole resulted in enhancement of the measured response during association between RanGTP and importin-β. This result would suggest that importazole might strengthen the RanGTP/importin-β interaction. We next immobilized the hydrolysis defective mutant RanQ69L (Stewart et al., 1998) on the sensor chip and applied importin-β in the presence of increasing concentrations of importazole (Figure 3.1, panel b). Similar to what was observed when importin-β was immobilized to the surface, increasing concentrations of importazole did not block the interaction but seemed to enhance the association between importin-β and RanQ69L. These results were initially unexpected because importazole was originally identified via its ability to disrupt a FRET interaction between CFP-RanGTP and YFP-importin-β (Figure 2.1). However, these results are consistent with what we have observed in other *in vitro* measurements of the Ran/importin-β interaction in the presence of importazole (Figure 2.4).

As a control for the specificity of importazole to the Ran/importin-β interaction, we next applied the importin-β related nuclear transport factor transportin to the RanQ69L surface in the presence of increasing concentrations of importazole (Figure 3.1, panel c). In contrast to what was observed in the presence of importin-β, increasing concentrations of importazole decreased the measured association between RanQ69L and transportin. As importazole does not inhibit transportin mediated nuclear import (Figure 2.8, panel c), these data could suggest that importazole's apparent ability to enhance association between RanGTP and importin-β may be critical for its function.

In order to quantify importazole's effect, we sought to determine a K_d for the RanQ69L/importin-β interaction in the absence and presence of 40 μM importazole, a concentration that displays strong effects *in vivo* (Figure 2.15). Fitting curves of 0-500 nM importin-β binding to surface-associated RanQ69L produced and estimated K_d of 28.2 nM in the presence of DMSO. In the presence of importazole, this estimated K_d was moderately reduced to 19.8 nM in agreement with the previously observed increase in Ran/importin-β association (Figure 3.1, panel c). The dissociation constant was also determined for the interaction between RanQ69L and transportin under identical conditions, and revealed a K_d of 83.2 nM in the presence of DMSO and of 90.6 nM in the presence of importazole (Figure 3.1, panel c). Taken together, these data suggest that importazole does not disrupt the RanGTP/importin-β interaction, but may in fact slightly stabilize the complex. However, the accuracy of these data may not be completely reliable for reasons discussed in the next section. Even so, when viewed in light of previous results (Figures 2.1, 2.5, and 2.14), these data could suggest a possible mechanism of importazole action in which importazole binds to and elicits a conformational change in importin-β that enhances its interaction with RanGTP, but prevents RanGTP-stimulated cargo release.

Figure 3.1

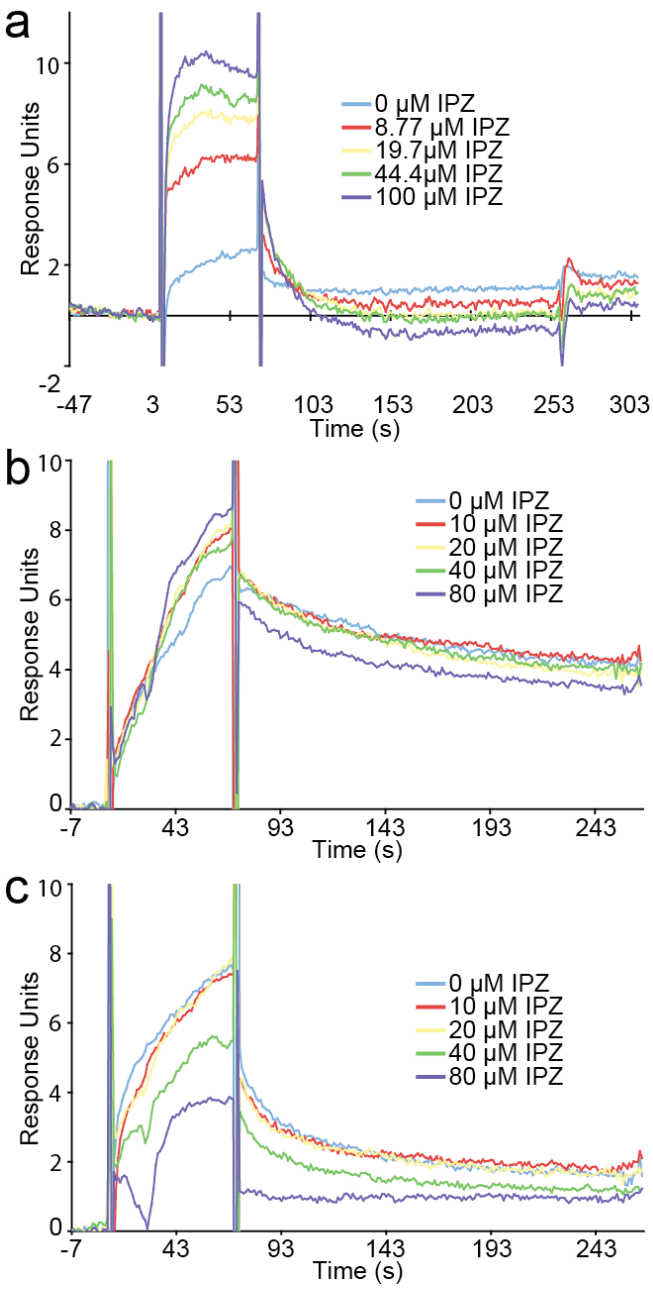

d

Condition	Kd
Imp-β	2.82E-08
Imp-β IPZ	1.98E-08
Transportin	8.32E-08
Transportin IPZ	9.06E-08

Figure 3.1: Importazole may stabilize the Ran/importin-β interaction
(a) Soluble RanGTP (10 nM) binding to surface conjugated importin-β in the presence of increasing concentrations of importazole.
(b) Soluble importin-β (100 nM) binding to surface conjugated RanQ69L in the presence of increasing concentrations of importazole.
(c) Soluble transportin (100 nM) binding to surface conjugated RanQ69L in the presence of increasing concentrations of importazole.

(d) Dissociation constants determined by fitting curves of 0-500 nM importin-β or transportin binding to surface conjugated RanQ69L in the presence of 40 μM importazole or DMSO.

Lessons learned from surface plasmon resonance

Surface plasmon resonance is a technique that can reveal a great deal of useful information about protein/protein interactions due to its ability to directly observe such interactions in real time with high sensitivity. However, there are several aspects of the technology that ultimately limited its usefulness in the study of importazole's effect on the Ran/importin-β interaction. The sensitivity of SPR is a great advantage of the technique, but this sensitivity proved to be a double-edged sword with regard to importazole. Though importazole displayed no effect on the melting temperature of transportin or on transportin mediated nuclear import (Figures 2.5, 2.8), SPR analysis indicated that importazole decreases the affinity of transportin for RanQ69L (Figure 3.1, panels c and d). While the decrease in affinity observed for this interaction was opposite of the increase in affinity observed for Ran and importin-β (Figure 3.1, panels a,b, and d), it still made interpretation of importazole's SPR results challenging, and cast doubt on the significance of the observed change in K_d for the RanQ69L/importin-β interaction in the presence of importazole.

A second aspect of surface plasmon resonance that affected its usefulness for analysis of the Ran/importin-β interaction is that it is not a truly solution-based assay. In order to observe the interaction between two ligands, SPR requires that one of the proteins be bound to sensor chip. Because the RanGTP and importin-β bind through use of three major interaction surfaces (Lee et al., 2005), it is likely that surface conjugation of these proteins partially affected their affinity for one another. Possibly as a result, the measured K_d for the RanQ69L/importin-β and RanQ69L/transportin interaction (28.2 nM and 83.2 nM respectively) were both about an order of magnitude higher than what was measured using a solution based assay (Figure 2.4) and previously reported in the literature (Bischoff and Gorlich, 1997).

Once a protein is conjugated to the sensor chip for use in SPR experiments, in principle, that surface can be used to observe many rounds of binding between the surface bound protein and soluble ligands. This approach is highly advantageous because it allows direct comparisons between the binding of different ligand conditions to the exact same surface. However, in order to make use of this essential feature of SPR, the surface must be regenerated between each round of ligand binding to provide an accurate estimation of K_d. Unfortunately, we were unable to ever find conditions that allowed for complete regeneration of the RanQ69L surface without denaturing the surface bound protein, thus introducing a source of error that limited the reproducibility of our experiments.

Identification of an importazole analogue

In an effort to limit potential non-specific effects of importazole treatment, we sought to identify a more potent importazole analogue. We screened a small library of 18 importazole analogues, generated by altering the side chains of importazole's 2,4-diaminoquinazoline structure, for disruption of mitotic spindle assembly in *Xenopus* egg extract (data not shown), as well as for inhibition of nuclear import of NFAT-GFP as described previously (Soderholm et al., 2011).

One importazole analogue, which we called compound 6 (Figure 3.2, panel a), efficiently inhibited nuclear import of NFAT-GFP in a pilot assay (data not shown). To further characterize compound 6, we quantified its ability to inhibit RanGTP/importin-β mediated import of NFAT-GFP. Cells were pretreated for one hour with compound 6 or importazole, after which cells were co-treated with ionomycin for 30 minutes to induce import. Compound 6 effectively inhibited NFAT-GFP import at a concentration of 5 μM at levels similar to importazole at 20 μM (Figure 3.2 panel b).

To test compound 6 for specificity to the Ran/importin-β interaction, we tested its ability to inhibit nuclear export of NFAT-GFP, which is exported from the nucleus by RanGTP and CRM1 (Kehlenbach et al., 1998; Zhu and McKeon, 1999). Cells pre-treated with NFAT-GFP already imported to the nucleus were washed and treated with 20 μM importazole or compound 6 for one hour. Similar to what was observed for importazole, compound 6 did not inhibit nuclear export of NFAT-GFP, and in fact decreased the observed percentage of cells displaying nuclear NFAT-GFP, as is expected for a compound that inhibits import but not export (Figure 3.2 panel c).

To assess the effects of compound 6 on mitosis, asynchronously dividing HeLa cells were treated with DMSO, 40 μM importazole, or various concentrations of compound 6 for one hour before fixation and staining for tubulin and DNA. Compound 6 caused dose-dependent defects in mitotic spindle assembly, chromosome congression, and mitotic spindle positioning, though increases in congression and positioning defects were moderate as compared to importazole treatment (Figure 3.3 panels a, b, and c). However, unlike importazole treatment, compound 6 did not affect mitotic spindle size, suggesting that decreased spindle size may be an indirect effect of importazole treatment, or that compound 6 may somehow uncouple spindle size from Ran pathway regulation (Figure 3.3 panel d).

Taken together, these data indicate that compound 6 has similar functional effects on Ran mediated pathways as importazole. However, at this point it remains unclear whether compound 6 is a more potent or specific inhibitor of the Ran/importin-β pathway than importazole. While compound 6 may well represent a viable alternative compound for studying the Ran pathway in mitosis, significant work still remains to be done in the characterization of this compound. Furthermore, additional experiments are warranted to determine the specificity and potential off-target effects of compound 6 and importazole. Therefore, until proven otherwise, importazole remains the best-characterized and most promising small molecule for use in inhibition of the RanGTP/importin-β pathway, and offers the best chance for understanding Ran's involvement in a variety of cellular processes including mitotic spindle positioning.

Figure 3.2

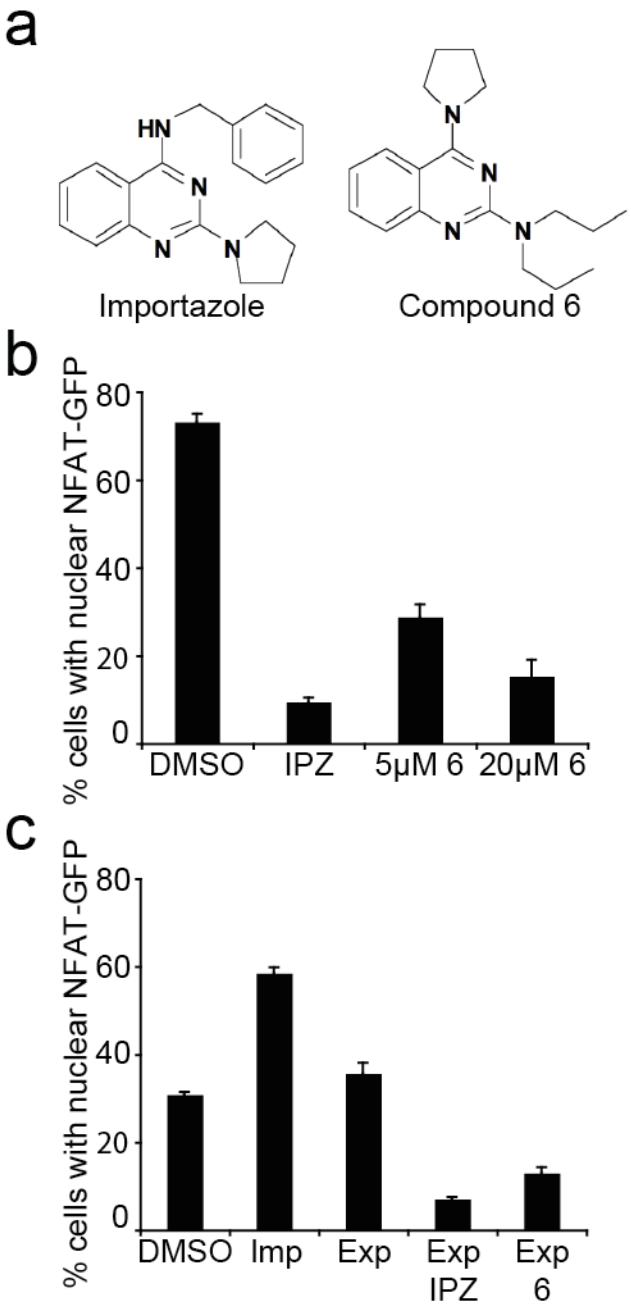

Figure 3.2: Compound 6 inhibits importin-β mediated import but not CRM1 mediated export

(a) The structure of importazole and the importazole analogue compound 6.
(b) HEK 293 cells stably expressing NFAT-GFP were treated with ionomycin to induce NFAT import. Quantification of the percentage of cells displaying nuclear NFAT-GFP in the presence of DMSO, 20 μM importazole, or the indicated concentrations of compound 6. N=3.
(c) Nuclear export of NFAT is not inhibited by compound 6. The percentage of cells displaying nuclear NFAT-GFP was quantified for all conditions. Cells were

treated with DMSO but not ionomycin (DMSO), or with ionomycin to induce import of NFAT-GFP (Imp). In other conditions, cells treated with ionomycin were washed and treated for one hour with DMSO (Exp), 20 μM importazole (Exp IPZ), or 20 μM compound 6 (Exp 6) to observe export. N=3, 100 cells were counted per condition. Bars represent standard error.

Figure 3.3

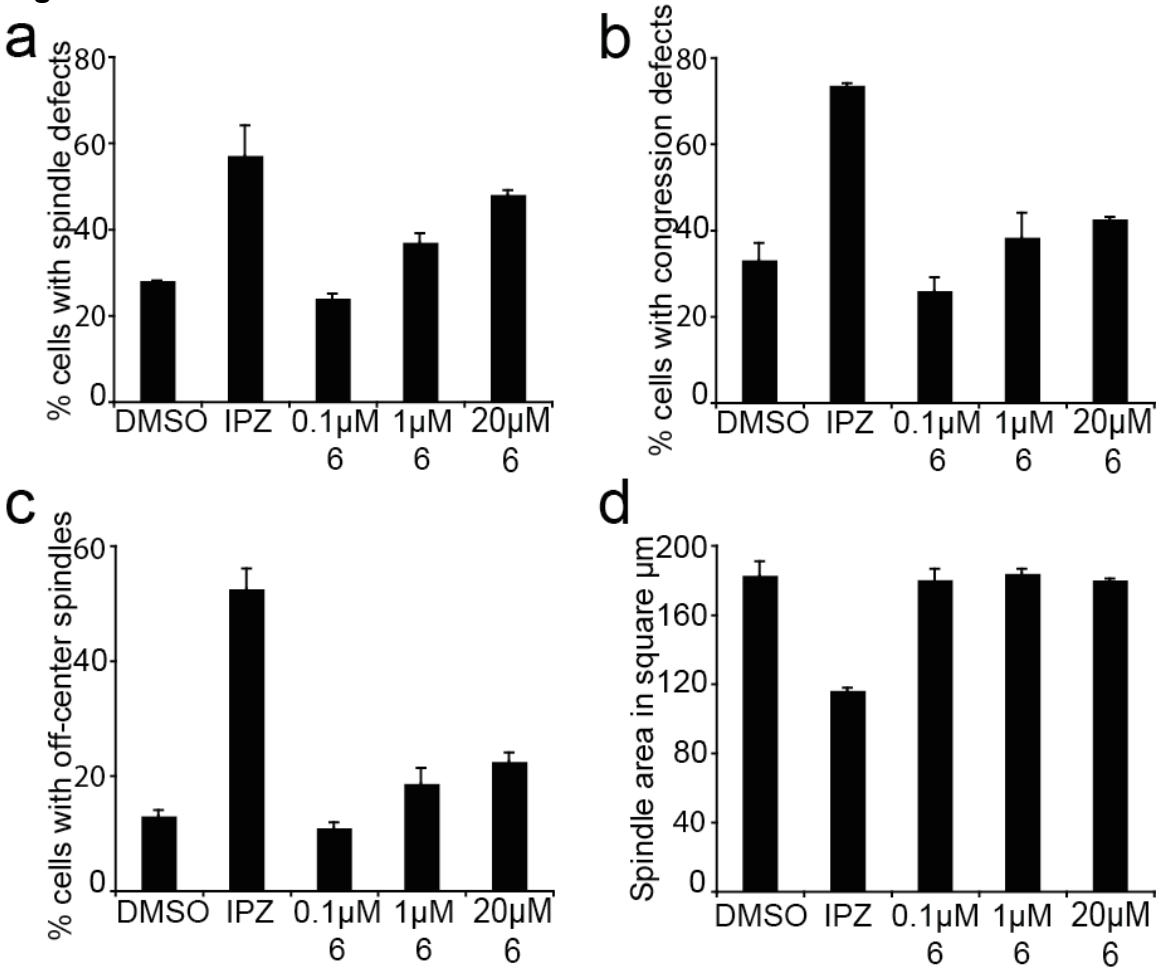

Figure 3.3: Compound 6 disrupts spindles in mitotic HeLa cells
(a) Percentage of mitotic HeLa cells displaying spindle assembly defects in the presence of DMSO, 40 μM importazole, or the indicated concentrations of compound 6.
(b) Percentage of mitotic HeLa cells displaying chromosome congression defects in the presence of DMSO, 40 μM importazole, or the indicated concentrations of compound 6.
(c) Percentage of mitotic HeLa cells displaying off-center spindles in the presence of DMSO, 40 μM importazole, or the indicated concentrations of compound 6.
(d) The size of spindles was measured for mitotic HeLa cells treated with DMSO, 40 μM importazole, or the indicated concentrations of compound 6. In each case, asynchronous HeLa cells were treated with drug for one hour prior to fixation. 100 mitotic cells per condition were scored for mitotic defects and spindle size was measured. N=3, bars represent standard error.

Materials and Methods

Protein expression and purification

A pET30a-derived construct encoding importin-β (pKW485) was transformed into BL21 cells (Invitrogen). Additionally, pQE32-derived Ran constructs (pKW356 [WT Ran], pKW 590 [RanQ69L]) and a pQE60-derived transportin construct (pKW738) were transformed in to SG13 cells. All constructs were induced with IPTG at room temperature. Harvested cells were lysed using a French press. Proteins were purified with Ni NTA resin using a standard protocol followed by gel filtration.

Surface Plasmon Resonance

All experiments were performed using a Biacore T100 at 25 ºC and in HBS-EP buffer (0.01 M HEPES pH 7.4, 0.15 M NaCl, 3 mM EDTA, 0.005 % Surfactant P20). 500 nM importin-β or 5 μM RanQ69L was coupled to the surface of a CM5 sensor chip via a standard amine coupling protocol. Importin-β surfaces were regenerated with a 30 s treatment of ionic buffer (0.92 M KCSN, 3.66 M $MgCl_2$, 1.84 M Urea, 3.66 M guanidine-HCl) followed by a 30 s treatment of HBS-EP buffer. RanQ69L surfaces were regenerated by a 30 s treatment of ionic buffer followed by a 30 s treatment of detergent buffer (0.6 % CHAPS, 0.6 % zwittergent 3-12, 0.6 % tween 80, 0.6 % tween 20, 0.6 % triton X-100), a 30 s treatment of HBS-EP buffer and a 30 s treatment of 1 mM GTP.

Cell lines and tissue culture

HEK 293 cells stably expressing NFAT-GFP were constructed as described previously (Soderholm et al., 2011), and were maintained in Opti-mem media (Gibco) plus 4 % fetal bovine serum, 1 % penicillin/streptomycin, and 200 μg/ml G418. HeLa cells were grown and maintained according to standard protocols.

NFAT-GFP nuclear import and export

For all import and export experiments, HEK 293 cells stably expressing NFAT-GFP were grown on glass coverslips to approximately 50% confluency prior to drug treatment. Importazole was used at 20 μM except where otherwise indicated. Compound 6 was used at the concentrations indicated. For controls, DMSO was used at a concentration of 0.4 %. Ionomycin was added at 1.25 μM. Importazole and compound 6 treatments were all for 1 hour. In all experiments cells were fixed with 4 % formaldehyde prior to fluorescence microscopy. DNA was visualized with 1 μg/ml Hoechst dye. For quantification, 100 cells from each condition were analyzed and the percentage that showed nuclear accumulation of NFAT-GFP calculated.

Immunofluorescence microscopy

Cells were fixed in 4 % formaldehyde with 0.1 % triton X-100 in PBS at 25 ºC for 5 minutes. Cells were then washed and blocked (PBS + 4 % BSA + 0.2 % saponin) and stained by standard techniques using the E7-A anti β tubulin

antibody (Developmental Studies Hybridoma Bank) diluted 1:1000 and Hoechst dye. For quantification, 100 mitotic cells were analyzed per experiment. Spindle size was measured in ImageJ.

Chapter 4:

Ran Pathway Control of Mitotic Spindle Positioning

Background

Multicellular organisms require proper regulation of both symmetric and asymmetric cell divisions to achieve proper development starting from a fertilized egg. In most eukaryotic cells, the cleavage plane bisects the middle of the mitotic spindle (Albertson, 1984; Glotzer, 1997; Grill and Hyman, 2005; Rappaport, 1971; Strome, 1993) and failure to properly position the mitotic spindle can result in a range of serious consequences including developmental defects, cell death, aneuploidy or cancer (Gonczy, 2008; O'Connell and Khodjakov, 2007). Control of spindle positioning is achieved through interactions between the cell cortex and the spindle's astral microtubules, which directly exert pushing forces on the mitotic spindle through microtubule polymerization, or more commonly apply pulling forces on the spindle either through microtubule depolymerization or the activity of microtubule or actin based motor proteins (Pearson and Bloom, 2004; Siller and Doe, 2009).

Control of mitotic spindle positioning has been historically studied in organisms that undergo asymmetric cell divisions, for example, the *Caenorhabditis elegans* zygote or *Drosophila melanogaster* neuroblasts. In these systems, after cell polarity is established, the mitotic spindle is positioned by pulling forces exerted on the astral microtubules by dynein/dynactin complexes which are linked to the cell cortex by an evolutionarily conserved tripartite protein complex (Gα/GPR-1/2/Lin-5 in worms and Gα-Pins-Mud in flies), which is required for spindle orientation (reviewed in (Gonczy, 2008; Siller and Doe, 2009)). While examples of asymmetric cell division in mammals are not as easily studied at the molecular level (Cayouette and Raff, 2002), a similar mechanism operates to position the spindle in symmetrically dividing mammalian cells, where the membrane-bound receptor-independent Gαi protein links the dynein/dynactin complex to the cortex through LGN and NuMA (Du and Macara, 2004).

Hence, some of the proteins involved in the positioning of the mammalian mitotic spindle have been fairly well established, but it is less clear how this process is regulated. Recent work has identified extrinsic cues that control spindle orientation (Thery et al., 2005; Toyoshima and Nishida, 2007), but a role for an intrinsic signal is also likely. One intriguing possibility for how this process is controlled is raised by the involvement of NuMA, a large coiled-coil protein that localizes and organizes the spindle poles during mitosis, and is known to be a Ran regulated importin-β cargo (Gaglio et al., 1995; Gordon et al., 2001; Joukov et al., 2006; Nachury et al., 2001; Wiese et al., 2001; Wong et al., 2006). Ran is a Ras-related small GTPase that is responsible for regulating a variety of processes throughout the cell cycle including nucleocytoplasmic transport, post-mitotic nuclear envelope assembly, nuclear pore complex assembly, protein ubiquitylation, primary cilium formation, and proper segregation of the genome (Clarke and Zhang, 2004; Dishinger et al., 2010; Goodman and Zheng, 2006; Harel et al., 2003; Pemberton and Paschal, 2005; Ryan et al., 2007; Song and Rape, 2010; Terry et al., 2007; Walther et al., 2003). In mitosis, Ran's guanine nucleotide exchange factor (GEF) RCC1 is bound to chromatin, and forms a

gradient of RanGTP centered around the chromosomes, which in turn generates a gradient of released cargoes triggering spindle assembly with high spatial specificity (Kalab et al., 2002; Kalab et al., 2006). Recent work has suggested a role for Ran in the regulation of spindle positioning of mammalian cells (Kiyomitsu and Cheeseman, 2012). However, studying the Ran pathway in mitosis is complicated by its multiple essential roles throughout the cell cycle, which limits the usefulness of traditional techniques such as genetics and RNAi. In order to overcome this problem, we made use of the small molecule inhibitor importazole, allowing us to demonstrate the Ran pathway's control of spindle positioning under endogenous protein levels and with high temporal precision (Soderholm et al., 2011).

Results and Discussion

Importazole specifically disrupts importin-β mediated spindle assembly and positioning

Previous work from our lab has shown that importazole specifically binds to importin-β *in vitro* and specifically inhibits importin-β meditated nuclear import *in vivo* (Figures 2.5, 2.9, 2.10, (Soderholm et al., 2011)). However, before using importazole to study mitotic spindle positioning, we first wanted to establish that the mitotic defects observed with importazole treatment (Figure 2.15) are due to specific inhibition of the RanGTP/importin-β pathway. As importazole binds to and inhibits importin-β, it is expected that overexpression of importin-β should at least partially alleviate the importazole-induced cellular phenotypes. In order to test this, we treated HeLa cells overexpressing importin-β-YFP or control cells overexpressing YFP alone with importazole, and quantified the mitotic phenotypes that we observed. Under both conditions, importazole treatment resulted in concentration dependent increases in mitotic spindle assembly, chromosome congression, and spindle positioning defects, as well as a concentration dependent decrease in spindle size (Figure 4.1). However, the number of mitotic cells displaying chromosome congression, spindle assembly, and spindle positioning defects was significantly reduced in importazole treated importin-β-YFP expressing cells (Figure 4.1, panels a, b, c), suggesting that these defects result specifically from importazole inhibition of the RanGTP/importin-β pathway. Interestingly, the observed reduction in mitotic spindle size with importazole treatment was not affected by importin-β-YFP overexpression, raising the possibility that this phenotype may result from an off-target effect of importazole treatment (Figure 4.1 panel d).

Importazole disrupts mitotic spindle positioning without destroying astral microtubules

As importazole treatment results in mitotic spindle assembly defects, we first surmised that the spindle positioning defects observed with importazole treatment resulted from a disruption of astral microtubules. To test this hypothesis, we took live cell movies of mitotic HeLa cells stably expressing GFP-

Figure 4.1

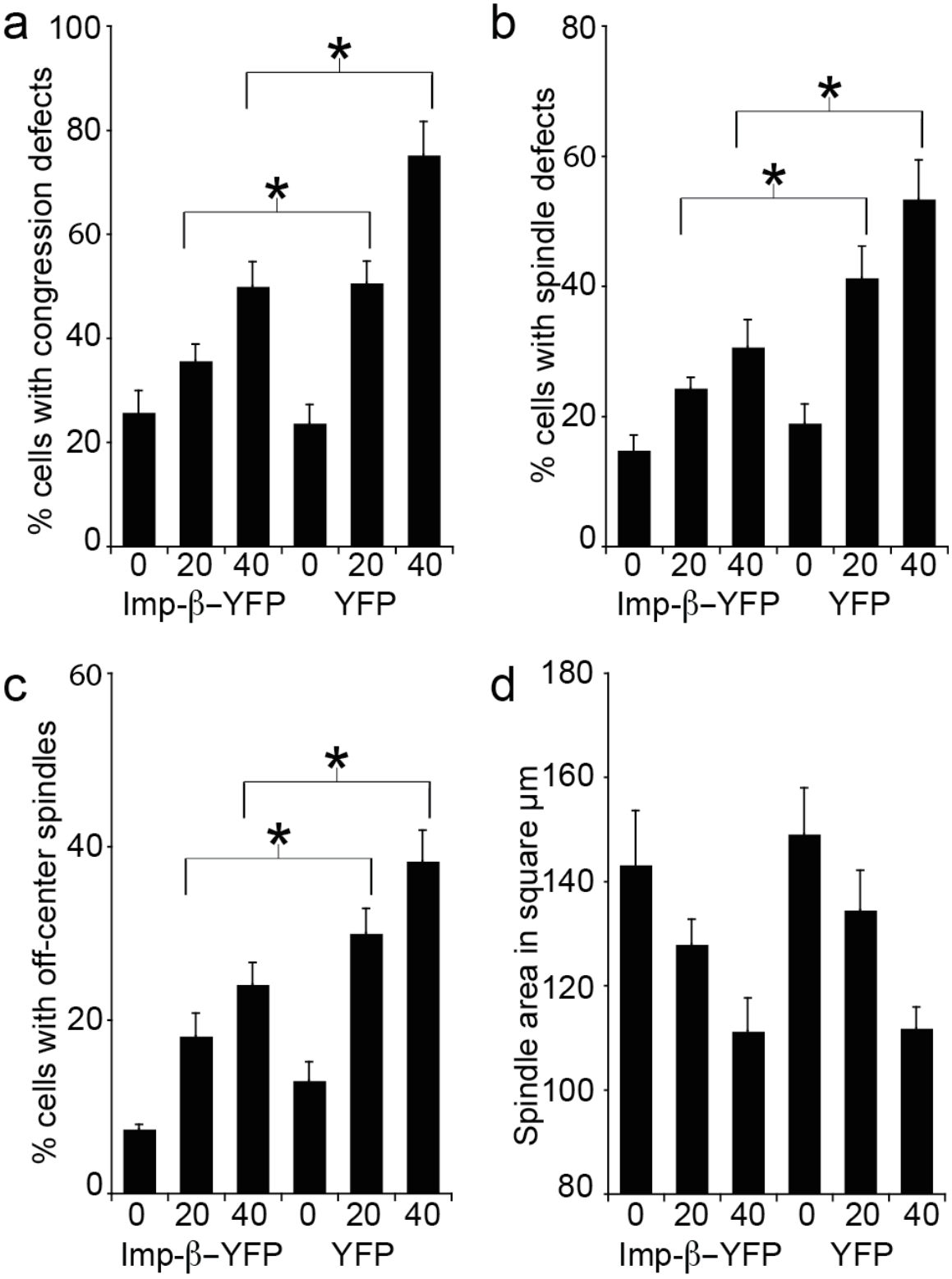
a
% cells with congression defects
100
80
60
40
20
0
*
*
0 20 40 0 20 40
Imp-β–YFP YFP
b
% cells with spindle defects
80
60
40
20
0
*
*
0 20 40 0 20 40
Imp-β–YFP YFP
c
% cells with off-center spindles
60
40
20
0
*
*
0 20 40 0 20 40
Imp-β–YFP YFP
d
Spindle area in square µm
180
160
140
120
100
80
0 20 40 0 20 40
Imp-β–YFP YFP

Figure 4.1: Importin-β overexpression reduces mitotic importazole phenotypes

Asynchronously growing HeLa cells were treated with DMSO, 20 μM, or 40 μM importazole for 1 hour before fixation.

(a) Quantification of cells expressing importin-β-YFP or YFP alone displaying chromosome congression defects.

(b) Quantification of cells expressing importin-β-YFP or YFP alone displaying mitotic spindle defects.

(c) Quantification of cells expressing importin-β-YFP or YFP alone displaying spindle positioning defects.

(d) Quantification of spindle size for cells expressing importin-β-YFP or YFP alone. N=5, 100 metaphase cells counted per condition. Bars represent standard error. Asterisks denote statistical significance ($p < 0.05$).

tubulin and mCherry-H2B. Asynchronously growing cells were treated with DMSO or 40 μM importazole, and early metaphase cells were imaged every 90 seconds starting 10 minutes after treatment. Spindles of DMSO treated cells displayed proper chromosome congression and aligned to the middle of the longitudinal axis of the cell before progressing through anaphase (Figure 4.2, panel a). In contrast, importazole treated cells failed to properly congress chromosomes to the metaphase plate, and displayed defects in spindle assembly including split spindle poles (Figure 4.2, panel b), consistent with previously observed results (Figures 2.15 and 4.1). Additionally, spindles in importazole treated cells did not adjust their position properly to the middle of the cell, but instead appeared to tumble through the cytoplasm in an uncontrolled manner before progressing through aberrant cell division (Figure 4.2, panel b). Importantly, astral microtubules appeared to be at least partially intact in importazole treated cells (Figure 4.2, panel b, arrowheads). This indicates that importazole's disruption of mitotic spindle positioning is not caused by a failure to form astral microtubules, but likely results from improper interaction of astral microtubules with the cell cortex.

Importazole treatment affects cortical factors involved in mitotic spindle positioning

In mammalian cells, spindle positioning is determined through pulling forces on the astral microtubules exerted by dynein/dynactin complexes. They are linked to the cortical membrane by LGN, NuMA, and a G-coupled receptor-independent Gαi protein (Du and Macara, 2004). To test the possibility that the Ran/importin-β regulates mitotic spindle positioning through any of these cortical factors, we first observed the endogenous mitotic localization of LGN in response to importazole treatment. Because the localization of LGN changes throughout mitosis (Kiyomitsu and Cheeseman, 2012), we synchronized HeLa cells using a double thymidine block and monitored LGN staining specifically at metaphase, nine hours after release from thymidine treatment. Synchronized cells were treated with DMSO or 40 μM importazole one hour before fixation. In DMSO treated cells, LGN localized to the cell cortex in a pattern of two arcs corresponding to the axis of the mitotic spindle (Figure 4.3, panel a). In importazole treated cells, this cortical staining pattern of LGN was disrupted, and in many cells little or no LGN was observed at the cortex (Figure 4.3, panel a, arrowheads). Additionally, in some importazole treated cells, LGN was still present at the cortex, but localized to a single arc in line with the axis of the metaphase plate (Figure 4.3, panel a, arrow). These results suggest that a functional Ran/importin-β pathway is required to regulate proper cortical LGN localization during mitosis.

To further characterize the role of the Ran pathway in cortical LGN localization, we quantified the mean cortical intensity of LGN in DMSO and importazole treated mitotic cells. Cortical intensity was measured starting at the axis of the metaphase plate, and moving in the direction of the wider arc of LGN staining (Figure 4.3, panel b). Quantification of DMSO treated cells revealed two large peaks of LGN localization at approximately 90º and 270º, corresponding to

Figure 4.2

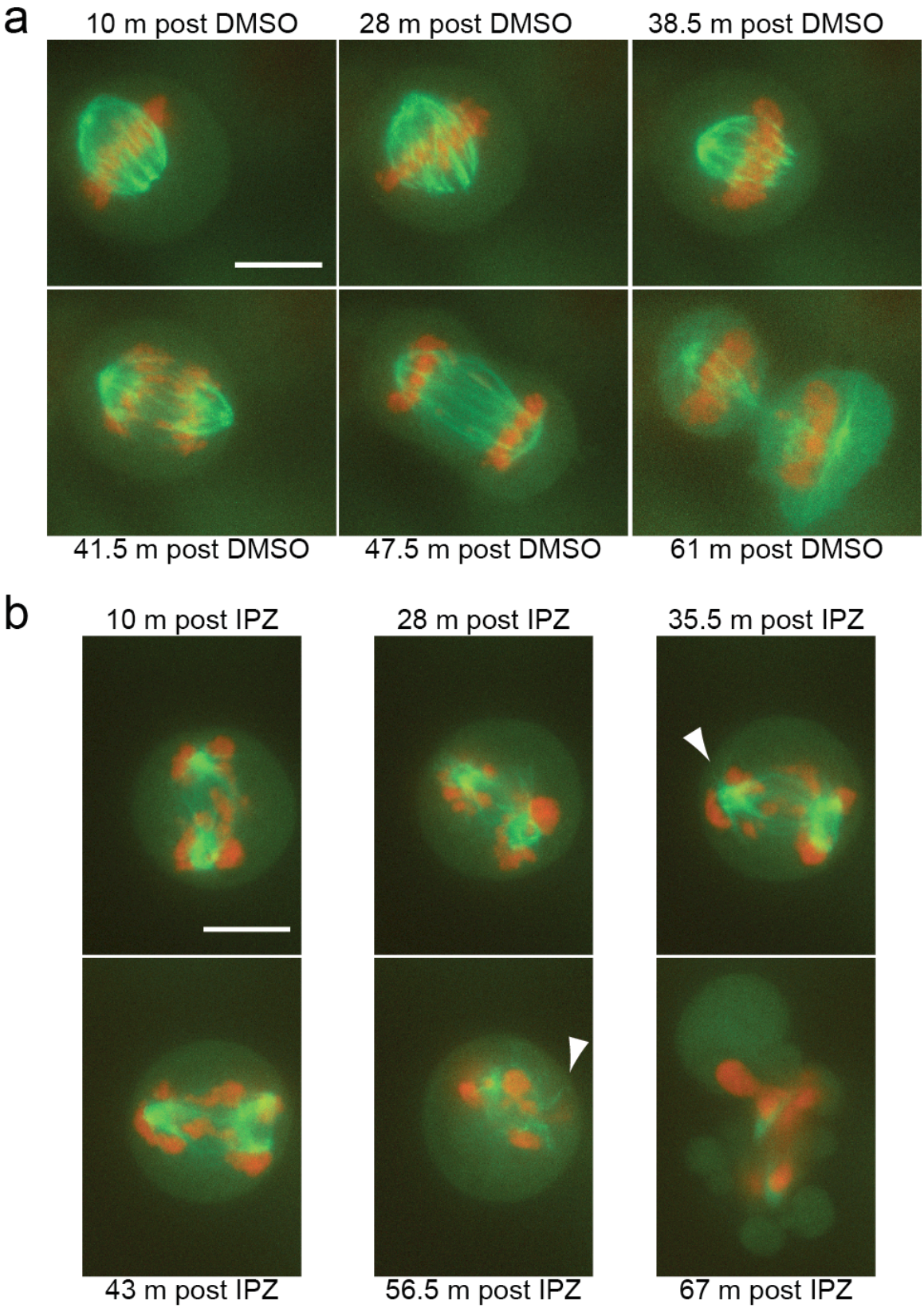
a
10 m post DMSO
28 m post DMSO
38.5 m post DMSO
41.5 m post DMSO
47.5 m post DMSO
61 m post DMSO
b
10 m post IPZ
28 m post IPZ
35.5 m post IPZ
43 m post IPZ
56.5 m post IPZ
67 m post IPZ

Figure 4.2: Importazole causes spindle movement during mitosis
(a) Time-lapse fluorescence microscopy of a mitotic HeLa cell expressing GFP-tubulin (green) and mCherry-H2B (red) treated with DMSO. Imaging began 10 minutes after treatment, and frames were captured every 1.5 minutes.
(b) Time-lapse fluorescence microscopy of a mitotic HeLa cell treated with 40 μM importazole. Arrowheads point to astral microtubules. Imaging began 10 minutes after treatment, and frames were captured every 1.5 minutes. Scale bars = 10 μm.

Figure 4.3

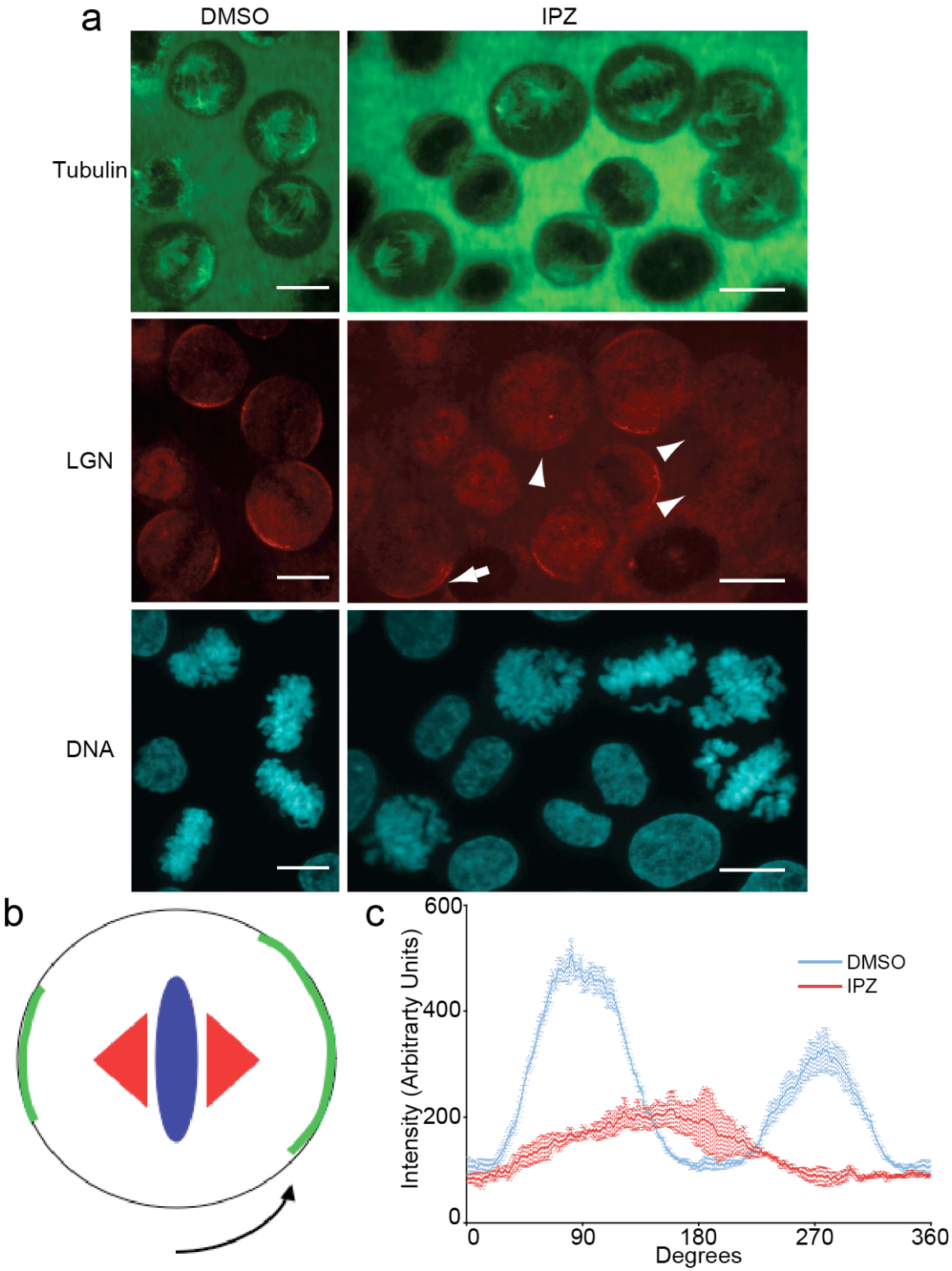

Figure 4.3: Importazole causes mislocalization of LGN
(a) Synchronized mitotic HeLa cells were treated with DMSO or 40 μM importazole for one hour prior to fixation and staining for tubulin (green), LGN

(red), and DNA (blue). Arrowheads point to cells with reduced cortical LGN staining. Arrow points to mislocalized cortical LGN. Scale bars = 10 μm.
(b) Diagram of how cortical intensity was measured. Measurement was started at the axis of the metaphase plate and proceeded around the cortex in the direction of the larger arc of cortical staining.
(c) Quantification of cortical LGN intensity in synchronized mitotic HeLa cells treated with DMSO or 40 μM importazole. N=3, 50 cells were measured per condition. Bars represent standard error.

the axis of the mitotic spindle (Figure 4.3, panel c). On the other hand, quantification of importazole treated cells revealed a single, smaller LGN peak at approximately 180º, corresponding to the axis of the metaphase plate. Additionally, in importazole treated cells, the overall cortical intensity of LGN was much lower than in DMSO treated cells, suggesting that Ran/importin-β activity promotes LGN localization to the cortex.

NuMA is a protein involved in cortical dynein localization that is known to be mitoticaly regulated by Ran and importin-β (Joukov et al., 2006; Nachury et al., 2001; Wiese et al., 2001; Wong et al., 2006). We therefore hypothesized that the direction of the RanGTP gradient regulates spindle positioning through NuMA. To test this possibility, we first observed the endogenous localization of NuMA in synchronized mitotic HeLa cells treated with DMSO or 40 μM importazole (Figure 4.4, panel a). In DMSO treated cells, NuMA localized to the spindle poles, as well as to the cell cortex in a pattern of two arcs that corresponded to the spindle axis. NuMA still localized to the spindle poles in importazole treated cells, but its cortical staining pattern was disrupted in a manner similar to LGN. In addition, NuMA formed cytoplasmic foci (Figure 4.4, panel a, arrowheads). This shows that the Ran/importin-β pathway is critical for the correct cortical localization of NuMA during mitosis.

To better understand the manner in which the Ran/importin-β pathway regulates the localization of NuMA at the cortex, we quantified the mean cortical intensity of NuMA for mitotic cells treated with either DMSO or importazole (Figure 4.4, panel b). Similar to what was observed for LGN, NuMA in DMSO treated cells formed two large peaks at approximately 90º and 270º, corresponding to the mitotic spindle axis. In importazole treated cells, this pattern of cortical NuMA localization was altered, displaying a single peak at approximately 180º, consistent with what was observed for LGN. Interestingly, the overall intensity of NuMA at the cortex in importazole treated cells was similar to what was observed for DMSO treated cells, suggesting that importazole inhibition of the Ran/importin-β does not prevent NuMA from getting to the cortex. The significance of the importazole-induced cytoplasmic NuMA foci remains unclear at this time.

It was recently suggested that the RanGTP/importin-β pathway may affect the stability of its mitotic targets (Song and Rape, 2010). In an effort to shed light on the mechanism of Ran/importin-β regulation of cortical LGN and NuMA, we measured overall intensity of both proteins in mitotic cells treated with DMSO or importazole. Importazole treatment significantly reduced overall LGN fluorescence, suggesting that inhibition of RanGTP/importin-β by importazole may destabilize LGN (Figure 4.5, panel a). On the other hand, overall NuMA intensity was not significantly altered by importazole, indicating that importazole treatment does not destabilize NuMA (Figure 4.5, panel b). This observation is consistent with our previous results showing that importazole treatment prevents release of Ran regulated cargos from importin-β (Figure 2.14). However, the strong polar staining of NuMA appeared to be unaffected by importazole treatment, which may have prevented observation of any change in NuMA

Figure 4.4

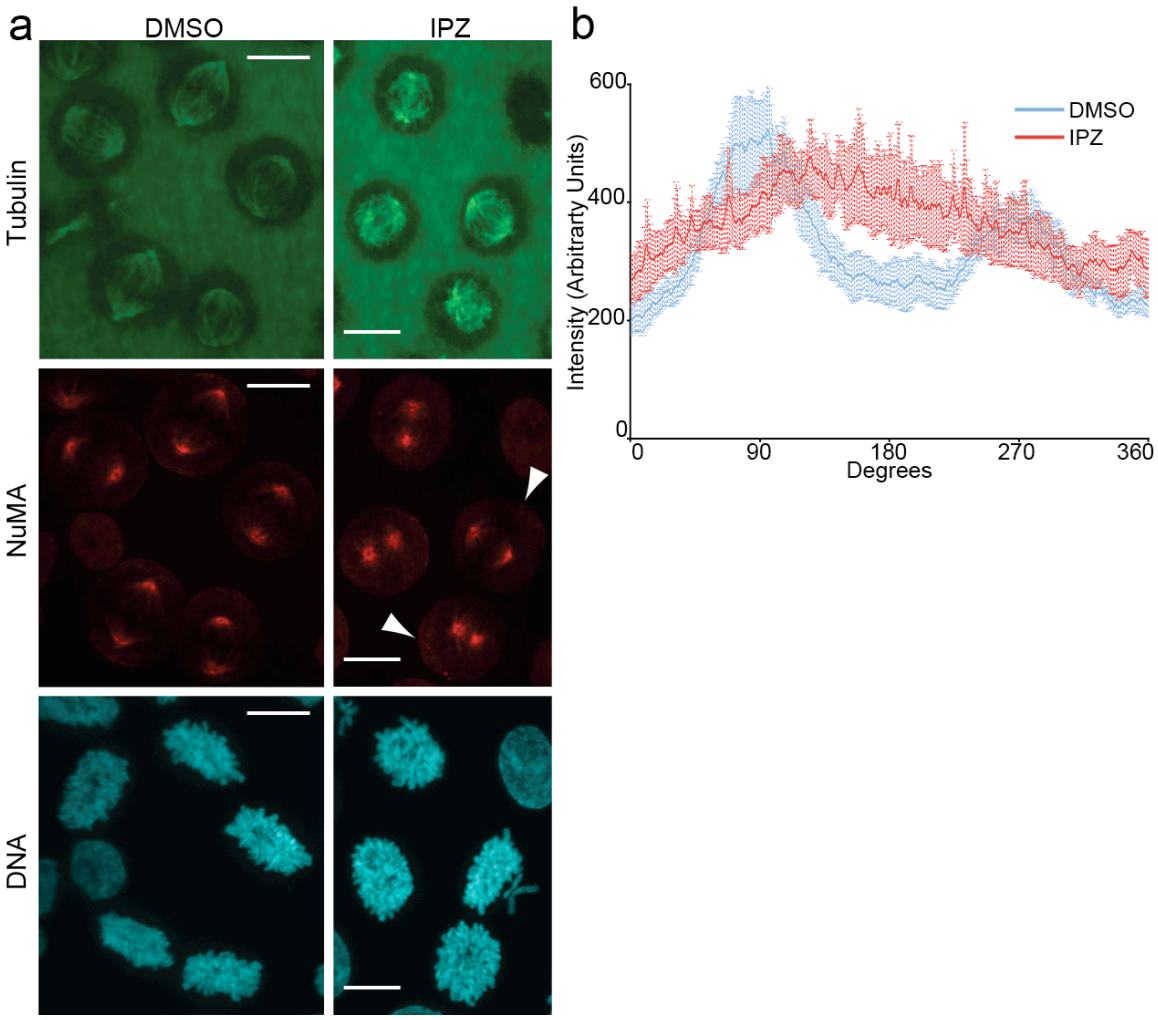

Figure 4.4: Importazole causes mislocalization of NuMA
(a) Synchronized mitotic HeLa cells were treated with DMSO or 40 μM importazole for one hour prior to fixation and staining for tubulin (green), NuMA (red), and DNA (blue). Arrowheads point to NuMA foci formed in importazole treated cells. Scale bars = 10 μm.
(c) Quantification of cortical NuMA intensity in synchronized mitotic HeLa cells treated with DMSO or 40 μM importazole. Cortical NuMA intensity was measured as in Figure 4.3, panel b. N=3, 50 cells were measured per condition. Bars represent standard error.

Figure 4.5

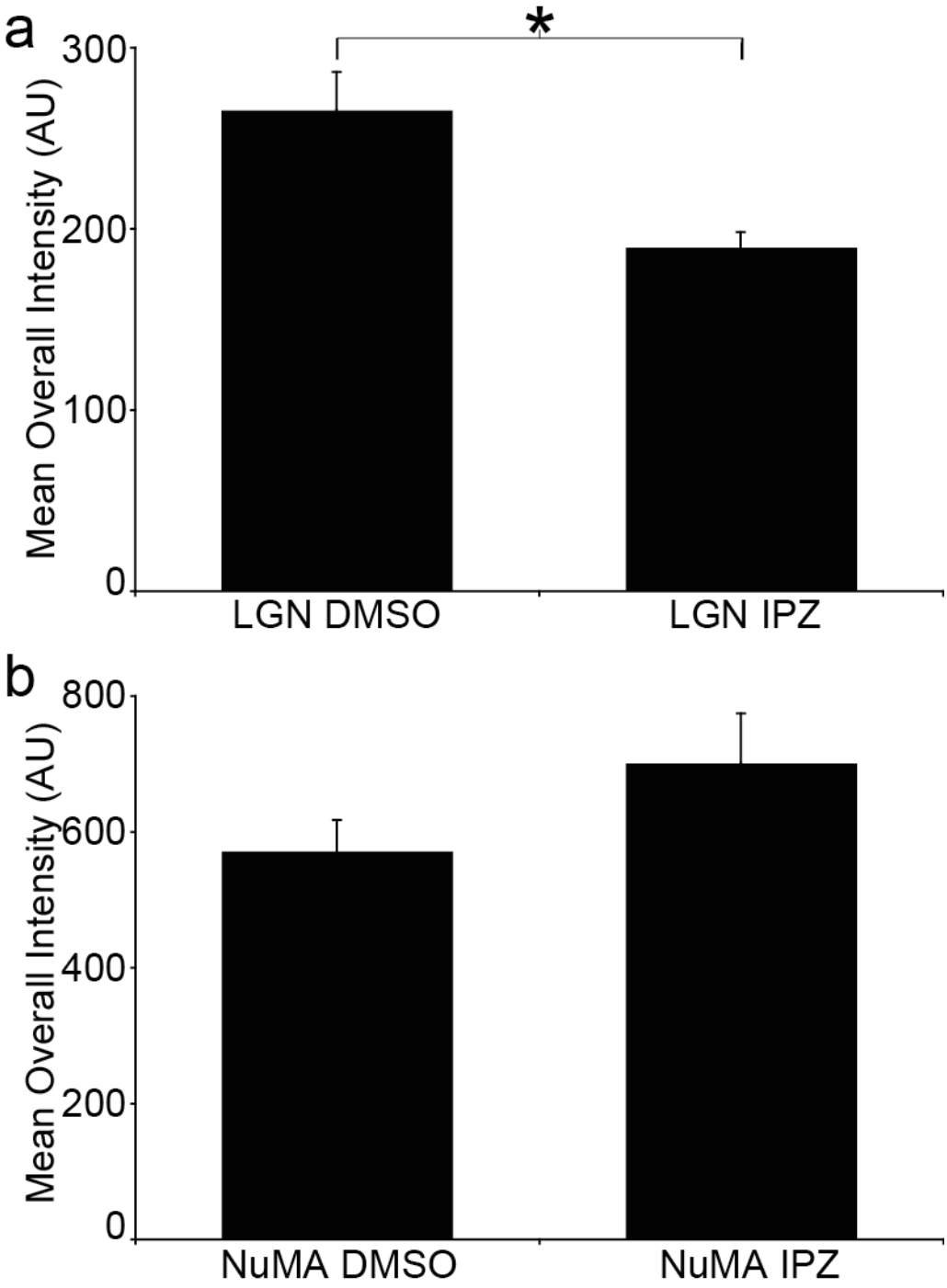

Figure 4.5: Overall cellular LGN and NuMA intensity
Overall cellular intensity of LGN (a) and NuMA (b) staining was measured in synchronized mitotic HeLa cells treated with DMSO or 40 μM importazole for one hour prior to fixation. N=3, 50 cells were measured per condition. Bars represent standard error. Asterisk denotes statistical significance ($p < 0.05$).

stability. Further analysis of protein levels will be required to definitively determine if and how importazole affects NuMA and LGN stability.

Finally, we asked how overexpression of importin-β-YFP would affect cortical localization of NuMA. Synchronized HeLa cells were transfected with importin-β-YFP or YFP alone, and cortical NuMA intensity was quantified as in Figure 4.3, panel b. Interestingly, importin-β-YFP expression decreased the overall intensity of NuMA at the cortex, but did not change the pattern of cortical NuMA localization observed with importazole treatment, suggesting that local activity of the Ran pathway may be important in determining the localization pattern of NuMA (Figure 4.6).

Conclusions and Future Directions

Our work, in combination with recent work from the Cheesman lab (Kiyomitsu and Cheeseman, 2012), clearly implies a role for Ran and importin-β in the regulation of mitotic spindle positioning in mammalian cells. However, the molecular nature of this regulation remains unclear. Live cell movies show that inhibition of RanGTP/importin-β with importazole disrupts spindle positioning without destabilizing astral microtubules (Figure 4.2), and that importazole treatment disrupts the cortical localization patterns of spindle positioning factors LGN and NuMA, preventing LGN from localizing to the cortex (Figures 4.3 and 4.4). How does the Ran pathway regulate localization of these proteins? NuMA is known to be a mitotically regulated importin-β cargo (Joukov et al., 2006; Nachury et al., 2001; Wiese et al., 2001; Wong et al., 2006), and is required for LGN localization to the cortex in mammalian cells (Du and Macara, 2004), making it the logical target for Ran regulation of spindle positioning factors. However, while importazole treatment disrupted NuMA's cortical localization pattern, it did not decrease NuMA's overall cortical intensity, suggesting proper Ran/importin-β activity is required for NuMA's localization at the cortex, but not for NuMA to get to the cortex (Figure 4.4). Additionally, while importin-β overexpression decreased the frequency of importazole treated HeLa cells that displayed mitotic spindle positioning defects (Figure 4.1), it did not rescue the cortical mislocalization of NuMA caused by importazole (Figure 4.6). One possibility suggested by these data is that additional factors besides the RanGTP/importin-β gradient may play a role in the regulation of cortical NuMA localization.

NuMA also binds microtubules and localizes to spindle poles during mitosis (Kalab and Heald, 2008), making microtubule binding a possible additional source of NuMA regulation, though we have yet to test this possibility. How could the theoretical interplay between the RanGTP/importin-β pathway and microtubule binding function to regulate cortical NuMA localization? One potential mechanism is through control of NuMA stability. Several Ran-regulated mitotic cargoes are degraded once released from importin-β by RanGTP (Song and Rape, 2010). Our current model is that release of NuMA from importin-β in the proximity of the Ran gradient makes it vulnerable to degradation. However, in the proximity of the spindle NuMA can bind microtubules, preventing its

Figure 4.6

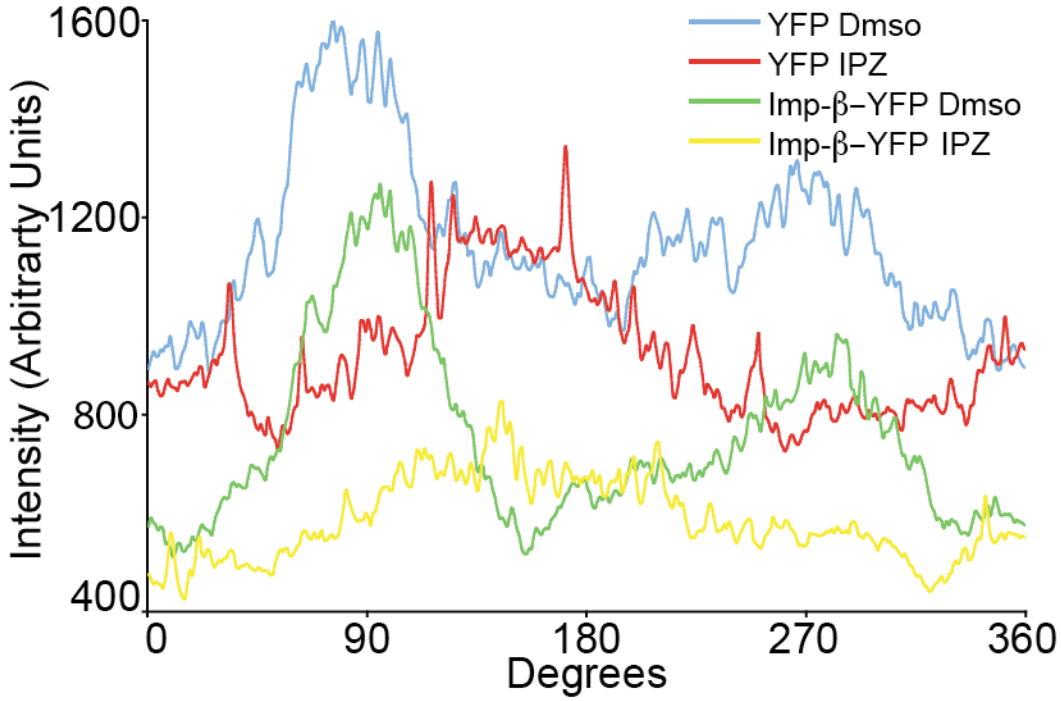

Figure 4.6: Importin-β overexpression does not alter NuMA's cortical localization pattern

Quantification of cortical NuMA intensity in synchronized mitotic HeLa cells expressing importin-β-YFP or YFP alone and treated with DMSO or 40 μM importazole. Cortical NuMA intensity was measured as in Figure 4.3, panel b. N=1, 40 cells were measured per condition.

Figure 4.7

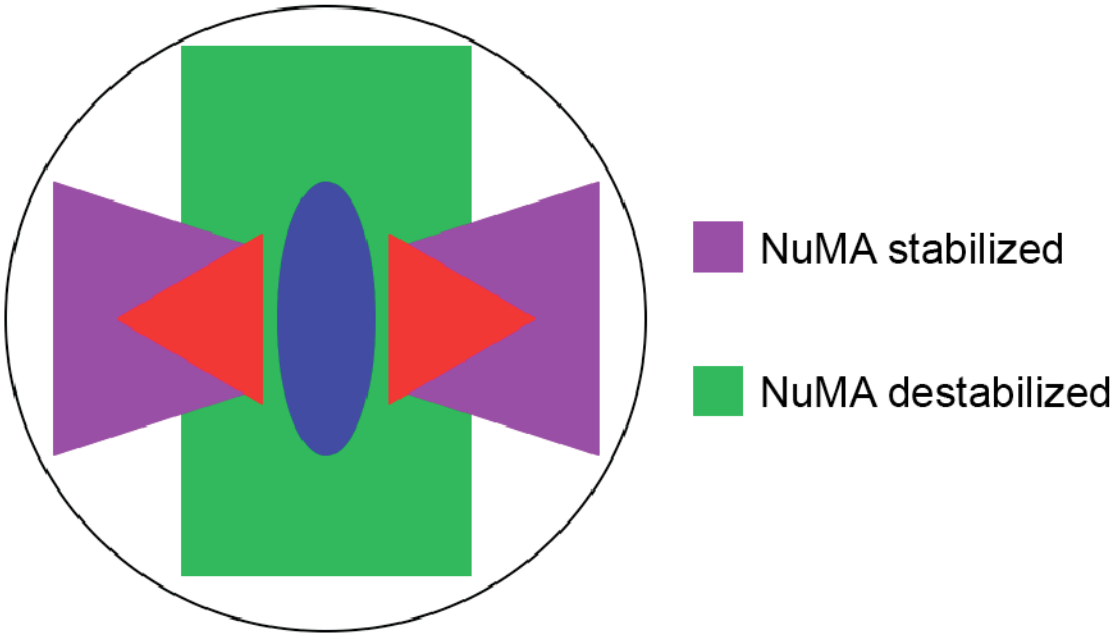

Figure 4.7: Working model for RanGTP/importin-β regulation of spindle positioning

Our current working model describing how RanGTP and importin-β may regulate mitotic spindle positioning through local stabilization or destabilization of NuMA. In the proximity of the RanGTP gradient NuMA is released from importin-β leading to its local destabilization. However, in the proximity of the spindle NuMA can bind microtubules, preventing its degradation and allowing it and LGN to localize to the cortex. The possible involvement of spindle microtubules remains to be tested.

degradation and allowing it to localize to the cortex along the spindle axis (Figure 4.7). As NuMA is required for LGN cortical localization (Du and Macara, 2004), LGN is likely recruited to the cortex where NuMA is stabilized, resulting in subsequent positioning of the mitotic spindle.

Much remains to be done in order to test our model for RanGTP/importin-β regulation of mitotic spindle positioning. For example, the effect of importazole treatment on LGN and NuMA protein stability needs to be more carefully analyzed by Western blot. The potential involvement of microtubules in the regulation of spindle positioning needs to be explored by using nocadazole and importazole in combination to determine their effects on LGN and NuMA cortical localization and stability. While many questions remain unanswered, importazole has proven to be a highly valuable tool for studying Ran regulation of spindle positioning, and promises to continue to be of great use for study of mitotic Ran/importin-β pathway function in the future.

Materials and Methods

Cell lines and tissue culture

HeLa cells stably expressing GFP-tubulin and mCherry-H2B were a gift of J. Ellenberg and were maintained in DMEM plus 10 % fetal bovine serum, 1 % penicillin/streptomycin, 500 μg/ml G418, and 0.5 μg/ml Purromycin. HeLa cells were grown and maintained according to standard protocols.

Protein overexpression

1.6 μg per well of importin-β-YFP (pKW1735) or YFP (pKW1258) plasmid DNA was transfected in to six well dishes containing 30 % - 40 % confluent HeLa cells using Lipofectamine™ LTX with PLUS™ reagent (Invitrogen). Cells were allowed to incubate for 45 hours post transfection before fixation. Only cells displaying visible YFP fluorescence were counted for quantification experiments.

Live cell movies

GFP-tubulin and mCherry-H2B HeLa cells were imaged at 37 ºC and 5 % CO_2 in Ringer's Buffer (155 mM NaCl, 5 mM KCl, 2 mM $CaCl_2$ 1 mM $MgCl_2$, 2 mM NaH_2PO_4, 10 mM HEPES pH 7.2, 10 mM Glucose) plus 10 % fetal bovine serum and 1 % OxyFluor™. Images were created from projections of 5 z slices (0.5 μm per z slice) captured with a Nikon TE2000 inverted spinning disc confocal microscope.

Cell synchronization

Cells were plated in dishes containing media (DMEM plus 10 % fetal bovine serum, 1 % penicillin/streptomycin) with 2 mM thymidine and allowed to incubate at 37 ºC and 5 % CO_2 for 18 h. Cells were washed 2x with clean media and incubated for 8.5 h. Cells were changed in to media plus 2 mM thymidine and incubated for 17 h. Cells were washed 2x with clean media to release from thymidine treatment, and cells were incubated for 9 h before fixation in mitosis.

Immunofluorescence microscopy

Cells were fixed in 4 % formaldehyde with 0.1 % triton X-100 in PBS at 25 ºC for 5 minutes. Cells were then washed and blocked (PBS + 4 % BSA + 0.2 % saponin) and stained by standard techniques using anti LGN antibody (a gift of Q. Du) diluted at 1:200 or anti NuMA antibody (a gift of D. Compton) diluted at 1:500 in addition to the E7-A anti β tubulin antibody (Developmental Studies Hybridoma Bank) diluted 1:1000 and Hoechst dye. Images were created from projections of 10 z slices (0.5 μm per z slice) captured with a Nikon TE2000 inverted spinning disc confocal microscope. Fluorescence intensity was measured in ImageJ.

References

Adam, S.A., Marr, R.S., and Gerace, L. (1990). Nuclear protein import in permeabilized mammalian cells requires soluble cytoplasmic factors. J Cell Biol *111,* 807-16.

Adames, N.R., and Cooper, J.A. (2000). Microtubule interactions with the cell cortex causing nuclear movements in Saccharomyces cerevisiae. J. Cell Biol. *149,* 863-874.

Albertson, D.G. (1984). Formation of the first cleavage spindle in nematode embryos. Dev. Biol. *101,* 61-72.

Ambrus, G., Whitby, L.R., Singer, E.L., Trott, O., Choi, E., Olson, A.J., Boger, D.L., and Gerace, L. (2010). Small molecule peptidomimetic inhibitors of importin alpha/beta mediated nuclear transport. Bioorg Med Chem *18,* 7611-20.

Amos, L.A., and Amos, W.B. (1991). The bending of sliding microtubules imaged by confocal light microscopy and negative stain electron microscopy. J. Cell Sci. Suppl. *14,* 95-101.

Andersen, S.S., Buendia, B., Dominguez, J.E., Sawyer, A., and Karsenti, E. (1994). Effect on microtubule dynamics of XMAP230, a microtubule-associated protein present in Xenopus laevis eggs and dividing cells. J. Cell Biol. *127,* 1289-1299.

Andersen, S.S., Ashford, A.J., Tournebize, R., Gavet, O., Sobel, A., Hyman, A.A., and Karsenti, E. (1997). Mitotic chromatin regulates phosphorylation of Stathmin/Op18. Nature *389,* 640-643.

Andersen, S.S., and Karsenti, E. (1997). XMAP310: a Xenopus rescue-promoting factor localized to the mitotic spindle. J. Cell Biol. *139,* 975-983.

Antonio, C., Ferby, I., Wilhelm, H., Jones, M., Karsenti, E., Nebreda, A.R., and Vernos, I. (2000). Xkid, a chromokinesin required for chromosome alignment on the metaphase plate. Cell *102,* 425-435.

Azuma, Y., Seino, H., Seki, T., Uzawa, S., Klebe, C., Ohba, T., Wittinghofer, A., Hayashi, N., and Nishimoto, T. (1996). Conserved histidine residues of RCC1 are essential for nucleotide exchange on Ran. J Biochem *120,* 82-91.

Bilbao-Cortes, D., Hetzer, M., Langst, G., Becker, P.B., and Mattaj, I.W. (2002). Ran binds to chromatin by two distinct mechanisms. Curr. Biol. *12,* 1151-1156.

Bischoff, F.R., and Gorlich, D. (1997). RanBP1 is crucial for the release of RanGTP from importin beta-related nuclear transport factors. FEBS Lett *419,* 249-54.

Blangy, A., Lane, H.A., d'Herin, P., Harper, M., Kress, M., and Nigg, E.A. (1995). Phosphorylation by p34cdc2 regulates spindle association of human Eg5, a kinesin-related motor essential for bipolar spindle formation in vivo. Cell *83,* 1159-69.

Bowman, S.K., Neumuller, R.A., Novatchkova, M., Du, Q., and Knoblich, J.A. (2006). The Drosophila NuMA Homolog Mud regulates spindle orientation in asymmetric cell division. Dev. Cell. *10,* 731-742.

Budde, P.P., Kumagai, A., Dunphy, W.G., and Heald, R. (2001). Regulation of Op18 during spindle assembly in Xenopus egg extracts. J. Cell Biol. *153,* 149-158.

Canman, J.C., Cameron, L.A., Maddox, P.S., Straight, A., Tirnauer, J.S., Mitchison, T.J., Fang, G., Kapoor, T.M., and Salmon, E.D. (2003). Determining the position of the cell division plane. Nature *424,* 1074-8.

Carminati, J.L., and Stearns, T. (1997). Microtubules orient the mitotic spindle in yeast through dynein-dependent interactions with the cell cortex. J. Cell Biol. *138,* 629-641.

Cassimeris, L. (2002). The oncoprotein 18/stathmin family of microtubule destabilizers. Curr. Opin. Cell Biol. *14,* 18-24.

Caudron, M., Bunt, G., Bastiaens, P., and Karsenti, E. (2005). Spatial coordination of spindle assembly by chromosome-mediated signaling gradients. Science *309,* 1373-1376.

Cayouette, M., Barres, B.A., and Raff, M. (2003). Importance of intrinsic mechanisms in cell fate decisions in the developing rat retina. Neuron *40,* 897-904.

Cayouette, M., and Raff, M. (2003). The orientation of cell division influences cell-fate choice in the developing mammalian retina. Development *130,* 2329-2339.

Cayouette, M., and Raff, M. (2002). Asymmetric segregation of Numb: a mechanism for neural specification from Drosophila to mammals. Nat. Neurosci. *5,* 1265-1269.

Chalfie, M., Tu, Y., Euskirchen, G., Ward, W.W., and Prasher, D.C. (1994). Green fluorescent protein as a marker for gene expression. Science *263,* 802-805.

Chi, N.C., Adam, E.J., and Adam, S.A. (1997). Different binding domains for Ran-GTP and Ran-GDP/RanBP1 on nuclear import factor p97. J Biol Chem *272,* 6818-22.

Clarke, P.R., and Zhang, C. (2004). Spatial and temporal control of nuclear envelope assembly by Ran GTPase. Symp. Soc. Exp. Biol. *(56),* 193-204.

Colombo, K., Grill, S.W., Kimple, R.J., Willard, F.S., Siderovski, D.P., and Gonczy, P. (2003). Translation of polarity cues into asymmetric spindle positioning in Caenorhabditis elegans embryos. Science *300,* 1957-1961.

Couwenbergs, C., Labbe, J.C., Goulding, M., Marty, T., Bowerman, B., and Gotta, M. (2007). Heterotrimeric G protein signaling functions with dynein to promote spindle positioning in C. elegans. J. Cell Biol. *179,* 15-22.

Desai, A., and Mitchison, T.J. (1997). Microtubule polymerization dynamics. Annu. Rev. Cell Dev. Biol. *13,* 83-117.

Desai, A., Verma, S., Mitchison, T.J., and Walczak, C.E. (1999). Kin I kinesins are microtubule-destabilizing enzymes. Cell *96,* 69-78.

Dimitrov, A., Quesnoit, M., Moutel, S., Cantaloube, I., Pous, C., and Perez, F. (2008). Detection of GTP-tubulin conformation in vivo reveals a role for GTP remnants in microtubule rescues. Science *322,* 1353-1356.

Dishinger, J.F., Kee, H.L., Jenkins, P.M., Fan, S., Hurd, T.W., Hammond, J.W., Truong, Y.N., Margolis, B., Martens, J.R., and Verhey, K.J. (2010). Ciliary entry of the kinesin-2 motor KIF17 is regulated by importin-beta2 and RanGTP. Nat Cell Biol *12,* 703-10.

Du, Q., and Macara, I.G. (2004). Mammalian Pins is a conformational switch that links NuMA to heterotrimeric G proteins. Cell *119,* 503-516.

Eshel, Y., Shai, Y., Vorherr, T., Carafoli, E., and Salomon, Y. (1993). Synthetic peptides corresponding to the calmodulin-binding domains of skeletal muscle myosin light chain kinase and human erythrocyte Ca2+ pump interact with and permeabilize liposomes and cell membranes. Biochemistry *32,* 6721-6728.

Farkasovsky, M., and Kuntzel, H. (2001). Cortical Num1p interacts with the dynein intermediate chain Pac11p and cytoplasmic microtubules in budding yeast. J. Cell Biol. *152,* 251-262.

Feng, B.Y., and Shoichet, B.K. (2006). A detergent-based assay for the detection of promiscuous inhibitors. Nat Protoc *1,* 550-3.

Flanagan, W.M., Corthesy, B., Bram, R.J., and Crabtree, G.R. (1991). Nuclear association of a T-cell transcription factor blocked by FK-506 and cyclosporin A. Nature *352,* 803-7.

Floer, M., and Blobel, G. (1996). The nuclear transport factor karyopherin beta binds stoichiometrically to Ran-GTP and inhibits the Ran GTPase activating protein. J Biol Chem *271,* 5313-6.

Fuller, B.G., Lampson, M.A., Foley, E.A., Rosasco-Nitcher, S., Le, K.V., Tobelmann, P., Brautigan, D.L., Stukenberg, P.T., and Kapoor, T.M. (2008). Midzone activation of aurora B in anaphase produces an intracellular phosphorylation gradient. Nature *453,* 1132-1136.

Funabiki, H., and Murray, A.W. (2000). The Xenopus chromokinesin Xkid is essential for metaphase chromosome alignment and must be degraded to allow anaphase chromosome movement. Cell *102,* 411-424.

Gadde, S., and Heald, R. (2004). Mechanisms and molecules of the mitotic spindle. Curr. Biol. *14,* R797-805.

Gaglio, T., Saredi, A., and Compton, D.A. (1995). NuMA is required for the organization of microtubules into aster-like mitotic arrays. J. Cell Biol. *131,* 693-708.

Gassmann, R., Carvalho, A., Henzing, A.J., Ruchaud, S., Hudson, D.F., Honda, R., Nigg, E.A., Gerloff, D.L., and Earnshaw, W.C. (2004). Borealin: a novel chromosomal passenger required for stability of the bipolar mitotic spindle. J. Cell Biol. *166,* 179-191.

Glotzer, M. (1997). The mechanism and control of cytokinesis. Curr. Opin. Cell Biol. *9,* 815-823.

Gonczy, P. (2008). Mechanisms of asymmetric cell division: flies and worms pave the way. Nat. Rev. Mol. Cell Biol. *9,* 355-366.

Goodman, B., and Zheng, Y. (2006). Mitotic spindle morphogenesis: Ran on the microtubule cytoskeleton and beyond. Biochem. Soc. Trans. *34,* 716-721.

Gordon, M.B., Howard, L., and Compton, D.A. (2001). Chromosome movement in mitosis requires microtubule anchorage at spindle poles. J. Cell Biol. *152,* 425-434.

Gorlich, D., Pante, N., Kutay, U., Aebi, U., and Bischoff, F.R. (1996). Identification of different roles for RanGDP and RanGTP in nuclear protein import. EMBO J *15,* 5584-94.

Gotta, M., Dong, Y., Peterson, Y.K., Lanier, S.M., and Ahringer, J. (2003). Asymmetrically distributed C. elegans homologs of AGS3/PINS control spindle position in the early embryo. Curr. Biol. *13,* 1029-1037.

Grill, S.W., and Hyman, A.A. (2005). Spindle positioning by cortical pulling forces. Dev. Cell. *8,* 461-465.

Gruss, O.J., Carazo-Salas, R.E., Schatz, C.A., Guarguaglini, G., Kast, J., Wilm, M., Le Bot, N., Vernos, I., Karsenti, E., and Mattaj, I.W. (2001). Ran induces spindle assembly by reversing the inhibitory effect of importin alpha on TPX2 activity. Cell *104,* 83-93.

Hannak, E., and Heald, R. (2006). Investigating mitotic spindle assembly and function in vitro using Xenopus laevis egg extracts. Nat Protoc *1,* 2305-14.

Harel, A., Chan, R.C., Lachish-Zalait, A., Zimmerman, E., Elbaum, M., and Forbes, D.J. (2003). Importin beta negatively regulates nuclear membrane fusion and nuclear pore complex assembly. Mol Biol Cell *14,* 4387-96.

Heald, R. (2000). Motor function in the mitotic spindle. Cell *102,* 399-402.

Heald, R., Tournebize, R., Blank, T., Sandaltzopoulos, R., Becker, P., Hyman, A., and Karsenti, E. (1996). Self-organization of microtubules into bipolar spindles around artificial chromosomes in Xenopus egg extracts. Nature *382,* 420-425.

Heald, R., and Walczak, C.E. (1999). Microtubule-based motor function in mitosis. Curr. Opin. Struct. Biol. *9,* 268-274.

Heil-Chapdelaine, R.A., Tran, N.K., and Cooper, J.A. (2000). Dynein-dependent movements of the mitotic spindle in Saccharomyces cerevisiae Do not require filamentous actin. Mol. Biol. Cell *11,* 863-872.

Hetzer, M., Gruss, O.J., and Mattaj, I.W. (2002). The Ran GTPase as a marker of chromosome position in spindle formation and nuclear envelope assembly. Nat. Cell Biol. *4,* E177-84.

Hintersteiner, M., Ambrus, G., Bednenko, J., Schmied, M., Knox, A.J., Meisner, N.C., Gstach, H., Seifert, J.M., Singer, E.L., Gerace, L., and Auer, M. (2010). Identification of a small molecule inhibitor of importin beta mediated nuclear import by confocal on-bead screening of tagged one-bead one-compound libraries. ACS Chem Biol *5,* 967-79.

Hwang, E., Kusch, J., Barral, Y., and Huffaker, T.C. (2003). Spindle orientation in Saccharomyces cerevisiae depends on the transport of microtubule ends along polarized actin cables. J. Cell Biol. *161,* 483-488.

Izumi, Y., Ohta, N., Hisata, K., Raabe, T., and Matsuzaki, F. (2006). Drosophila Pins-binding protein Mud regulates spindle-polarity coupling and centrosome organization. Nat. Cell Biol. *8,* 586-593.

Joukov, V., Groen, A.C., Prokhorova, T., Gerson, R., White, E., Rodriguez, A., Walter, J.C., and Livingston, D.M. (2006). The BRCA1/BARD1 heterodimer modulates ran-dependent mitotic spindle assembly. Cell *127,* 539-552.

Kalab, P., and Heald, R. (2008). The RanGTP gradient - a GPS for the mitotic spindle. J. Cell. Sci. *121,* 1577-1586.

Kalab, P., Pralle, A., Isacoff, E.Y., Heald, R., and Weis, K. (2006). Analysis of a RanGTP-regulated gradient in mitotic somatic cells. Nature *440,* 697-701.

Kalab, P., Solc, P., and Motlik, J. (2011). The role of RanGTP gradient in vertebrate oocyte maturation. Results Probl. Cell Differ. *53,* 235-267.

Kalab, P., Weis, K., and Heald, R. (2002). Visualization of a Ran-GTP gradient in interphase and mitotic Xenopus egg extracts. Science *295,* 2452-6.

Kalderon, D., Roberts, B.L., Richardson, W.D., and Smith, A.E. (1984). A short amino acid sequence able to specify nuclear location. Cell *39,* 499-509.

Kapoor, T.M., Mayer, T.U., Coughlin, M.L., and Mitchison, T.J. (2000). Probing spindle assembly mechanisms with monastrol, a small molecule inhibitor of the mitotic kinesin, Eg5. J Cell Biol *150,* 975-88.

Kashina, A.S., Scholey, J.M., Leszyk, J.D., and Saxton, W.M. (1996). An essential bipolar mitotic motor. Nature *384,* 225.

Kehlenbach, R.H., Dickmanns, A., and Gerace, L. (1998). Nucleocytoplasmic shuttling factors including Ran and CRM1 mediate nuclear export of NFAT In vitro. J Cell Biol *141,* 863-74.

Kelly, A.E., Sampath, S.C., Maniar, T.A., Woo, E.M., Chait, B.T., and Funabiki, H. (2007). Chromosomal enrichment and activation of the aurora B pathway are coupled to spatially regulate spindle assembly. Dev. Cell. *12,* 31-43.

Khodjakov, A., Cole, R.W., Oakley, B.R., and Rieder, C.L. (2000). Centrosome-independent mitotic spindle formation in vertebrates. Curr. Biol. *10,* 59-67.

Khodjakov, A., Copenagle, L., Gordon, M.B., Compton, D.A., and Kapoor, T.M. (2003). Minus-end capture of preformed kinetochore fibers contributes to spindle morphogenesis. J Cell Biol *160,* 671-83.

Kilner, J., Corfe, B.M., and Wilkinson, S.J. (2011). Modelling the microtubule: towards a better understanding of short-chain fatty acid molecular pharmacology. Mol. Biosyst *7,* 975-983.

Kimura, A., and Onami, S. (2005). Computer simulations and image processing reveal length-dependent pulling force as the primary mechanism for C. elegans male pronuclear migration. Dev. Cell. *8,* 765-775.

Kiyomitsu, T., and Cheeseman, I.M. (2012). Chromosome- and spindle-pole-derived signals generate an intrinsic code for spindle position and orientation. Nat. Cell Biol. *14,* 311-317.

Klebe, C., Bischoff, F.R., Ponstingl, H., and Wittinghofer, A. (1995). Interaction of the nuclear GTP-binding protein Ran with its regulatory proteins RCC1 and RanGAP1. Biochemistry *34,* 639-647.

Knoblich, J.A. (2008). Mechanisms of asymmetric stem cell division. Cell *132,* 583-597.

Konno, D., Shioi, G., Shitamukai, A., Mori, A., Kiyonari, H., Miyata, T., and Matsuzaki, F. (2008). Neuroepithelial progenitors undergo LGN-dependent planar divisions to maintain self-renewability during mammalian neurogenesis. Nat. Cell Biol. *10,* 93-101.

Kosugi, S., Hasebe, M., Entani, T., Takayama, S., Tomita, M., and Yanagawa, H. (2008). Design of peptide inhibitors for the importin alpha/beta nuclear import pathway by activity-based profiling. Chem Biol *15,* 940-9.

Lanford, R.E., and Butel, J.S. (1984). Construction and characterization of an SV40 mutant defective in nuclear transport of T antigen. Cell *37,* 801-813.

Lawrence, C.J., Dawe, R.K., Christie, K.R., Cleveland, D.W., Dawson, S.C., Endow, S.A., Goldstein, L.S., Goodson, H.V., Hirokawa, N., Howard, J.*, et al.* (2004). A standardized kinesin nomenclature. J. Cell Biol. *167,* 19-22.

Lee, S.J., Matsuura, Y., Liu, S.M., and Stewart, M. (2005). Structural basis for nuclear import complex dissociation by RanGTP. Nature *435,* 693-6.

Lee, W.L., Oberle, J.R., and Cooper, J.A. (2003). The role of the lissencephaly protein Pac1 during nuclear migration in budding yeast. J. Cell Biol. *160,* 355-364.

Li, H.Y., and Zheng, Y. (2004). Phosphorylation of RCC1 in mitosis is essential for producing a high RanGTP concentration on chromosomes and for spindle assembly in mammalian cells. Genes Dev. *18,* 512-527.

Li, Y.Y., Yeh, E., Hays, T., and Bloom, K. (1993). Disruption of mitotic spindle orientation in a yeast dynein mutant. Proc. Natl. Acad. Sci. U. S. A. *90,* 10096-10100.

Lowe, A.R., Siegel, J.J., Kalab, P., Siu, M., Weis, K., and Liphardt, J.T. (2010). Selectivity mechanism of the nuclear pore complex characterized by single cargo tracking. Nature *467,* 600-3.

Mahajan, R., Delphin, C., Guan, T., Gerace, L., and Melchior, F. (1997). A small ubiquitin-related polypeptide involved in targeting RanGAP1 to nuclear pore complex protein RanBP2. Cell *88,* 97-107.

Maiato, H., Khodjakov, A., and Rieder, C.L. (2005). Drosophila CLASP is required for the incorporation of microtubule subunits into fluxing kinetochore fibres. Nat. Cell Biol. *7,* 42-47.

Mans, B.J., Anantharaman, V., Aravind, L., and Koonin, E.V. (2004). Comparative genomics, evolution and origins of the nuclear envelope and nuclear pore complex. Cell. Cycle *3,* 1612-1637.

Matunis, M.J., Coutavas, E., and Blobel, G. (1996). A novel ubiquitin-like modification modulates the partitioning of the Ran-GTPase-activating protein RanGAP1 between the cytosol and the nuclear pore complex. J. Cell Biol. *135,* 1457-1470.

Mayer, T.U., Kapoor, T.M., Haggarty, S.J., King, R.W., Schreiber, S.L., and Mitchison, T.J. (1999). Small molecule inhibitor of mitotic spindle bipolarity identified in a phenotype-based screen. Science *286,* 971-4.

McNally, F.J., and Vale, R.D. (1993). Identification of katanin, an ATPase that severs and disassembles stable microtubules. Cell *75,* 419-429.

Melchior, F. (2001). Ran GTPase cycle: One mechanism -- two functions. Curr. Biol. *11,* R257-60.

Merdes, A., Ramyar, K., Vechio, J.D., and Cleveland, D.W. (1996). A complex of NuMA and cytoplasmic dynein is essential for mitotic spindle assembly. Cell *87,* 447-458.

Miller, R.K., D'Silva, S., Moore, J.K., and Goodson, H.V. (2006). The CLIP-170 orthologue Bik1p and positioning the mitotic spindle in yeast. Curr. Top. Dev. Biol. *76,* 49-87.

Mitchison, T., and Kirschner, M. (1984). Dynamic instability of microtubule growth. Nature *312,* 237-242.

Mitchison, T.J., and Kirschner, M.W. (1985). Properties of the kinetochore in vitro. II. Microtubule capture and ATP-dependent translocation. J. Cell Biol. *101,* 766-777.

Mitchison, T.J., and Salmon, E.D. (2001). Mitosis: a history of division. Nat. Cell Biol. *3,* E17-21.

Morgan-Lappe, S.E., Tucker, L.A., Huang, X., Zhang, Q., Sarthy, A.V., Zakula, D., Vernetti, L., Schurdak, M., Wang, J., and Fesik, S.W. (2007). Identification of Ras-related nuclear protein, targeting protein for xenopus kinesin-like protein 2, and stearoyl-CoA desaturase 1 as promising cancer targets from an RNAi-based screen. Cancer Res. *67,* 4390-4398.

Moritz, M., Braunfeld, M.B., Sedat, J.W., Alberts, B., and Agard, D.A. (1995). Microtubule nucleation by gamma-tubulin-containing rings in the centrosome. Nature *378,* 638-640.

Moroianu, J. (1998). Distinct nuclear import and export pathways mediated by members of the karyopherin beta family. J. Cell. Biochem. *70,* 231-239.

Murakoshi, H., Lee, S.J., and Yasuda, R. (2008). Highly sensitive and quantitative FRET-FLIM imaging in single dendritic spines using improved non-radiative YFP. Brain Cell Biol *36,* 31-42.

Nachury, M.V., Maresca, T.J., Salmon, W.C., Waterman-Storer, C.M., Heald, R., and Weis, K. (2001). Importin beta is a mitotic target of the small GTPase Ran in spindle assembly. Cell *104,* 95-106.

Nemergut, M.E., Mizzen, C.A., Stukenberg, T., Allis, C.D., and Macara, I.G. (2001). Chromatin docking and exchange activity enhancement of RCC1 by histones H2A and H2B. Science *292,* 1540-1543.

Nguyen-Ngoc, T., Afshar, K., and Gonczy, P. (2007). Coupling of cortical dynein and G alpha proteins mediates spindle positioning in Caenorhabditis elegans. Nat. Cell Biol. *9,* 1294-1302.

Niederstrasser, H., Salehi-Had, H., Gan, E.C., Walczak, C., and Nogales, E. (2002). XKCM1 acts on a single protofilament and requires the C terminus of tubulin. J. Mol. Biol. *316,* 817-828.

Niesen, F.H., Berglund, H., and Vedadi, M. (2007). The use of differential scanning fluorimetry to detect ligand interactions that promote protein stability. Nat Protoc *2,* 2212-21.

Niethammer, P., Bastiaens, P., and Karsenti, E. (2004). Stathmin-tubulin interaction gradients in motile and mitotic cells. Science *303,* 1862-1866.

Nilsson, J., Askjaer, P., and Kjems, J. (2001). A role for the basic patch and the C terminus of RanGTP in regulating the dynamic interactions with importin beta, CRM1 and RanBP1. J. Mol. Biol. *305,* 231-243.

Nipper, R.W., Siller, K.H., Smith, N.R., Doe, C.Q., and Prehoda, K.E. (2007). Galphai generates multiple Pins activation states to link cortical polarity and spindle orientation in Drosophila neuroblasts. Proc. Natl. Acad. Sci. U. S. A. *104,* 14306-14311.

Nishi, K., Yoshida, M., Fujiwara, D., Nishikawa, M., Horinouchi, S., and Beppu, T. (1994). Leptomycin B targets a regulatory cascade of crm1, a fission yeast nuclear protein, involved in control of higher order chromosome structure and gene expression. J Biol Chem *269,* 6320-4.

Nogales, E. (1999). A structural view of microtubule dynamics. Cell Mol. Life Sci. *56,* 133-142.

O'Connell, C.B., and Khodjakov, A.L. (2007). Cooperative mechanisms of mitotic spindle formation. J. Cell. Sci. *120,* 1717-1722.

Ohi, R., Sapra, T., Howard, J., and Mitchison, T.J. (2004). Differentiation of cytoplasmic and meiotic spindle assembly MCAK functions by Aurora B-dependent phosphorylation. Mol. Biol. Cell *15,* 2895-2906.

Ohtsubo, M., Okazaki, H., and Nishimoto, T. (1989). The RCC1 protein, a regulator for the onset of chromosome condensation locates in the nucleus and binds to DNA. J. Cell Biol. *109,* 1389-1397.

Ossareh-Nazari, B., Bachelerie, F., and Dargemont, C. (1997). Evidence for a role of CRM1 in signal-mediated nuclear protein export. Science *278,* 141-4.

Park, D.H., and Rose, L.S. (2008). Dynamic localization of LIN-5 and GPR-1/2 to cortical force generation domains during spindle positioning. Dev. Biol. *315,* 42-54.

Parmentier, M.L., Woods, D., Greig, S., Phan, P.G., Radovic, A., Bryant, P., and O'Kane, C.J. (2000). Rapsynoid/partner of inscuteable controls asymmetric division of larval neuroblasts in Drosophila. J. Neurosci. *20,* RC84.

Pearson, C.G., and Bloom, K. (2004). Dynamic microtubules lead the way for spindle positioning. Nat. Rev. Mol. Cell Biol. *5,* 481-492.

Pemberton, L.F., and Paschal, B.M. (2005). Mechanisms of receptor-mediated nuclear import and nuclear export. Traffic *6,* 187-198.

Pollard, V.W., Michael, W.M., Nakielny, S., Siomi, M.C., Wang, F., and Dreyfuss, G. (1996). A novel receptor-mediated nuclear protein import pathway. Cell *86,* 985-94.

Rappaport, R. (1971). Cytokinesis in animal cells. Int. Rev. Cytol. *31,* 169-213.

Reinsch, S., and Gonczy, P. (1998). Mechanisms of nuclear positioning. J. Cell. Sci. *111 (Pt 16),* 2283-2295.

Ryan, K.J., Zhou, Y., and Wente, S.R. (2007). The karyopherin Kap95 regulates nuclear pore complex assembly into intact nuclear envelopes in vivo. Mol Biol Cell *18,* 886-98.

Sampath, S.C., Ohi, R., Leismann, O., Salic, A., Pozniakovski, A., and Funabiki, H. (2004). The chromosomal passenger complex is required for chromatin-induced microtubule stabilization and spindle assembly. Cell *118,* 187-202.

Sawin, K.E., LeGuellec, K., Philippe, M., and Mitchison, T.J. (1992). Mitotic spindle organization by a plus-end-directed microtubule motor. Nature *359,* 540-3.

Schaefer, M., Petronczki, M., Dorner, D., Forte, M., and Knoblich, J.A. (2001). Heterotrimeric G proteins direct two modes of asymmetric cell division in the Drosophila nervous system. Cell *107,* 183-194.

Schaefer, M., Shevchenko, A., Shevchenko, A., and Knoblich, J.A. (2000). A protein complex containing Inscuteable and the Galpha-binding protein Pins orients asymmetric cell divisions in Drosophila. Curr. Biol. *10,* 353-362.

Schatz, C.A., Santarella, R., Hoenger, A., Karsenti, E., Mattaj, I.W., Gruss, O.J., and Carazo-Salas, R.E. (2003). Importin alpha-regulated nucleation of microtubules by TPX2. EMBO J. *22,* 2060-2070.

Schneider, S.Q., and Bowerman, B. (2003). Cell polarity and the cytoskeleton in the Caenorhabditis elegans zygote. Annu. Rev. Genet. *37,* 221-249.

Schuyler, S.C., and Pellman, D. (2001). Microtubule "plus-end-tracking proteins": The end is just the beginning. Cell *105,* 421-424.

Sharp, D.J., Yu, K.R., Sisson, J.C., Sullivan, W., and Scholey, J.M. (1999). Antagonistic microtubule-sliding motors position mitotic centrosomes in Drosophila early embryos. Nat. Cell Biol. *1,* 51-54.

Sheeman, B., Carvalho, P., Sagot, I., Geiser, J., Kho, D., Hoyt, M.A., and Pellman, D. (2003). Determinants of S. cerevisiae dynein localization and activation: implications for the mechanism of spindle positioning. Curr. Biol. *13,* 364-372.

Shibasaki, F., Price, E.R., Milan, D., and McKeon, F. (1996). Role of kinases and the phosphatase calcineurin in the nuclear shuttling of transcription factor NF-AT4. Nature *382,* 370-3.

Siegrist, S.E., and Doe, C.Q. (2005). Microtubule-induced Pins/Galphai cortical polarity in Drosophila neuroblasts. Cell *123,* 1323-1335.

Siller, K.H., Cabernard, C., and Doe, C.Q. (2006). The NuMA-related Mud protein binds Pins and regulates spindle orientation in Drosophila neuroblasts. Nat. Cell Biol. *8,* 594-600.

Siller, K.H., and Doe, C.Q. (2009). Spindle orientation during asymmetric cell division. Nat. Cell Biol. *11,* 365-374.

Soderholm, J.F., Bird, S.L., Kalab, P., Sampathkumar, Y., Hasegawa, K., Uehara-Bingen, M., Weis, K., and Heald, R. (2011). Importazole, a small molecule inhibitor of the transport receptor importin-beta. ACS Chem. Biol. *6,* 700-708.

Song, L., and Rape, M. (2010). Regulated degradation of spindle assembly factors by the anaphase-promoting complex. Mol Cell *38,* 369-82.

Stewart, M., Kent, H.M., and McCoy, A.J. (1998). The structure of the Q69L mutant of GDP-Ran shows a major conformational change in the switch II loop that accounts for its failure to bind nuclear transport factor 2 (NTF2). J. Mol. Biol. *284,* 1517-1527.

Strom, A.C., and Weis, K. (2001). Importin-beta-like nuclear transport receptors. Genome Biol *2,* REVIEWS3008.

Strome, S. (1993). Determination of cleavage planes. Cell *72,* 3-6.

Summers, K., and Kirschner, M.W. (1979). Characteristics of the polar assembly and disassembly of microtubules observed in vitro by darkfield light microscopy. J. Cell Biol. *83,* 205-217.

Terry, L.J., Shows, E.B., and Wente, S.R. (2007). Crossing the nuclear envelope: hierarchical regulation of nucleocytoplasmic transport. Science *318,* 1412-1416.

Thery, M., Racine, V., Pepin, A., Piel, M., Chen, Y., Sibarita, J.B., and Bornens, M. (2005). The extracellular matrix guides the orientation of the cell division axis. Nat. Cell Biol. *7,* 947-953.

Toyoshima, F., and Nishida, E. (2007). Integrin-mediated adhesion orients the spindle parallel to the substratum in an EB1- and myosin X-dependent manner. EMBO J. *26,* 1487-1498.

Tsou, M.F., Hayashi, A., and Rose, L.S. (2003). LET-99 opposes Galpha/GPR signaling to generate asymmetry for spindle positioning in response to PAR and MES-1/SRC-1 signaling. Development *130,* 5717-5730.

Uniewicz, K.A., Ori, A., Xu, R., Ahmed, Y., Wilkinson, M.C., Fernig, D.G., and Yates, E.A. (2010). Differential scanning fluorimetry measurement of protein stability changes upon binding to glycosaminoglycans: a screening test for binding specificity. Anal Chem *82,* 3796-802.

van der Merwe, P.A., and Barclay, A.N. (1996). Analysis of cell-adhesion molecule interactions using surface plasmon resonance. Curr. Opin. Immunol. *8,* 257-261.

Vernos, I., Raats, J., Hirano, T., Heasman, J., Karsenti, E., and Wylie, C. (1995). Xklp1, a chromosomal Xenopus kinesin-like protein essential for spindle organization and chromosome positioning. Cell *81,* 117-127.

Walczak, C.E., Verma, S., and Mitchison, T.J. (1997). XCTK2: a kinesin-related protein that promotes mitotic spindle assembly in Xenopus laevis egg extracts. J. Cell Biol. *136,* 859-870.

Walker, R.A., Inoue, S., and Salmon, E.D. (1989). Asymmetric behavior of severed microtubule ends after ultraviolet-microbeam irradiation of individual microtubules in vitro. J. Cell Biol. *108,* 931-937.

Walther, T.C., Askjaer, P., Gentzel, M., Habermann, A., Griffiths, G., Wilm, M., Mattaj, I.W., and Hetzer, M. (2003). RanGTP mediates nuclear pore complex assembly. Nature *424,* 689-94.

Wee, B., Johnston, C.A., Prehoda, K.E., and Doe, C.Q. (2011). Canoe binds RanGTP to promote Pins(TPR)/Mud-mediated spindle orientation. J. Cell Biol. *195,* 369-376.

Weis, K. (2003). Regulating access to the genome: nucleocytoplasmic transport throughout the cell cycle. Cell *112,* 441-451.

Wiese, C., Wilde, A., Moore, M.S., Adam, S.A., Merdes, A., and Zheng, Y. (2001). Role of importin-beta in coupling Ran to downstream targets in microtubule assembly. Science *291,* 653-6.

Wittmann, T., Wilm, M., Karsenti, E., and Vernos, I. (2000). TPX2, A novel xenopus MAP involved in spindle pole organization. J. Cell Biol. *149,* 1405-1418.

Wollman, R., Cytrynbaum, E.N., Jones, J.T., Meyer, T., Scholey, J.M., and Mogilner, A. (2005). Efficient chromosome capture requires a bias in the 'search-and-capture' process during mitotic-spindle assembly. Curr. Biol. *15,* 828-832.

Wolpert, L. (1995). Evolution of the cell theory. Philos. Trans. R. Soc. Lond. B. Biol. Sci. *349,* 227-233.

Wong, R.W., Blobel, G., and Coutavas, E. (2006). Rae1 interaction with NuMA is required for bipolar spindle formation. Proc. Natl. Acad. Sci. U. S. A. *103,* 19783-19787.

Xia, F., Lee, C.W., and Altieri, D.C. (2008). Tumor cell dependence on Ran-GTP-directed mitosis. Cancer Res *68,* 1826-33.

Yang, F., Moss, L.G., and Phillips, G.N.,Jr. (1996). The molecular structure of green fluorescent protein. Nat. Biotechnol. *14,* 1246-1251.

Yu, F., Morin, X., Cai, Y., Yang, X., and Chia, W. (2000). Analysis of partner of inscuteable, a novel player of Drosophila asymmetric divisions, reveals two distinct steps in inscuteable apical localization. Cell *100,* 399-409.

Yuen, H.F., Chan, K.K., Grills, C., Murray, J.T., Platt-Higgins, A., Eldin, O.S., O'Byrne, K., Janne, P., Fennell, D.A., Johnston, P.G., Rudland, P.S., and El-Tanani, M. (2012). Ran is a potential therapeutic target for cancer cells with molecular changes associated with activation of the PI3K/Akt/mTORC1 and Ras/MEK/ERK pathways. Clin. Cancer Res. *18,* 380-391.

Zhang, J.H., Chung, T.D., and Oldenburg, K.R. (1999). A Simple Statistical Parameter for Use in Evaluation and Validation of High Throughput Screening Assays. J Biomol Screen *4,* 67-73.

Zhang, X., Lan, W., Ems-McClung, S.C., Stukenberg, P.T., and Walczak, C.E. (2007). Aurora B phosphorylates multiple sites on mitotic centromere-associated kinesin to spatially and temporally regulate its function. Mol. Biol. Cell *18,* 3264-3276.

Zheng, Y., Wong, M.L., Alberts, B., and Mitchison, T. (1995). Nucleation of microtubule assembly by a gamma-tubulin-containing ring complex. Nature *378,* 578-583.

Zhu, J., and McKeon, F. (1999). NF-AT activation requires suppression of Crm1-dependent export by calcineurin. Nature *398,* 256-60.